A Storage Ring for Neutral Molecules

A Storage Ring for Neutral Molecules

een wetenschappelijke proeve op het gebied van
de Natuurwetenschappen, Wiskunde en Informatica

PROEFSCHRIFT

ter verkrijging van de graad van doctor
aan de Radboud Universiteit Nijmegen,
op gezag van de Rector Magnificus
Prof. Dr. C. W. P. M. Blom,
volgens besluit van het College van Decanen
in het openbaar te verdedigen
op donderdag 20 januari 2005,
des namiddags om 3.30 uur precies
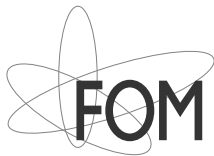
door

Floris Maria Hermansz Crompvoets

geboren op 27 februari 1976
te Meijel

Promotor : Prof. Dr. G. J. M. Meijer

Manuscriptcommissie : Prof. Dr. J. J. ter Meulen

Prof. Dr. H. J. Loesch
Universität Bielefeld

Dr. H. L. Bethlem
Fritz-Haber-Institut der
Max-Planck-Gesellschaft, Berlin

aan Cécile

Woord vooraf

De eerste stappen van het onderzoek dat ik in mijn proefschrift beschrijf, zijn nu ruim vijf jaar geleden gezet. Na mijn afstudeerstage wilde ik graag een natuurkundig promotieonderzoek doen en Gerard Meijer bood mij die kans. Hij had in Nijmegen net een onderzoek gestart om koude moleculen te maken. Mijn interesse was gewekt en terwijl ik nog op het zonnige La Palma verbleef om sterren te kijken, besloot ik me te gaan verdiepen in het koude en het kleine.

Mijn promotieonderwerp werd het bouwen van een opslagring voor neutrale moleculen. De Stark-afremmer die Rick Bethlem net operationeel had, zou gebruikt gaan worden om de moleculen in de ring te injecteren. Het eerste jaar bestond vooral uit het leren kennen van de apparatuur, zoals omgaan met hoogspanning, vacuüm en de lasersystemen. Het ontwerp voor de opslagring was vrij snel klaar en de ring kon gebouwd worden.

Inmiddels was de hele Koude-Moleculengroep verhuisd naar het FOM-instituut voor Plasmafysica Rijnhuizen. Dat betekende voor mij dagelijks op en neer reizen van Nijmegen naar Nieuwegein in het paarse Mazdaatje.

Op 5 december 2000, Sinterklaasavond, was de opslagring voor neutrale moleculen een feit: een pakketje moleculen had een rondje gevlogen in de ring. Al gauw konden we meer rondjes meten en bij verschillende snelheden. Deze eerste metingen met de ring en de publicatie ervan in Nature behoorden tot de betere, zij het enigszins verlate, Sinterklaascadeautjes die ik gehad heb.

De natuurkunde beperkte zich niet alleen tot het lab. De wetenschappelijke conferenties en summer schools, die ik bezocht heb, waren erg interessant en leerzaam. Je ziet bijvoorbeeld niet elke dag Nobelprijswinnaars in het wild. Leuk waren ook de ontmoetingen met collega-promovendi en onderzoekers. Vooral aan de bijeenkomsten in Les Houches in de zomer én in de winter en de US Particle Accelerator School in Boulder heb ik prettige herinneringen. Al deze zaken hebben mij meer dan eens duidelijk gemaakt dat ik aan het front van een zeer interessant vakgebied mocht vertoeven.

Tijdens mijn promotieonderzoek heb ik veel hulp gehad van anderen en daarom bedank ik hen graag in dit woord vooraf.

Zonder technicus ben je nergens als experimenteel fysicus. Gelukkig kon ik een beroep doen op André van Roij. André is een technicus die aan een half woord genoeg heeft om precies dat te maken of te tekenen wat jij nodig hebt. Zonder zijn hulp zouden er maar weinig rondjes in de opslagring gemeten zijn.

Op Rijnhuizen kon ik ook altijd een beroep doen op Paul Smeets en zijn on-geëvenaarde kennis van het instituut. Als ik een apparaat nodig had, wist hij het wel ergens op te duikelen. Ook voor kleine klusjes stond hij altijd klaar. Wim Melissen, Martin van der Kaaij en Ton van der Grift hebben mij weg-wijs gemaakt in de wereld van de (hoogspannings)electronica en mooie pulsers voor mij gebouwd. De tekeningen van mijn opstelling gemaakt door Frank van Amerongen hebben diverse publicaties opgesierd.

Magda Speijers en Erna Gouwens van Oss hebben allerlei geregel voor mij uit handen genomen en mijn basis in Nijmegen in stand gehouden. De mensen op het FOM-bureau handelden vragen en kwesties altijd snel en accuraat af.

Hans ter Meulen, prof. dr. H. J. Loesch en Rick Bethlem hebben mijn manuscript gelezen en nuttige suggesties ter verbetering gegeven.

Tijdens de momenten dat ik in Nijmegen was, kon ik rekenen op de interesse en gezelligheid van de MLF-ers. Ik zal met plezier terugdenken aan de gezellige lunches en borrels met de bewoners van het HFML. Dankzij de Rijnhuizenaren was er op het instituut in Nieuwegein een aangename, haast familiaire sfeer.

Met de leden van de zusterteams Moleculaire Dynamica en FELIX was het prettig samenwerken. Er was altijd gelegenheid voor een praatje en in tijden van nood was het lenen van een apparaat nooit een probleem.

De Koude-Moleculengroep is een bijzondere groep met slimme en aardi-ge mensen. Rick Bethlem, Bas van de Meerakker, Jacqueline van Veldhoven, André van Roij, Rienk Jongma, Paul Smeets, Jochen Küpper, David Carty, So-phie Schlunk, Wieland Schöllkopf, Allard Mosk, Giel Berden, Boris Sartakov, Michael Ziskind en Irena Labazan, it was very nice to have such wonderful and helpful colleagues. Good luck to you and the new members of the Cold Molecules group.

Bas en Jacqueline, mede-oio's van het eerste uur, fijn dat jullie paranimf willen zijn. Rick, je was een aangename kamergenoot en ik heb veel van je geleerd, zowel op natuurkundig als op muzikaal gebied. Gerard, ik heb mogen profiteren van je uitgebreide, gedetailleerde kennis, je onuitputtelijke energie en je enthousiaste en motiverende gesprekken.

Mijn ouders, familie en vrienden zorgden voor de broodnodige afwisseling in het leven van een promovendus; etentjes, bezoekjes, momenten van rust, weekendjes weg en skivakanties.

Cécile, ik kon altijd op jou rekenen. Als ik eens een dip had dan pepte jij mij weer op; vaak met een simpele glimlach. Als een experiment gelukt was of een artikel geaccepteerd was dan vierden we dat; met lekker uit eten en een brede lach. Cécile, we hebben het voor elkaar gekregen: ieder apart maar uiteindelijk samen op een dag promoveren.

<div align="right">

Floris Crompvoets
November 2004

</div>

Contents

Chapter 1

General introduction

1.1   Manipulation of molecules

Obtaining full control over both the internal and external degrees of freedom of molecules has been an important goal in molecular physics during the past decades. Full control over internal and external degrees of freedom of molecules can be achieved, in principle, with appropriately tailored electromagnetic fields. Radiation fields can be used, for instance, to prepare molecules in a single selected quantum state, thereby controlling their electronic, vibrational, and rotational degrees of freedom [1,2]. Static inhomogeneous electric and magnetic fields have been used for a long time to (de-)focus polar molecules in a beam, thereby manipulating their transverse position and velocity and controlling their orientation [3,4]. Time-varying electric fields can be used to change the forward (longitudinal) position and velocity of these molecules as well [5].

The ultimate form of control is the situation when the motion of molecules is spatially confined (control of external degrees of freedom) and when all the molecules are in a selected quantum state (control of internal degrees of freedom). Two requirements have to be fulfilled in order to confine a group of molecules. First, it must be possible to apply a force on the molecules. Second, the kinetic energy of the molecules must be (made) low enough so that they cannot break free from this force. As the force that can be exerted on a molecule depends in general on the quantum state of the molecule, a specific internal quantum state is selected. In this thesis a storage ring is presented in which cold neutral deuterated ammonia molecules, $^{14}ND_3$, are spatially confined in one specific quantum state.

1.2   Applications of cold molecules

The motivations for trapping molecules are, like for atoms and charged particles, high-precision measurements and the study of interactions between the trapped molecules. Especially, at low temperatures, where the realm of quan-

tum physics is entered and particles behave like waves, interesting phenomena are to be expected. A comprehensive overview of applications of trapped cold molecules in the fields of high-precision measurements and collision studies is given by Bethlem and Meijer [6]. The applications described in this article cannot (easily) be performed with atoms or ions and justify or even necessitate the use of molecules. These applications are briefly summarized in the following two Paragraphs.

1.2.1 High-precision measurements

The spectral resolution $\Delta\nu$ in molecular spectroscopy is ultimately limited by the time Δt a molecule spends in a measuring device: $\Delta\nu\Delta t \geq 1/2\pi$. In this case the linewidth is said to be Fourier transform limited. By lowering the velocity and/or storing the molecule over long time intervals, the interaction time with the measuring device can be increased, improving the attainable resolution.

Increased resolution helps, for instance, to determine an upper bound for the value of the electron's permanent electric dipole moment (EDM). The existence of an EDM is a violation of time-reversal symmetry and has profound consequences for the evolution of the universe as it is related to the matter/anti-matter symmetry in the universe. The value of the EDM predicted by the Standard Model is orders of magnitude smaller than the value predicted by some extensions to this model. Therefore a measurement of the EDM is an important test of these different models. Currently, the most accurate determination of the upper limit of the EDM has been performed on atoms but it is expected that ultimately the highest accuracy will be obtained by using cold polar molecules [7–9].

The study of parity-violating interactions in chiral molecules is another field that would benefit from increased resolution. In nature, there is a preference for the 'left-handed' forms of amino-acids. Based on parity considerations one would expect equal amounts of 'left-handed' and 'right-handed' forms. The question is: how did this imbalance happen? The only parity violating mechanism known is the weak interaction. Hence, the spectroscopic measurement of an energy difference between left-handed and right-handed molecules is a crucial experiment to reveal the manifestation of the weak interaction in molecules [10].

Time dependence of fundamental constants like the proton-electron mass ratio m_p/m_e, which could be a consequence of the expansion of the universe, can be tested by precisely measuring those ro-vibrational transitions in molecules that have a strong dependence on the ratio m_p/m_e [11].

Another interesting application of stored molecules is the possibility to determine the lifetime of an excited quantum state directly by looking at the trap loss of stored molecules in these excited quantum states. This can be used, for instance, to determine the lifetimes of vibrationally excited or electronically excited metastable states, which are difficult to obtain otherwise.

1.2.2   Interactions between particles

At very low temperatures the wave properties of particles become important and the particles behave fundamentally different than at room temperature where they can be considered to be like hard spheres. When the temperature is sufficiently low, trapped bosonic particles all occupy the lowest energy level in the trap and condense into one giant wavefunction: a Bose-Einstein condensate [12,13]. Trapped fermionic particles cannot occupy the same energy level and all energy levels in the trap will be filled up one by one. In the end the cloud of particles can no longer shrink owing to the Fermi pressure due to the Pauli exclusion principle [14]. These degenerate quantum gases are a macroscopic manifestation of quantum mechanics. Compared to atoms, molecules also have rotational and vibrational degrees of freedom and in the degenerate regime this leads to interesting, new behavior.

One of the interesting novelties in molecules compared to atoms is that they have electric dipole moments. The interaction between the electric dipole moments is typically three orders of magnitude larger than the interaction between their magnetic counterparts. At very low temperatures, when the translational energy becomes comparable to the dipole-dipole interaction energy between two polar molecules, trapped molecules will feel each other's dipoles and it is predicted that the molecules will form a crystalline structure similar to an ionic crystal in ion traps [15]. This dipole-dipole interaction is anisotropic and therefore the mean field interaction energy of the cold sample of molecules depends on the trap geometry. By changing the geometry one has a knob to tune the interaction, offering new possibilities for controlling and engineering macroscopic quantum states [16].

In a sufficiently cold gas of fermionic particles, interparticle interactions can lead to weakly bound pairs of particles whose motions are correlated. These pairs act like bosons. This mechanism shows strong resemblance to the Cooper pairing of electrons in the Bardeen-Cooper-Schrieffer (BCS) theory of superconductivity. For identical fermions the interaction vanishes at very low temperatures due to the Pauli-principle. Therefore, in order to observe the BCS-transition in dilute atomic gases one needs simultaneous trapping of two different fermionic species. The constraint on the relative concentrations of these species is rather severe. Dipole-dipole interactions in ultracold polar gases, though, do not vanish at ultralow temperatures. Therefore, it is predicted that a BCS-transition can be obtained in a single species polar Fermi-gas [17].

A proposal has been put forward that polar molecules trapped in an optical lattice can be used for quantum computation [18]. The qubits would be the electric dipole moments of ultracold molecules, oriented along or against an externally applied electric field. Individual qubits can be addressed when they are in a well-defined inhomogeneous external electric field and the coupling between the qubits will occur via the electric dipole-dipole interaction.

1.3   Production of cold molecules

Laser cooling and trapping [19], the technique that has been so successfully applied to cool and to confine neutral atoms, cannot be applied to molecules unfortunately due to their more complex energy level structure. Laser cooling requires a closed cycling scheme without off-resonance fluorescence. Although a rotationally and electronically closed two-level system can be found for many molecules as well, it is generally not possible to find a vibrationally closed cycle. The vibrational transitions are governed by Franck-Condon factors and after spontaneous emission the molecules generally end up in different vibrational levels and are lost from the laser cooling cycle.

Therefore, other experimental schemes to produce cold molecules have to be pursued. By now, trapped samples of neutral molecules have been created by means of buffer gas cooling in a magnetic trap [20], by using Stark-deceleration of a molecular beam in combination with an electrostatic trap [21], and by pairing cold atoms to form molecules, which are subsequently held in an optical [22] or magnetic trap [23]. Recently, spectacular progress has been made with association of ultra-cold atoms assisted by magnetically induced Feshbach resonances, resulting in the first molecular Bose-Einstein condensates [24–27].

1.3.1   Stark deceleration of a molecular beam

For the experiments described in this thesis the Stark deceleration technique is employed to create samples of cold molecules. This technique uses time-varying electric fields to manipulate the motion of a package of neutral polar molecules. This technique is applicable to a wide range of molecules, as long as they have a sufficiently large Stark-shift-to-mass ratio. The source of cold molecules in these experiments is a pulsed, supersonic molecular beam. By letting a gas expand adiabatically from a high-pressure container through a small nozzle into vacuum most of the rotational, vibrational, and translational energy of the molecules is converted into forward motion (kinetic energy). This results in a package of molecules in the lowest rotational and vibrational levels, with a high forward velocity in the laboratory frame (300–2000 m/s) but with a low translation temperature in the moving frame. Details about molecular beams and their applications are extensively described in the books on Molecular Beams edited by Scoles [3, 4]. The Stark deceleration technique is applied to lower the forward velocity of the molecules in the beam to an arbitrarily low value. This deceleration process is in fact the neutral analogue of the linear acceleration of charged particles. Techniques successfully applied in charged particle accelerator physics can hence be transferred to neutral molecules; important principles like phase stability [28, 29] and alternate gradient focusing [30] are applicable to neutral molecules as well. The important difference between charged particles and neutral particles is that the force on a charged particle in an electric field is proportional to the field while the force on a neutral particle is proportional

to the gradient of the electric field strength. The force on a charged particle is many orders of magnitude larger than the force on a neutral particle. For instance, in an hexapole focuser with a voltage difference of 10 kV between adjacent rods and with an inner radius of 3 mm, as used in the experiments reported in this thesis, a positively charged ammonia ion experiences a maximum force of $8.0 \cdot 10^{-13}$ N. A neutral ammonia molecule in its $|J, K\rangle = |1, 1\rangle$ ground-state level experiences in the same hexapole focuser a maximum force of $8.3 \cdot 10^{-21}$ N, almost eight orders of magnitude smaller.

1.4   Confinement of molecules in a ring

The first storage rings to be constructed were rings for charged particles. In these rings confinement is achieved with magnetic fields that generate a Lorentz force holding the charged particles in circular orbits. Acceleration of the charged particles is achieved by radio frequency modulated electric fields. An overview of the development of storage rings for charged particles can be found in various textbooks [31, 32]. In charged particle storage rings particles are swept up to velocities close to the speed of light. Counterpropagating beams are forced to collide with each other resulting in highly energetic collisions. The counterpropagating geometry allows for the highest possible center-of-mass energy and this is the energy that is available to be dissipated in collisions. Only under these circumstances traces of fundamental particles and their interactions become observable. Seminal knowledge has been gathered about the fundamentals of modern physics with charged particle storage rings.

A central theme in charged particles physics is the concept of 6-dimensional position-momentum space or in short: phase-space. Liouville's theorem [33] states that the phase-space density for a group of particles, i.e., the number of particles per unit volume and per unit momentum space, remains constant in the absence of dissipative forces. This has important consequences throughout.

Electrostatic and magnetostatic multipole lenses have been used for a long time to control the transverse motion of beams of neutral particles, for instance, to create a collimated beam or a beam focus. Inside these lenses a trapping potential well is created for the particles in the transverse direction. Bending such a lens around in a circle and connecting the exit of the lens to its entrance, creates a storage ring in which the neutral particles are transversely confined.

The first storage ring for neutral particles was a ring for thermal neutrons. The original design was based on a straight magnetic hexapole focuser that is bent into a circle, as proposed by Kügler et al. [34]. The interaction between the magnetic spin of the neutrons and the magnetic field leads to a force that confines the neutrons inside the ring. Experimental demonstration of this storage ring resulted in the direct measurement of the natural beta decay lifetime for free neutrons [35]. The second class of neutral particles to be confined in a ring were neutral polar molecules [36]. Shortly after this a miniaturized

magnetostatic storage ring for atoms has been realized as well [37].

In this thesis the experimental results of the first storage ring for neutral polar molecules are presented. A proposal for a storage ring for neutral molecules can already be found in a paper by Auerbach et al. in 1966 [38] although it is very likely that it has even been considered by those working with hexapole focusers before. In this paper [38] alternate-gradient focusing of molecular beams is discussed. This focusing technique is quite general as it is applicable to both high-field seeking and low-field seeking particles (*vide infra*). In practice this technique is difficult to implement as it requires electric field gradients that alternate at the right time and position. It is also shown in this paper, however, that under the right conditions circular motion can be exploited to store a beam of high-field seeking molecules in a static electric field. This type of motional stabilization has been used, for example, to guide a molecular beam around the inner electrode of a cylindrical capacitor [39–41].

In 1997, a design for an hexapole storage ring for low-field seeking neutral molecules was proposed [42]. A storage ring for low-field seeking molecules is easier to realize than a ring for high-field seeking molecules because Maxwell's equations only allow the existence of an electric field minimum in free space. The proposed design [42] is based on the design of the neutron storage ring mentioned before: electrode rods in a hexagonal configuration are bent round to create a torus. Applying appropriate voltages on the ring shaped electrodes creates an electric field that exerts the required centripetal force on the neutral dipolar molecules to confine them in circular orbits.

In the theoretical proposals for the storage ring for neutral molecules loading of the ring is considered using the low velocity tail of the thermal distribution of an effusive molecular beam. To capture a reasonable amount of molecules the ring must accept rather high velocities in that case. It would be highly advantageous to load the storage ring directly from a (pulsed) supersonic beam. This has the advantage that one can start with a high density package of molecules at low transverse temperatures (1 K) and at the lowest rotational and vibrational temperatures. The disadvantage is the high velocity in the laboratory frame, which is typically in the 300–2000 m/s range. The maximum attainable electric field strength then sets a limit on the minimum diameter of the ring, which scales with the square of the mean velocity of the injected molecules. In order to keep the ring compact, the molecules are decelerated in our experimental setup using the Stark deceleration scheme before they are injected into the ring. Subsequent improvements can be made to the injection beamline with the addition of devices for transverse and longitudinal focusing, which are also based on (time-varying) electric fields. With these improvements, more molecules at lower translational temperatures can be loaded in the storage ring.

The storage ring presented in this thesis can generally be used to confine polar neutral molecules. The advantage of a storage ring over a trap is that bunches of molecules in a ring can be made to interact repeatedly, at well

defined times and at distinct locations, with electromagnetic fields and/or other particles. This can be used, for instance, to study ultracold collisions and reactions [43, 44]. In such experiments, the effect of weak interactions can be enhanced by increasing the storage time in the ring, i.e., by accumulating weak effects during many round trips. A sectional version of a storage ring allows implementation of field-free interaction regions and various out-coupling regions. This yields unique opportunities for high-resolution molecular spectroscopy as well as for a large variety of collision studies. Different molecules can be stored simultaneously in the ring; slowly overtaking or counter-propagating bunches can be stored and used for collision studies. By incorporating a re-bunching element in the ring, the gradual spreading out of the package of molecules due to the velocity spread can be avoided and the stored molecules can be confined to the same region in phase-space over a time-period only limited by collisions with background gas. Optical access to the storage ring makes it feasible to use laser detection schemes to accurately determine where the molecules are in the ring at each given moment in time. If this is done in a non-intrusive manner, for instance via two-level laser-induced fluorescence or by detecting the change in refractive index when they pass through an optical cavity, this information can be used to actively correct the trajectories of individual molecules towards the ideal, circular orbit, thus increasing the phase-space density of the stored molecules [45]. This cooling method, known as stochastic cooling, has been successfully applied in storage rings for charged particles where it has been used to create high brightness beams of anti-protons [46].

Whenever any cooling scheme on molecules stored in the ring is proven to work (stochastic cooling, evaporative cooling, laser cooling on ro-vibrational transitions, cavity-mediated cooling [47]), the number of molecules in the ring can be increased by reloading of the ring. Such reloading might be a viable way of achieving phase-space densities of stored molecules that are sufficiently high to permit experimental study of molecular quantum-collective effects.

1.5 Outline

In Chapter 2, the concept of phase-space, Liouville's theorem and how this theorem affects the experiments described in this thesis are explained. After that, the motion of molecules in phase-space is described, phase-space matching is introduced and we discuss how nonlinearities lead to unwanted, irreversible perturbations in the phase-space distribution, hindering the phase-space matching. How the motion of polar molecules can be manipulated with (time-varying) electric fields is discussed in the last part of this Chapter. Hexapole focusing and Stark deceleration of a molecular beam are detailed. Effects of nonlinear forces on the motion of molecules in real space as well as in phase-space are discussed.

Chapter 3 starts with a theoretical description of the motion of molecules

in a storage ring. The design of the storage ring for neutral molecules is presented, including its theoretical possibilities and limitations. The molecular beam machine — injection beamline for the ring — is explained together with the detection scheme for the ammonia molecules that is used in the experiments. Finally, the experimental results obtained with a prototype storage ring are shown and discussed.

In Chapter 4 an improved injection beamline for the storage ring is described. A so-called buncher is inserted in the beamline to adjust the longitudinal phase-space distribution of the molecular beam. Furthermore, the beamline is upgraded with extra hexapoles to keep the molecular beam transversely together. It is experimentally demonstrated that it is possible with this buncher to longitudinally focus and cool a molecular beam.

The improved injection beamline is then used to inject molecules into the storage ring as described in Chapter 5. The hexapoles and buncher make it possible to load more molecules into the ring at lower translational (longitudinal) temperatures resulting in higher densities of the stored molecules.

In Chapter 6 the design of a sectional storage ring is presented. In such a storage ring a package of molecules can be kept together as buncher sections are part of the ring. These buncher sections will counteract the tangential spreading out of the package in the ring due to the forward velocity spread of the package of molecules. Calculations are performed to investigate the stability of a sectional storage ring and to find the right parameters for operation of the ring.

Chapter 2

Manipulating polar molecules in 6D phase-space

2.1 Liouville's theorem

In this Section the trajectories of particles moving in six dimensional position-momentum space, known as phase-space, are investigated. The Hamiltonian for a particle is given by $H(\mathbf{q}, \mathbf{p}, t)$, where $\mathbf{q}$ and $\mathbf{p}$ are the spatial coordinates and the canonical conjugated momentum coordinates, respectively, and t is the time. The Hamiltonian provides a complete description of the motion of a particle in phase-space and the equations of motion can generally be written as

$$\dot{\mathbf{q}} = \boldsymbol{\nabla}_p H, \tag{2.1}$$

$$\dot{\mathbf{p}} = -\boldsymbol{\nabla}_q H + \mathbf{Q}. \tag{2.2}$$

Here, $\mathbf{Q}$ is a force that is not derivable from a potential, such as frictional forces that depend on the velocity of the particle. $\boldsymbol{\nabla}_q$ and $\boldsymbol{\nabla}_p$ are the gradient operators for the three spatial coordinates and for the three momentum coordinates, respectively. For a large group of particles, a phase-space density function $\rho(\mathbf{q}, \mathbf{p}, t)$ is defined for the number of particles per unit volume in six dimensional phase-space. In order to know how the phase-space density and hence the motion of a group of particles evolves in time, it is useful to define a six dimensional current [48] for the motion of the ensemble of particles in phase-space by

$$\mathbf{J}_6 = (\rho \dot{\mathbf{q}}, \rho \dot{\mathbf{p}}), \tag{2.3}$$

where the dot implies the time derivative d/dt. The continuity equation for this current is then

$$\frac{\partial \rho}{\partial t} + \boldsymbol{\nabla}_6 \cdot \mathbf{J}_6 = 0 \tag{2.4}$$

with $\boldsymbol{\nabla}_6 = (\boldsymbol{\nabla}_q, \boldsymbol{\nabla}_p)$. The continuity equation just states that the rate of change of particles inside an arbitrary volume, V, is equal to the negative of the

total flux leaving that volume. Differentiating the second term in the continuity equation by parts yields

$$\boldsymbol{\nabla}_6 \cdot \mathbf{J}_6 = (\boldsymbol{\nabla}_q \rho) \cdot \dot{\mathbf{q}} + (\boldsymbol{\nabla}_p \rho) \cdot \dot{\mathbf{p}} + \rho (\boldsymbol{\nabla}_q \cdot \dot{\mathbf{q}} + \boldsymbol{\nabla}_p \cdot \dot{\mathbf{p}}). \tag{2.5}$$

The last term of this equation can be rewritten using Hamilton's equations (2.1, 2.2) resulting in

$$\boldsymbol{\nabla}_6 \cdot \mathbf{J}_6 = (\boldsymbol{\nabla}_q \rho) \cdot \dot{\mathbf{q}} + (\boldsymbol{\nabla}_p \rho) \cdot \dot{\mathbf{p}} + \rho (\boldsymbol{\nabla}_p \cdot \mathbf{Q}) . \tag{2.6}$$

Now, it is easy to see what happens to the time evolution of the phase-space density ρ. The total derivative of ρ with respect to time is

$$\frac{d\rho}{dt} = (\boldsymbol{\nabla}_q \rho) \cdot \dot{\mathbf{q}} + (\boldsymbol{\nabla}_p \rho) \cdot \dot{\mathbf{p}} + \frac{\partial \rho}{\partial t}. \tag{2.7}$$

Substituting Eq. (2.6) and using the continuity equation yields

$$\frac{d\rho}{dt} = -\rho (\boldsymbol{\nabla}_p \cdot \mathbf{Q}). \tag{2.8}$$

Hence, the time evolution of the phase-space density ρ depends on the non-Hamiltonian forces $\mathbf{Q}$. If these forces are not present or do not depend on the velocity, phase-space density remains constant:

$$\frac{d\rho}{dt} = 0. \tag{2.9}$$

This is Liouville's theorem [33]. It states that in the absence of dissipative forces, i.e., forces that depend on the velocity and that change the energy in the system, the phase-space density remains constant. This theorem implies that once you have a beam of particles, for instance a molecular beam, there is no way to increase or decrease the phase-space density of particles in the beam with conservative forces, i.e., forces that only depend on the position of the molecules. Two important properties of phase-space can be inferred from Liouville's theorem. First, different trajectories in phase-space do not intersect at any given instant of time. This is evident from the fact that in a Hamiltonian system the initial conditions and time uniquely determine the subsequent motion. Hence, if two trajectories crossed at a certain time, they would have the same position and momentum at that time and their subsequent motion would be identical. Second, a boundary B_1 in phase-space, which bounds a group of particles at time t_1 will transform into a boundary B_2 at time t_2, which bounds the same group of particles. This follows directly from the first property. As a consequence, the motion of a group of particles in phase-space can be calculated by tracking the boundary of that group in phase-space. In phase-space representation, the group of particles behaves as an incompressible fluid: the shape of the six dimensional volume can change but the volume itself can not.

This has major consequences for the molecular beam experiments described in this thesis. The phase-space density is defined during the supersonic expansion and can not be increased with forces generated by (time-varying) electric fields as these forces are not velocity dependent. The momentum spread, which is a measure for the translational temperature of the molecules in the beam, can be lowered ("cooling") but only at the expense of the number density. Liouville's theorem does not hold when dissipative forces act on the system of particles. In this case lowering the momentum spread, and hence the temperature, leads to real cooling as it is accompanied by an increase in phase-space density. A few of these real cooling schemes and their applicability to molecules are discussed in the next Section.

2.2   Cooling schemes

In laser cooling [49–51] atoms are cooled by many consecutive photon absorption-emission cycles leading to a significant momentum transfer from the photons of the laser beam to the atoms. In this cooling process the phase-space density is increased. The momentum transfer and thus the force on the atoms is velocity dependent due to the Doppler effect: an atom absorbs only those photons that match the Doppler shift. Unfortunately, laser cooling is not as amenable to molecules as it is to atoms due to the far more complex energy level structure of molecules.

In a cloud of trapped particles, thermodynamic equilibrium will be established by energy exchange in elastic collisions between the particles. At equilibrium, the energy distribution of the particles corresponds to the Maxwell-Boltzmann distribution. However, in a trap of finite depth, a certain fraction of the particles will have an energy larger than the trap depth and these particles will escape from the trap. Then, the particles left behind will establish a new thermodynamic equilibrium by means of elastic collisions but at a lower temperature, as the particles that left the trap had a higher energy than the average. This so-called evaporative cooling process strongly depends on the density of particles. At higher densities, a thermodynamic equilibrium is more quickly established. By gradually lowering the trap depth to allow particles with lower energy to escape, the evaporation process can be sustained until competing heating processes, such as inelastic collisions between particles or collisions with background gas, grow too large. The collisions between the particles gives the required velocity dependent 'force' and evaporative cooling can increase phase-space density considerably [52]. This is the final cooling step needed for the creation of atomic Bose-Einstein condensates. When sufficiently high densities are obtained in a dilute molecular gas with favorable collisional properties, evaporative cooling might be similarly rewarding for molecules.

An interesting alternative method for cooling, a method that does not rely on a velocity dependent force, is stochastic cooling [45]. Stochastic cooling is

used to increase the brightness of charged particle beams in storage rings [46]. Phase-space density is hereby increased without violating Liouville's theorem by realizing that Liouville's theorem only holds for an infinite number of particles, i.e., a continuous distribution. For a finite number of particles the density is not continuous in phase-space and one has a discrete distribution of point-like particles surrounded by empty space. In this case phase-space may be distorted such that individual particles are displaced towards the center of the distribution and the empty space is squeezed outwards. The momenta of the particles are hereby reduced (hence cooling) and the particle density is increased, leading to an increase in phase-space density near the center of the original volume. It must be noted that this is only valid in the classical regime where the individual particle wave packets are small compared to the separation between the particles in phase-space. In experimental implementations of stochastic cooling, the fluctuations in the average positions and momenta of particles are measured at a certain time. A feedback signal is then sent to a correction element that damps these fluctuations. Stochastic cooling has been applied very successfully in charged particles storage rings, where it enabled the discovery of the W-boson and Z-boson, communicators of the weak interaction. In 1984 S. van der Meer was awarded the Nobel prize for his invention and implementation of stochastic cooling. Recently, proposals to apply stochastic cooling to atoms using laser detection schemes for feedback control have been put forward [53, 54]. Similar schemes might be applicable to molecules as well.

It should be noted that in the description of the phase-space density function ρ and Liouville's theorem thus far, only the external degrees of freedom of a particle are taken into account. However, molecules also have many internal degrees of freedom. It is possible in principle to increase the external phase-space density, and thereby to lower the translational temperature, by decreasing the internal phase-space density [55]. One example of translational cooling by heating internal degrees of freedom is adiabatic demagnetization [56] in which energy is extracted from a sample by means of a change in magnetic field strength. Another way to increase the phase-space density is based on the fact that the potential energy of a neutral particle in a trap depends on the quantum state of that particle. A proposal has been put forward to accumulate NH molecules in a magnetic trap [57]. This can be accomplished by optically pumping the NH molecules from a non-trappable quantum state to a trappable quantum state via a uni-directional path using spontaneous emission from an intermediate state. Molecules already stored in the magnetic trap are not lost in this way and the phase-space density is hence increased.

2.3   Phase-space transformations

There are two important and general transformations in phase-space: translation and rotation. Translation corresponds to linear free flight of a particle
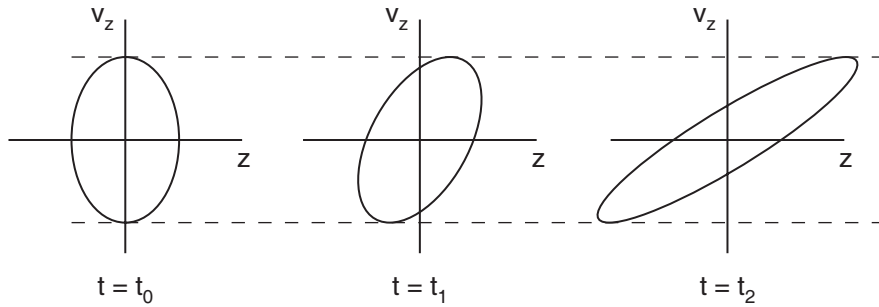
Figure 2.1: *Phase-space representation of free flight motion. Ellipses represent phase-space distributions in the z direction at $t = t_0$, $t = t_1$, and $t = t_2$ during free flight. The position spread grows but the velocity spread remains unchanged as does the area of the ellipse.*

in real space, while rotation corresponds to the situation when a linear force is applied to a particle. As both transformations are linear in nature, the transformation of the position and velocity coordinates in phase-space can be conveniently expressed in matrix notation.

In free flight there are no forces acting on the particles and therefore the velocity spread is constant. For free flight during a time t with velocity v_z along the z-axis the transformation of coordinates is given by

$$\begin{pmatrix} z_f \\ v_{z_f} \end{pmatrix} = \begin{pmatrix} 1 & t \\ 0 & 1 \end{pmatrix} \begin{pmatrix} z_i \\ v_{z_i} \end{pmatrix}, \tag{2.10}$$

where the subscripts i and f indicate the initial and final coordinates, respectively. A phase-space representation of free flight of a package of molecules is shown schematically in Fig. 2.1 for motion along the z-axis. At $t = t_0$, the boundary of the distribution of molecules in phase-space is indicated by an ellipse. Later, at $t = t_1$ the position spread is wider due to the velocity spread and the ellipse is tilted and stretched. At $t = t_2$, the ellipse is tilted and stretched even more. The area ('volume') of the ellipse remains constant in this process.

If a group of particles resides in an harmonic potential well then a linear force acts on the particles. The position of a particle in phase-space starts to rotate as long as the force is present. This leads to a change in both the positions and the momenta of the particles. For particles in an harmonic potential well the transformation of coordinates is given by

$$\begin{pmatrix} z_f \\ v_{z_f} \end{pmatrix} = \begin{pmatrix} \cos \omega t & \frac{1}{\omega} \sin \omega t \\ -\omega \sin \omega t & \cos \omega t \end{pmatrix} \begin{pmatrix} z_i \\ v_{z_i} \end{pmatrix}, \tag{2.11}$$

where the subscripts i and f denote the initial and final coordinates, respectively. In this case the molecules rotate at a constant angular frequency ω during
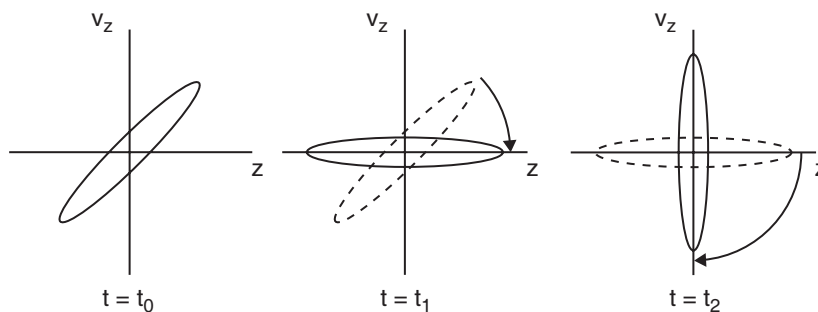
Figure 2.2: *Rotation in phase-space. Ellipses represent the phase-space distribution along one direction (z) at $t = t_0$, $t = t_1$, and $t = t_2$ during rotation in an harmonic potential well. The distribution rotates clockwise. The initial orientation of the distribution is shown at $t = t_0$. At $t = t_1$ the distribution is rotated such that the velocity spread is minimized. Rotating further ($t = t_2$) the distribution is such that the position spread is minimal.*

a time t and the rotation is uniform or isochronous for all molecules in the potential well and the shape of the phase-space distribution remains constant. Fig. 2.2 schematically shows this rotation of the distribution of molecules in phase-space. Phase-space rotations are conveniently used to minimize the velocity spread and hence to create a velocity focus, as shown in the figure at $t = t_1$. As the phase-space volume remains constant, the position spread increases in this process. Reducing the velocity spread is in fact reducing the translational temperature of the package of molecules but as the phase-space density is not increased, this is not 'real' cooling as opposed to the cooling schemes, mentioned in Section 2.2, where phase-space density is increased. If the phase-space distribution is rotated 90° further ($t = t_2$) then the position spread is minimized leading to a spatial focus. The velocity spread is thereby increased.

2.4 Nonlinearities in phase-space transformations

In practice, it is rather difficult to make perfectly linear transformations due to mechanical limitations and/or due to the nonlinear nature of the force acting on the particles. Although this does not lead to a real increase in phase-space volume, nonlinearities lead to an increase in *effective* phase-space volume. The effective phase-space volume is defined as the envelope that encloses all (trapped) particles in phase-space. This increase is irreversible and the original phase-space distribution cannot be retrieved.

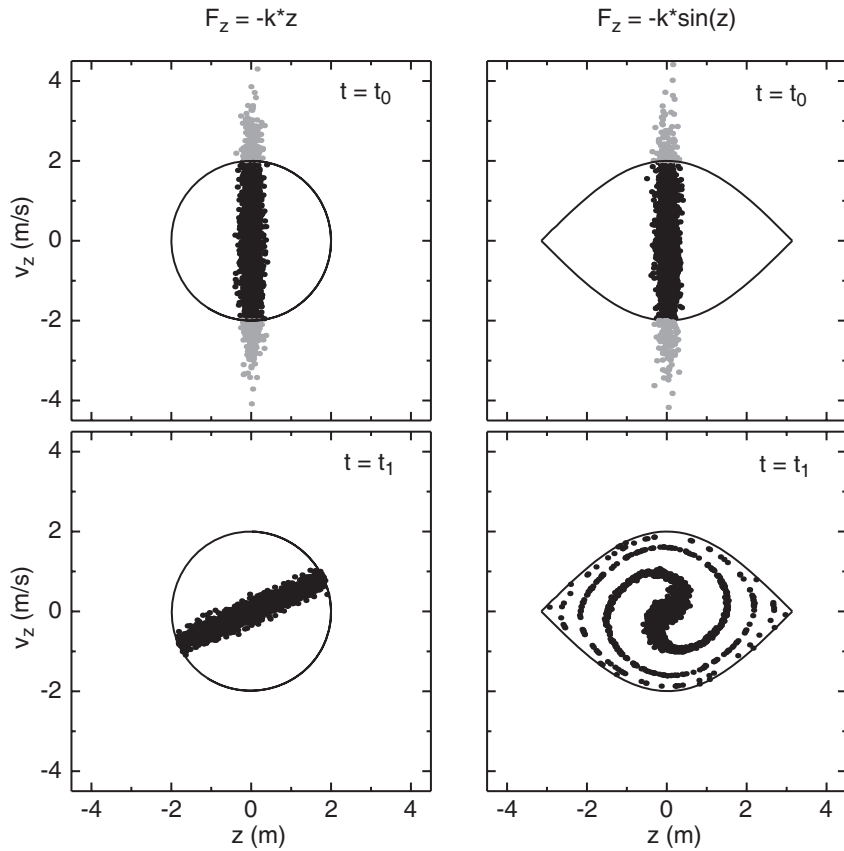In an anharmonic potential well, molecules near the edge of the well have

Figure 2.3: *Numerically calculated distributions of molecules in phase-space (z,v_z) at t_0 and at $t_1 > t_0$ for an harmonic potential well (left column) and for an anharmonic potential well (right column). The closed contours indicate the acceptances of the corresponding potential wells. The molecules that are not accepted by the potential wells are gray shaded.*

a different oscillation frequency from molecules near the bottom of the potential well. In phase-space the distribution therefore does not rotate uniformly but spirals as shown in the right column in Fig. 2.3. Eventually, the spiraling distribution will fill up the entire effective phase-space volume whose envelope is given by the acceptance. The acceptance is defined as the maximum phase-space volume that can be captured by a potential well. It must be noted that Liouville's theorem still applies and the phase-space volume that the molecules occupy is in principle still the same. However, due to the spiraling effect, the distribution in phase-space has been smeared out and is so sparse now that the effective phase-space volume is increased. As the number of trapped molecules in the potential well remains constant, the effective phase-space density is decreased. In an harmonic potential well on the other hand, all the molecules have the same oscillation frequency and the package of molecules rotates uni-

formly in phase-space. Here the spiraling does not occur and the envelope of the distribution in phase-space remains the same as shown in the left column in Fig. 2.3. Consequently, the effective phase-space density stays constant.

Clearly, the transformation needed for phase-space matching (next Section) should be as linear as possible in order to prevent filamentation processes as these decrease the effective phase-space density and frustrate phase-space matching; in practice this leads to a decrease in signal as fewer molecules can be transported and trapped.

2.5 Phase-space matching

In the experiments presented in this thesis, we want to load as many molecules as possible, at the highest possible density, and at the lowest possible temperature from the supersonic expansion into the storage ring, i.e., we want to get the highest possible phase-space density in the storage ring. The methods employed to load the ring use time-varying electric fields. Phase-space density cannot be increased with time-varying electric fields [55], and thus it is important to start with a source with a high initial phase-space density.

We start with a pulsed molecular beam created in a supersonic expansion. The initial package of molecules occupies a certain volume in phase-space. This initial phase-space volume of the molecular beam is called the emittance of the molecular beam. According to Liouville's theorem, the emittance is constant (in absence of dissipative forces) but the shape of the emittance or the boundary of the phase-space volume may change.

The injection beamline for the storage ring consists further of free-flight sections and sections that exert forces on the molecules. These forces arise from the interaction of the molecules with the electric field and as these forces are conservative they can be associated with potential wells. The equipotential lines of the potential well indicate the shape of the acceptance. The trajectories of the molecules that happen to be within the acceptance are closed orbits in phase-space and the molecules perform an oscillatory motion in real space as well as in momentum space. The phase-space volume occupied by the molecules at the exit of a certain section is the emittance of that section. Upon entering a section whose acceptance is smaller than the emittance of the previous section, the molecules outside the acceptance volume will be cut off and are lost from the beamline. Fig. 2.4 shows this cutoff of an arbitrary emittance by the acceptance of an arbitrary one-dimensional potential well. Besides a cutoff by the acceptance, the molecular beam can also be skimmed by physical apertures in the machine.

Not only the size but also the shape of the emittance at the exit of one beamline section must be mapped onto the shape of the acceptance of the next beamline section. This process is called phase-space matching [58]. The principle of phase-space matching is shown schematically in Fig. 2.5. An interposed
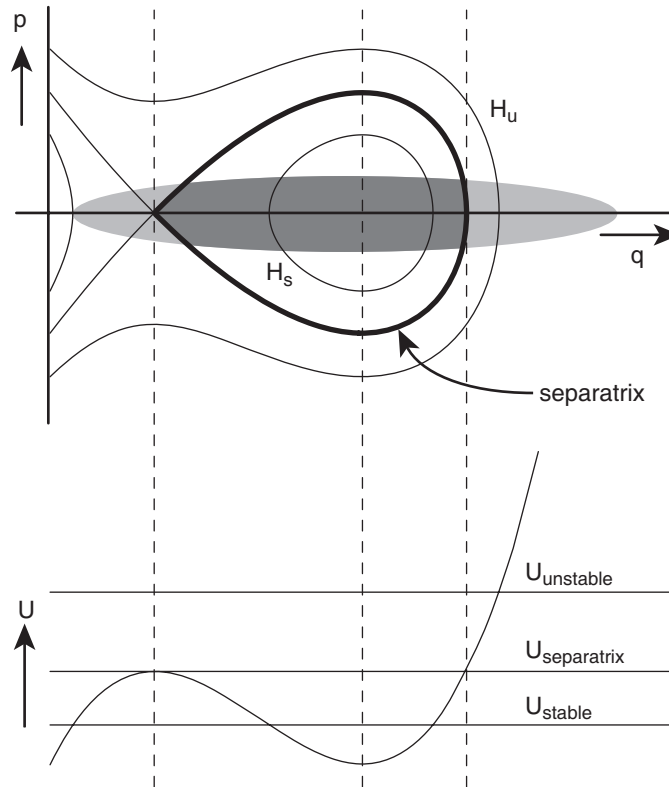
Figure 2.4: *The upper part of the figure shows the equipotential lines H in phase-space for an arbitrary one-dimensional potential well (shown below). The thick equipotential line is the separatrix: the boundary describing the acceptance of the potential well. The shaded ellipse represents the emittance of the incoming particles. The darker shaded area indicates the part of the emittance that is accepted by the potential well. The horizontal lines in the potential energy curve are the energy levels corresponding to (un)stable trajectories and trajectories on the separatrix in the phase-space plot.*

transformation section is necessary to transform the shape of the emittance at the exit of section A such that it fits the acceptance of section B. Phase-space matching is necessary to keep the phase-space density constant, especially in view of nonlinearities in potential wells. If the emittance is not properly matched onto the acceptance then filamentation of the phase-space distribution occurs and the effective phase-space volume becomes bigger. This is shown in Fig. 2.6(a). At $t = t_0$ particles with an elliptical phase-space distribution, the emittance, are coupled into a nonlinear potential well. It is immediately clear from this figure that the emittance does not match the acceptance of the potential well: both the shape of the emittance and its position in phase-space are wrong. The particles reside in the potential well until $t = t_1$ $(t_1 > t_0)$. Due to the phase-space mismatching and the nonlinearity of the potential well, fila-
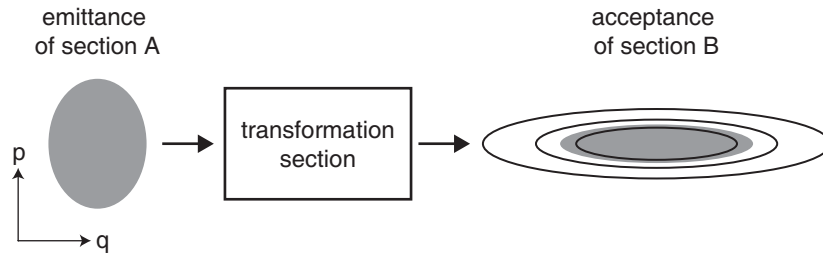
Figure 2.5: *Schematic representation of phase-space matching. The gray shaded emittance of section A is mapped onto the acceptance, or the equipotential lines, of section B using an interposed transformation section. Note that the volume in phase-space, i.e., the shaded area in this two dimensional plot remains constant under this transformation.*

(a) No phase-space matching

(b) Perfect phase-space matching
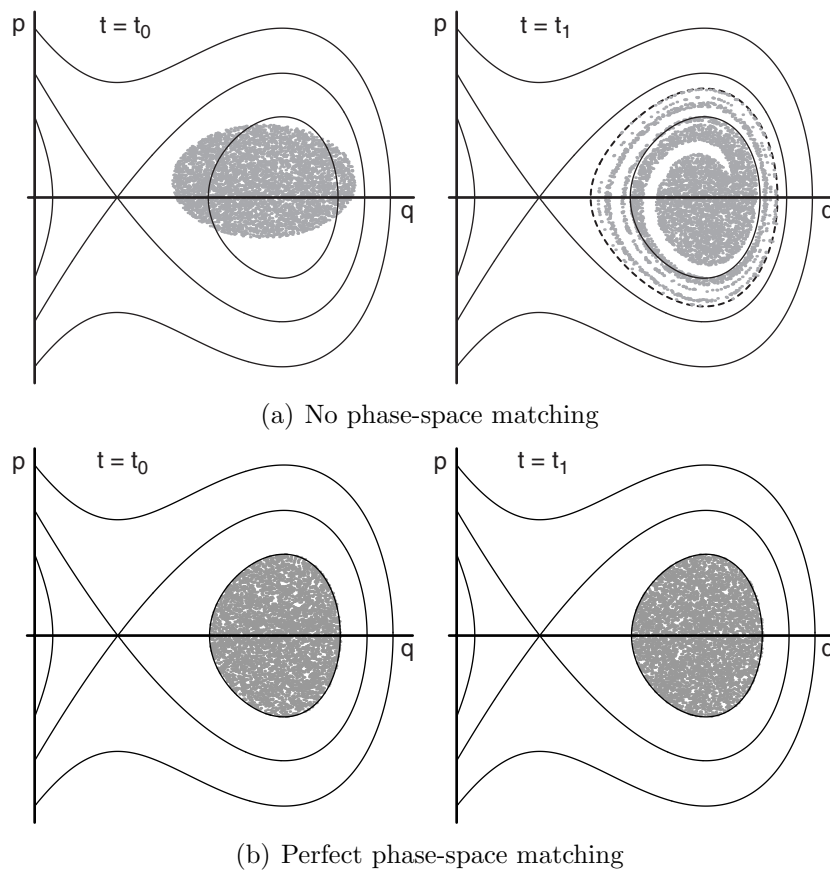
Figure 2.6: *Matching the emittance onto the acceptance of the potential well. No phase-space matching (a) and perfect phase-space matching (b).*

mentation occurs. This leads to an increase of the effective phase-space volume, which is indicated in the figure with the dashed contour line. Compared to the original phase-space volume, the effective phase-space volume is almost twice as large. This increase in effective phase-space volume does not occur when the emittance is properly matched onto the acceptance, as shown in Fig. 2.6(b). Here, the shape and position in phase-space of the elliptical phase-space distribution are altered with a transformation section, as schematically shown in Fig. 2.5, to match the acceptance of the potential well at $t = t_0$. In this process the volume, i.e., the area of the distribution, remains constant. Again, the particles reside in the potential until $t = t_1$. In this case, no filamentation occurs and the shape and volume of the phase-space distribution is unchanged: the effective phase-space density remains constant.

2.6   Polar molecules

2.6.1   Electric dipole moment

Neutral molecules are said to be polar and hence have an electric dipole moment when the (time-averaged) centers of positive charge density and negative charge density do not coincide [59].

Classically, the dipole of a molecule can be viewed as one positive point charge $+q$ and one negative point charge $-q$ separated by a distance a (Fig. 2.7). The electric dipole moment $\boldsymbol{\mu}$ is defined as $\boldsymbol{\mu} = q\mathbf{a}$, having a magnitude of $q|\mathbf{a}|$ and pointing from the negative charge towards the positive charge. In a uniform electric field there will be no net force on the dipole as the forces on the positive and negative charges exactly cancel. Only a torque $\mathbf{N} = \boldsymbol{\mu} \times \mathbf{E}$ will act on the dipole trying to orient it along the electric field lines. As soon as the dipole swings across the electric field lines, the torque changes sign and the dipole is forced to swing the other way. Due to the librational motion that the molecule thus performs along the electric field lines [60,61] we can adopt a time-averaged orientation of the dipole. The dipole spends most of its time at the turning points of the librating motion where the angular velocity changes sign. This means that the time-averaged orientation of the dipole can even be anti-parallel to the electric field.

2.6.2   Stark effect

In quantum mechanics the classical picture of the dipole of a molecule has to be adjusted. The point charges have to be replaced by charge density distributions and the orientation angles are quantized. When a neutral molecule with an electric dipole moment resides in an electric field, the (degenerate) zero-field energy levels of the molecule will split due to the interaction of the dipole moment with the electric field. This is called the Stark effect. In general, for
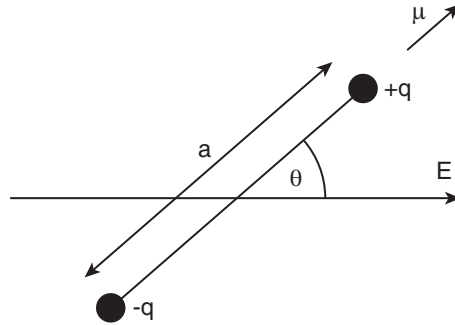
Figure 2.7: *Electric dipole q***a** *in an electric field* **E**. *The dipole moment points from the negative charge toward the positive charge and is at an angle θ with the electric field.*

an arbitrary charge distribution ρ in an external electrical potential $\varphi(\mathbf{r})$, the potential energy W is given by the volume integral

$$W = \int_V \rho(\mathbf{r})\varphi(\mathbf{r})dV. \tag{2.12}$$

Taking the origin to be the average of the centers of the positive and negative charge distributions, the potential $\varphi(\mathbf{r})$ can be written as a multipole expansion around $\mathbf{r} = 0$ [62]:

$$\varphi(\mathbf{r}) = \varphi_0 + \mathbf{r} \cdot (\boldsymbol{\nabla}\varphi)_0 + \ldots \tag{2.13}$$

If the potential is nearly constant over a distance comparable with the size of the molecule, the higher order terms in the multipole expansion can be neglected[1]. Inserting this multipole expansion back into Eq. (2.12) yields the potential energy as

$$W = q\varphi(0) - \boldsymbol{\mu} \cdot \mathbf{E}(0). \tag{2.14}$$

Here, $\varphi(0)$ and $\mathbf{E}(0)$ are the potential and electric field at $\mathbf{r} = 0$, respectively, $q = \int \rho(\mathbf{r})dV$ is the monopole term, and $\boldsymbol{\mu} = \int \mathbf{r}\rho(\mathbf{r})dV$ is the dipole term of the multipole expansion. The first term of Eq. (2.14) is the potential energy of the total charge of the molecule in the electric potential. This term is zero for a neutral molecule. The second term is the potential energy of a dipole in an electric field. For a polar molecule, having a dipole moment, this term is nonzero and hence the molecule's potential energy will change with an amount that depends on the orientation of the dipole in the electric field. This second term in the potential energy expansion is the Stark energy

$$W_{Stark} = -\boldsymbol{\mu} \cdot \mathbf{E}. \tag{2.15}$$

---

[1]Higher order terms such as the quadrupole term, which interacts with the electric field gradient, are of particular interest for nuclear physics as atomic nuclei can possess quadrupole moments and their magnitudes and signs reflect the nature of the forces between neutrons and protons, as well as the shapes of the nuclei themselves [62].
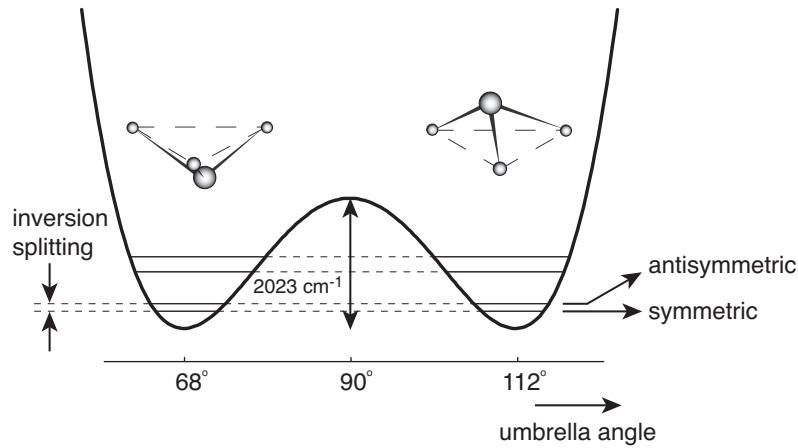
Figure 2.8: *Potential energy of the ν_2 (umbrella) mode of ammonia. The energy splitting between the two lowest levels is 0.053 cm^{-1} for deuterated ammonia.*

As we have used an arbitrary charge distribution in the derivation, this expression is of course also valid for the potential energy of a classical dipole consisting of point charges.

Quantum mechanically the (time-averaged) orientation of the dipole with respect to the electric field cannot take an arbitrary value anymore due to space quantization. Only discrete orientations are allowed that, in case of a symmetric top molecule, depend on the total angular momentum **J**, its projection M on the space fixed axis defined by the electric field direction, and its projection K on the molecular symmetry axis.

2.6.3   Stark effect in deuterated ammonia

For the experiments described in this thesis an isotopomer of ammonia, $^{14}ND_3$, is used as a test molecule. Ammonia is the textbook example of a molecule with fluxional behavior: the molecule rapidly inverts its tetrahedral geometry when all the hydrogen atoms tunnel from one side of the nitrogen atom to the other side. The energy barrier associated with this tunneling motion is shown in Fig. 2.8. The horizontal lines indicate the levels of the ν_2 umbrella vibration of ammonia where the two lowest levels correspond to $\nu_2 = 0$ and $\nu_2 = 1$ for the case of a single potential well (barrier is absent). Due to the finite barrier height, the levels are split into a symmetric level and an antisymmetric level and the energy difference between these two levels, the inversion splitting W_{inv}, is 0.053 cm^{-1} for $^{14}ND_3$ [63]. The inversion splitting for normal ammonia, $^{14}NH_3$, is 0.79 cm^{-1} [64]. The magnitude of the inversion splitting is important because it affects the linearity of the Stark effect as will be discussed at length later. In the experiments described in this thesis a beam of deuterated ammonia is formed

in a supersonic expansion. Because of the adiabatic cooling in the expansion, only the lowest rotational levels of the vibronic ground state are populated and about 60% of all $^{14}ND_3$ molecules reside in the $|J, K\rangle = |1, 1\rangle$ level which is the ground state level of para-ammonia[2].

The Stark shifted energy levels are found by calculating the eigenvalues of the Stark Hamiltonian $H_{Stark} = -\boldsymbol{\mu} \cdot \mathbf{E}$. As the Stark shift is small compared to the vibrational and electronic energies in a molecule, only the rotational part of the molecular wave function has to be taken into account. For symmetric tops, such as ammonia, a full basis set of rotational wave functions is given by the rigid rotor wave functions $|J, K, M\rangle$ [66]. The Stark operator has odd parity, so it is convenient to use a basis of rotational eigenfunctions with a definite parity by creating linear combinations of the rigid rotor wave functions $|J, K, M\rangle$:

$$|J, K, M, \pm\rangle = \frac{1}{\sqrt{2}}\Big(|J, K, M\rangle \pm |J, -K, M\rangle\Big). \quad (2.16)$$

The only nonzero matrix elements of H_{Stark} are then given by [67]

$$\langle J, K, M \pm |H_{Stark}|J, K, M \mp\rangle = -\mu|\mathbf{E}|\frac{|MK|}{J(J+1)}, \quad (2.17)$$

$$\langle J, K, M \pm |H_{Stark}|J+1, K, M \pm\rangle =$$
$$-\frac{\mu|\mathbf{E}|}{J+1}\sqrt{\frac{((J+1)^2 - K^2)((J+1)^2 - M^2)}{(2J+1)(2J+3)}}, \quad (2.18)$$

with $|\mathbf{E}|$ the absolute electric field strength and μ the permanent electric dipole moment. At low electric field strengths and for molecules with a large separation of rotational energy levels, the first term, Eq. (2.17), dominates. In first order perturbation theory the Stark shift W_{Stark} of ammonia including the zero-field inversion splitting is given by

$$W_{Stark} = \pm\sqrt{\left(\frac{W_{inv}}{2}\right)^2 + \left(-\mu|\mathbf{E}|\frac{MK}{J(J+1)}\right)^2}, \quad (2.19)$$

where the electric dipole moment of $^{14}ND_3$ is $\mu = 1.497$ D (Debye units) [68]. It is clear from this expression that at low electric fields, the inversion splitting gives rise to a quadratic dependence of the Stark shift on the applied electric field. The choice of $^{14}ND_3$ over $^{14}NH_3$ is made because the magnitude of the inversion splitting is significantly reduced upon deuteration. This leads to a

---

[2]Deuterated ammonia, $^{14}ND_3$, is a boson [63] and the Pauli exclusion principle demands that the total wave function including the nuclear spin has to be symmetric if two deuterium atoms are interchanged. Levels with nuclear spin wave functions of E symmetry are denoted para-ammonia while levels with A_1 or A_2 symmetry are denoted ortho-ammonia [65].
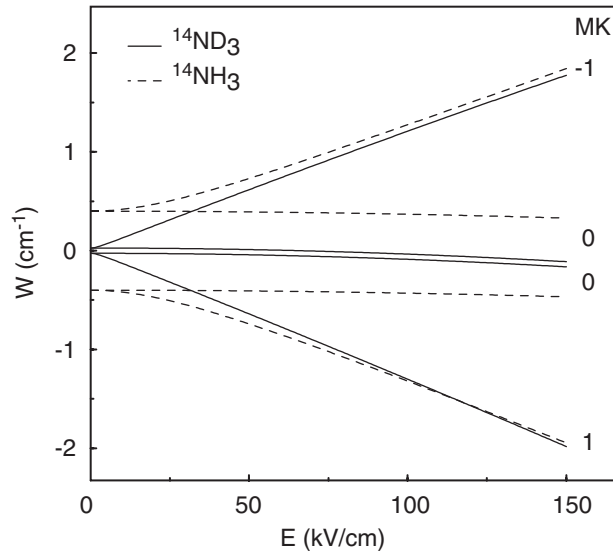
Figure 2.9: *Stark shift of* $^{14}ND_3$ *and* $^{14}NH_3$ *shown for electric fields up to 150 kV/cm.*

more linear Stark effect, and therefore to fewer nonlinearities, in the range of electric fields used in the experiments. In addition, the kinetic energy that can be extracted from an ammonia molecule per electric field section in the Stark decelerator is larger for $^{14}ND_3$ than for $^{14}NH_3$ due to this decreased inversion splitting, as will be discussed later.

At higher electric field strengths and/or for heavier molecules with a closer spacing of rotational levels different J-levels will start to mix and off-diagonal terms in the Stark matrix, Eq. (2.18), which couple different J-levels, have to be taken into account. Fig. 2.9 shows the Stark shift of $^{14}ND_3$ for the $|J, K\rangle = |1, 1\rangle$ state. Coupling up to $J = 7$ is taken into account. It is clear from this figure that for electric field strengths above 2 kV/cm and below 100 kV/cm the Stark shift is almost linear. For reference, the Stark shift of $^{14}NH_3$ is plotted as well (dashed lines). This plot shows that upon deuteration the magnitude of the Stark shift is increased and that the linearity of the Stark shift in the region below 50 kV/cm is greatly improved. The hyperfine splitting due to the coupling of the total angular momentum **J** with the nuclear spins of the nitrogen and the deuterium (hydrogen) nuclei is neglected in this calculation as it is much smaller than the Stark shift for the electric fields used in the experiments. Nevertheless, due to this coupling there are many hyperfine levels present. For instance, the $|J, K\rangle = |1, 1\rangle$ low-field seeking state of $^{14}ND_3$ consists of 48 separate hyperfine components in an electric field [63].

Molecules with a positive Stark shift, i.e., molecules whose Stark energy increases with increasing electric field strength as indicated by the positive sign

in Eq. (2.19), move to lower electric fields in order to lower their potential energy. These molecules are therefore referred to as low-field seekers. Molecules with a negative Stark shift, i.e., molecules whose Stark energy decreases with increasing electric field strength, move to higher electric fields in order to lower their potential energy. These molecules are therefore referred to as high-field seekers.

2.7 Force on a polar molecule

The Stark energy that a molecule acquires in an electric field, is the potential energy of that molecule in the electric field. Using Hamilton's equation of motion, Eq. (2.2), the force that a molecule experiences can easily be derived and one finds, in the absence of dissipative forces or any other forces that cannot be derived from a potential, that the force on the molecule at a point $\mathbf{r}$ is given by the gradient of the Stark energy in that point:

$$
\begin{align}
\mathbf{F}(\mathbf{r}) &= -\boldsymbol{\nabla} W_{Stark}(\mathbf{r}) \tag{2.20}\\
&= \underbrace{-\left(\frac{\partial W_{Stark}}{\partial E}\right)}_{\mu_{eff}} \boldsymbol{\nabla}|\mathbf{E}(\mathbf{r})|. \tag{2.21}
\end{align}
$$

Here, $-\partial W_{Stark}/\partial E$ can be regared as the effective electric dipole moment μ_{eff}. The angle θ between the dipole moment vector and the electric field vector, which depends on the quantum state of the molecule, is included in this effective dipole moment. The molecule will only experience a force when the electric field is inhomogeneous: $\boldsymbol{\nabla}|\mathbf{E}(\mathbf{r})| \neq 0$. The force does not depend on the direction of the electric field but solely on the magnitude of the electric field $|\mathbf{E}(\mathbf{r})|$ and on the quantum state of the molecule. Therefore, molecules, if in the right quantum state, can be confined in a static electric field geometry with zero electric field strength in the center and with increasing electric field strength in all three directions. This is fundamentally different from charged particles. For charged particles Earnshaw's theorem applies, which states that it is not possible to trap a particle with charge q with purely static electric fields. This is a direct consequence of Maxwell's equations which state that there can be no restoring forces in all three directions at once: $\boldsymbol{\nabla} \cdot \mathbf{F} = q\boldsymbol{\nabla} \cdot \mathbf{E} = 0$.

2.7.1 Focusing a beam of polar molecules

In this Section it is shown that electric multipole fields and in particular the hexapole field are convenient means with which to focus molecular beams of low-field seekers. Electrostatic focusing was developed independently by Gordon, Zieger, and Townes [69] and by Bennewitz, Paul, and Schlier [70]. An electrostatic multipole focuser consists of a number of rods placed equidistantly

on the outside of a circle. The rods are alternately at ground potential and at high voltage (voltage difference V), creating a cylindrically symmetric electric field whose magnitude is zero at the centerline on the symmetry axis. The multipole focuser is placed such that the molecular beam axis and the symmetry axis of the multipole focuser coincide. Molecules in low-field seeking states will then experience a force towards the beam axis. Focusing a beam of high-field seekers is more difficult as Maxwell's equations forbid the existence of a global electric field maximum in free space. It is possible however, to create an electric field with a saddle point, having a maximum electric field in one direction and a minimum in the orthogonal direction. By alternating the orientation of such fields appropriately, an average focusing force can be achieved in both directions. This so-called alternate gradient (AG) focusing technique was first proposed and implemented for charged particles, which are natural high-field seekers [30]. Later, AG-focusing was proposed to focus a beam of neutral molecules [38] which was soon afterwards experimentally demonstrated [71].

The electric potential of a multipole configuration obeys the Laplace equation in absence of any free charges. It can be derived by recognizing that because the multipole potential does not depend on the coordinate along the molecular beam axis z, any complex analytical function $f(\zeta) = \phi(x, y) + i\psi(x, y)$, $\zeta = x + iy$ can be used to describe the equipotential lines. Generally, a $2n$-pole configuration can be derived from the complex function

$$f(\zeta) = A\zeta^n \tag{2.22}$$

with n a positive integer and $A = V/2R^n$, a constant that depends on the voltage difference V between two adjacent electrodes of the multipole and on the inner radius R of the multipole. The real part of $f(\zeta)$, $\phi(x, y)$, defines the equipotential lines of normal multipoles whereas the imaginary part, $\psi(x, y)$, defines the equipotential lines of skew multipoles. The skew multipoles are rotated around the symmetry axis over an angle $2\pi/4n$ with respect to the normal multipoles. As the electrode surfaces of a physical multipole are in fact equipotential surfaces, the functions $\phi(x, y)$ and $\psi(x, y)$ give the physical shape of the electrodes, which is hyperbolic in nature.

The equipotential lines for an ideal hexapole are given for $n = 3$:

$$f(\zeta) = \underbrace{A\left(x^3 - 3xy^2\right)}_{\phi(x,y)} + i\underbrace{A\left(3x^2y - y^3\right)}_{\psi(x,y)} \tag{2.23}$$

The electric fields of the normal hexapole and skew hexapole can be calculated by taking the gradient of the potentials $\phi(x, y)$ and $\psi(x, y)$, respectively. The magnitude of the electric field $|\mathbf{E}|$ is in both cases the same and as it depends solely on the radial distance from the axis of the hexapole, r, the direction of the electric field points in the radial direction:

$$\mathbf{E} = 3A(x^2 + y^2)\hat{\mathbf{r}} = \frac{3V}{2R^3}r^2\,\hat{\mathbf{r}} \tag{2.24}$$

25

From Eq. (2.17) and Eq. (2.24) it is clear that an hexapole is the ideal focuser for molecules having only a first order Stark effect. As the electric field and hence the Stark energy increases quadratically in r, the force on the molecules will be harmonic and molecules coming from a point are focused again into a point. As the electric field in a $2n$-pole focuser depends on r like $|\mathbf{E}| \propto r^{n-1}$, molecules with a quadratic Stark effect are better served with a quadrupole focuser.

For deuterated ammonia the harmonic force is slightly perturbed due to the zero field inversion splitting. The force exerted by the hexapole electric field on an ammonia molecule is calculated by inserting Eq. (2.24) into Eq. (2.19) and then applying Eq. (2.21):

$$\mathbf{F} = -\boldsymbol{\nabla}\left[\pm\sqrt{\left(\frac{W_{inv}}{2}\right)^2 + \left(\frac{1}{2}kr^2\right)^2}\right] \tag{2.25}$$

$$= \mp\frac{k^2 r^3\,\hat{\mathbf{r}}}{\sqrt{W_{inv}^2 + k^2 r^4}} \tag{2.26}$$

$$= \mp\frac{kr\,\hat{\mathbf{r}}}{\sqrt{1 + \left(\frac{W_{inv}}{kr^2}\right)^2}}. \tag{2.27}$$

The upper sign corresponds here to low-field seeking states and the lower sign corresponds to high-field seeking states. In these equations k is the harmonic force constant given by

$$k = \mu\frac{3V}{R^3}\frac{|MK|}{J(J+1)}. \tag{2.28}$$

It is obvious from Eq. (2.27) that when the magnitude of the inversion splitting would be zero, the molecule would experience a perfect harmonic force with an angular frequency given by $\omega = \sqrt{k/m}$. The inversion splitting leads to a reduction of the force near the hexapole axis compared to the situation without inversion splitting. Molecules flying closest to the hexapole axis are affected the most by this and are focused less than molecules flying further off-axis.

For an ideal hexapole the hyperbolic surfaces of the electrodes would nearly touch at large radii, leading to electrical discharges when a high voltage difference is applied between adjacent electrodes. To prevent this, and for ease of manufacturing, the electrodes are commonly approximated with cylindrical rods.

The hexapoles that are used in the experiments described in this thesis are composed of six cylindrical rods equidistantly placed on the outside of a circle with radius R. In most experiments a voltage difference of 10 kV is applied to adjacent hexapole rods. The rods have a radius of $R/2$, following Reuss in [3]. The electric field of the approximated hexapole geometry and the ideal hexapole field are shown in Fig. 2.10(a) and Fig. 2.10(b), respectively. The field in the approximated hexapole geometry is calculated using a finite element
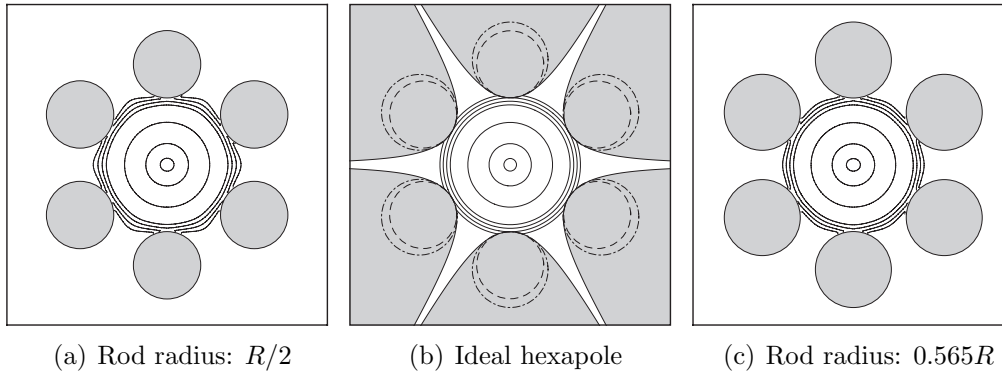
(a) Rod radius: $R/2$ (b) Ideal hexapole   (c) Rod radius: $0.565R$

Figure 2.10: *Lines of equal electric field strength in three different hexapole configurations. In all geometries the inner radius R is 3 mm and the potential on the electrodes is alternately at +10 kV and -10 kV. The lines of equal electric field strength are from the inside out: 1, 10, 40, 80, 90, 100, and 110 kV/cm. (a) Approximated hexapole with a radius of the rods equal to R/2. (b) Ideal hexapole with hyperbolic electrodes. (c) Approximated hexapole with a radius of the rods equal to 0.565R. The contours of the rods in (a,c) are shown in the ideal hexapole geometry (b) as well.*

program [72]. The ideal field is calculated using Eq. (2.24). The contour lines of the electric field in our hexapole geometry show a hexagonal perturbation close to the electrodes. This deviation from the cylindrical symmetry has been experimentally observed in two-dimensional imaging experiments [73].

A better approximation of the ideal hexapole field can be obtained for a rod radius of $0.565R$, as recommended by Anderson [74]. The contour lines of the electric field in the hexapole geometry as suggested by Anderson are more circular close to the electrodes, as shown in Fig. 2.10(c). This becomes clearer if one looks at the difference between the ideal field and the approximated fields. In Fig. 2.11 this difference is shown as a function of radial position r along the dashed lines indicated in the hexapole cross sections. It is seen from the figure that for $r > 0.5R$ the hexapole geometry as proposed by Reuss deviates more from the ideal field than the geometry proposed by Anderson. The latter one is also less dependent on the angular coordinate as the difference curves are similar in the 0° and 30° plots. This is also reflected in the more circular electric field contour lines in Fig. 2.10(c). For a radial position r close to the hexapole inner radius R, both approximated geometries deviate strongly from the ideal hexapole geometry. The small dip in the 0°-plot around $r = 0$ is an artefact of the finite element calculation. A calculation with more grid points should resolve this but a more powerful computer is needed for that. For future experiments it might be better to use the hexapole geometry as proposed by Anderson because it approximates the ideal hexapole field better. One has to
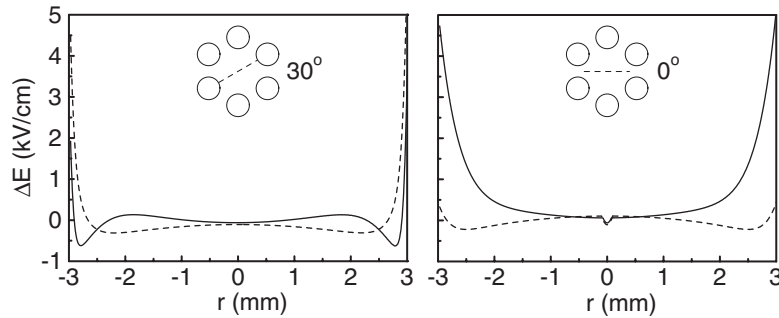
Figure 2.11: *Electric field differences between the ideal hexapole field and the fields of the approximated geometries as proposed by Reuss (solid line) and by Anderson (dashed line) are plotted as a function of the radial position r. Same hexapole settings are used as in Fig. 2.10. The differences are shown for two different cuts through the hexapole: 0° and 30°.*

take into account, however, that due to the larger radius of the rods the smallest distance between two adjacent electrodes is $0.435R$ compared to $0.5R$ for the geometry as proposed by Reuss. Hence, for the same voltage settings discharges are likelier to occur in the geometry as proposed by Anderson. If one wants to use a rod radius of $R/2$ then the effects due to the not cylindrically symmetrical fields close to the hexapole rods can largely be avoided by making the hexapole radius R sufficiently large and the voltages on the electrodes sufficiently high.

To visualize the operation of the hexapole the equations of motion for molecules flying through the hexapole have been solved and their trajectories have been calculated. Edge effects at the hexapole entrance and exit are neglected in the calculations. This is allowed as the hexapoles that are used are long compared to the length of the package of molecules and as they are rapidly switched on and off when the package of molecules is completely inside. In this case all the molecules experience a force during an equal time and 'chromatic aberration' of the hexapole lens is avoided.

The trajectories of a few $^{14}ND_3$ molecules flying through an ideal hexapole oriented along the z-axis are numerically calculated and shown in Fig. 2.12. The molecules are assumed to originate from a single point. The values of the molecular and hexapole parameters that have been used for these calculations are given in Table 2.1 and are taken from the experiment. The force constant of the (ideal) hexapole is $k = 0.14$ cm^{-1}/mm^2 and the corresponding rotation frequency in phase-space is $\omega/2\pi = 1450$ Hz. In the left figure the inversion splitting is set to zero and the molecular beam that is originating from a single point is focused into a single point again. The right figure demonstrates the effect of nonlinearities in the equations of motion resulting from a nonzero value of the inversion splitting. The trajectories in this figure show that molecules with inversion splitting moving close to the hexapole axis are less well focused

$|J, K\rangle$	$|1, 1\rangle$
μ	1.497 D
W_{inv}	0.053 cm^{-1}
velocity v_z	91.8 m/s
inner radius hexapole R	3 mm
voltage difference V	10 kV
mass, m	20 amu

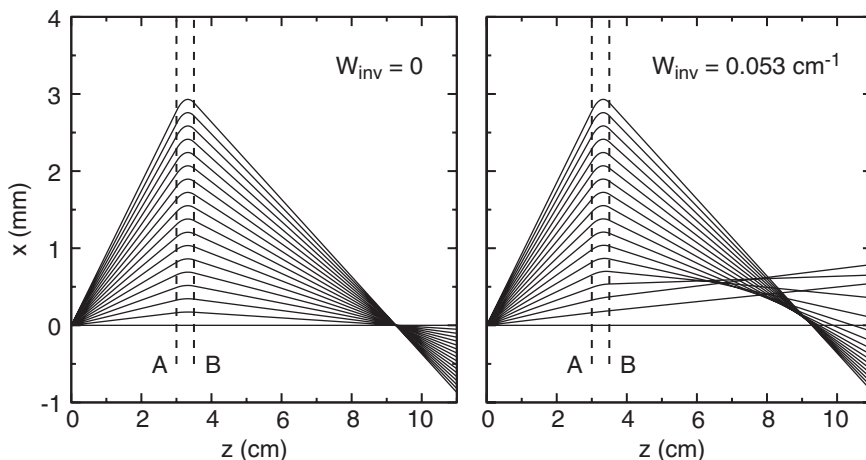**Table 2.1:** *Parameters used for trajectory calculations through the hexapole.*

Figure 2.12: *Trajectories of ^{14}ND$_3$ molecules flying through an hexapole with z along the molecular beam axis and x perpendicular to the beam axis. Curves are calculated for molecules without (left) and with (right) inversion splitting. It is assumed that all molecules start in one point and fly freely towards the hexapole which is assumed to be ideal. The hexapole is switched on when the molecules are at position A and switched off when the molecules are at position B. The field is on for a duration of 54 μs. A voltage difference of 10 kV is put between adjacent rods ($R = 3$ mm). The molecular package is completely inside the hexapole when the field is applied. After the hexapole is switched off, the molecules continue in free flight.*

than molecules that have no inversion splitting. The inversion splitting blurs the focus of the molecular beam: the sharp point like focus changes into a ring-shaped focus (cylindrically symmetric around the hexapole axis). This has been experimentally observed in two-dimensional imaging experiments [73]. The effect is similar to the spherical aberration caused by optical lenses that leads to caustics. The nonlinearity introduced by the inversion splitting leads to filamentation of the phase-space distribution in the transverse direction and hence to an increase in effective phase-space volume as shown in Fig. 2.13. Numerically

29
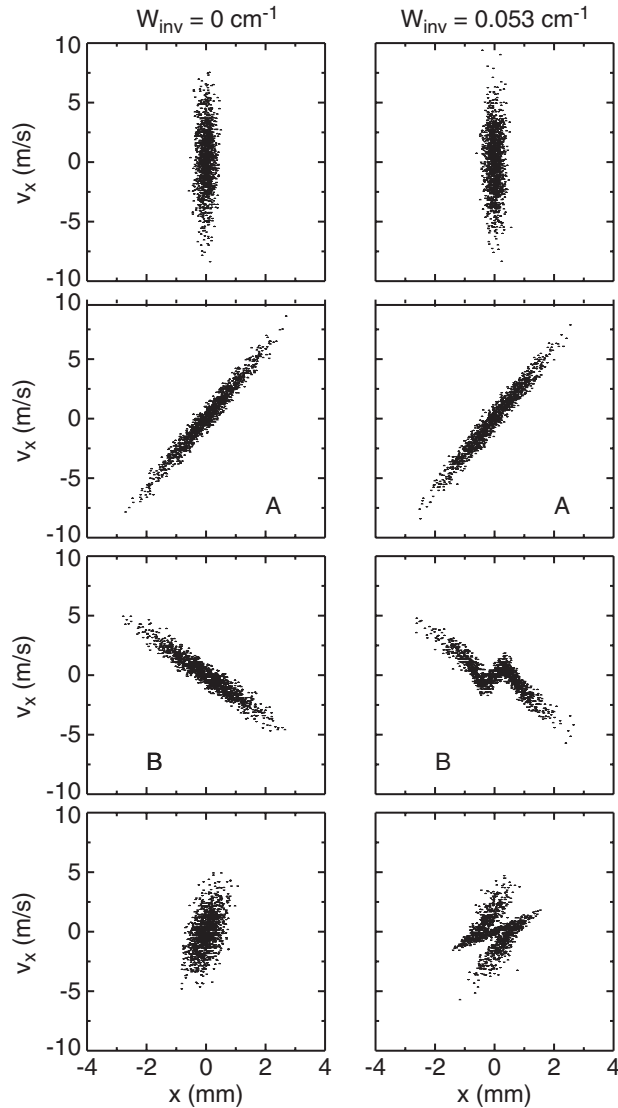
Figure 2.13: *Phase-space plots in the transverse direction for a distribution of molecules flying through an ideal hexapole. The left column shows the phase-space plots without inversion splitting and the right column shows them with inversion splitting. The upper row shows the initial distribution at $z = 0$. Full widths at half maximum are $\Delta x = 0.4$ mm and $\Delta v_x = 6$ m/s. The second row shows the distribution after free flight to the hexapole (position A in Fig. 2.12). The third row shows the distribution in phase-space after passing through the hexapole (position B in Fig. 2.12). Finally, the fourth row shows the distribution near the focus of the hexapole.*

calculated transverse phase-space distributions are shown at four different positions along the beam axis (z-axis). From top to bottom: at $z = 0$, at the moment when the hexapole is switched on (position A), at the moment when the hexapole is switched off (position B), and near the focus of the molecular beam (at $z \approx 0.093$ m). Calculations are shown for molecules *without* (left column) and *with* (right column) inversion splitting. Due to the inversion splitting, the force near the hexapole axis is weaker and hence the rotation frequency in phase-space is lower. This leads to a spiraling of the phase-space distribution: molecules further off-axis rotate faster than molecules close to the hexapole axis. As the calculation was done in one direction (x) the spiraling effect is rather pronounced. The effect is less pronounced when the calculation is performed in three dimensions as most molecules in the distribution then reside off-axis. The filamentation of the phase-space distribution leads to an increase in effective phase-space volume. The phase-space transformation by the hexapole is hence imperfect and results in less than ideal phase-space matching conditions.

2.7.2 Decelerating polar molecules

As discussed in the previous Section the transverse motion of molecules in a beam can readily be manipulated with static inhomogeneous electric multipole fields. These multipole lenses have a minimum field strength on the molecular beam axis and increase radially outwards. Inhomogeneous electric fields can also be used to manipulate the longitudinal motion of the molecules. When molecules in a low-field seeking state enter a region of high electric field, they will gain Stark energy. This gain in Stark energy is compensated by a loss in kinetic energy. If the electric field is greatly reduced before the molecules have left this region, the molecules will not regain the lost kinetic energy and continue their motion at their instantaneous (reduced) velocities. The maximum amount of kinetic energy that can be taken out of a molecule depends on its Stark shift at the maximum obtainable electric field strength. For $^{14}ND_3$ molecules in the low-field seeking $|1,1\rangle$ state the Stark shift in an electric field of 100 kV/cm is 1.2 cm^{-1}. The Stark shift of $^{14}NH_3$ molecules in the same state and electric field is only 0.9 cm^{-1}. The kinetic energy of a molecule in a supersonic beam is typically on the order of 100 cm^{-1}. So in order to make a significant change in kinetic energy, this deceleration process needs to be repeated by letting the molecules pass through an array of inhomogeneous electric field stages, that are switched synchronously with the arrival time of the decelerating package of molecules [5]. This process is referred to as Stark deceleration and the array of electric field stages is accordingly referred to as a Stark decelerator. As already mentioned in Chapter 1 Stark deceleration of neutral molecules shows a great resemblance to the acceleration of charged particles in linear accelerators. The Stark deceleration technique has been extensively described elsewhere [65, 75]. Here, the basic operation principle is briefly described, focusing mainly on the longitudinal motion of the molecules in the Stark decelerator as this is also
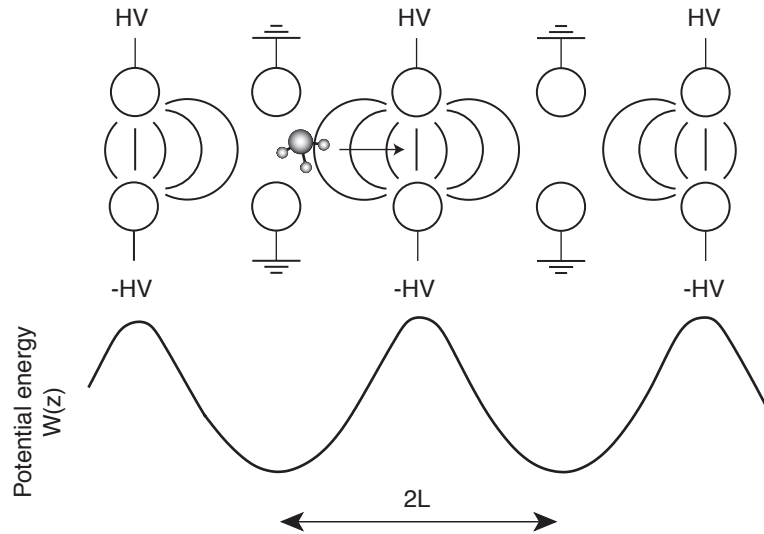
Figure 2.14: *Array of electric field stages. Each stage consists of two parallel cylindrical rods. The potential energy of a $^{14}ND_3$ molecule in the $|1, 1\rangle$ low-field seeking state is shown below as a function of the position z along the molecular beam axis.*

important for the working of the buncher as described in Chapter 4.

The Stark decelerator consists of an array of electric field stages as schematically depicted in Fig. 2.14. Each stage consists of two parallel cylindrical metal rods with radius r and centered a distance $2r + d$ apart. The experimental values for r and d are 1.5 mm and 2 mm, respectively. The distance L between two adjacent stages is 5.5 mm. One of the rods is connected to a positive and the other to a negative switchable high voltage power supply. Alternating stages are connected to each other. The strength of the electric field created by the high voltages on the electrodes is higher near the electrodes than on the molecular beam axis. Therefore, molecules in a low-field seeking state will be focused towards the beam axis. This focusing occurs only in the direction perpendicular to the electrodes; in the direction parallel to the electrodes there is practically no focusing. To achieve a net focusing effect in both transverse directions throughout the Stark decelerator, the electric field stages are alternately oriented vertically and horizontally (not shown in Fig. 2.14). For the experiments described in this thesis a Stark decelerator with 64 electric field stages is used.

In Fig. 2.14 the potential energy, $W(z)$, of a $^{14}ND_3$ molecule in the $|1, 1\rangle$ low-field seeking state is depicted as a function of its position z along the beam axis. For clarity all electrodes are depicted in the same direction. The energy a molecule loses per stage depends on its position at the time that the fields are being switched. In analogy with concepts used in charged particle accelerators,

this position is expressed in terms of a 'phase angle' ϕ that has a periodicity of $2L$. Molecules that are in maximum electric field just prior to the time at which the fields are switched are assigned a phase angle $\phi = 90°$.

The (virtual) molecule that has always travelled exactly a distance L between two switching times of the electric fields, is referred to as the synchronous molecule. Its phase and longitudinal velocity are designated as the equilibrium phase ϕ_s and the equilibrium velocity v_s, respectively. Let us look at the situation in which the electric fields are switched at equal time intervals ΔT. The synchronous molecule in this case has an equilibrium phase $\phi_s = 0°$. A nonsynchronous molecule that has a slightly larger phase angle relative to this synchronous molecule will lose more kinetic energy per stage than the synchronous molecule. It is slowed down relative to the synchronous molecule and its phase will get smaller until it lags behind the synchronous molecule. Then the molecule will gain kinetic energy with respect to the synchronous molecule and is accelerated. From this argument it is clear that the nonsynchronous molecules oscillate around the synchronous molecule in phase-space. This is known as phase stability, which was independently conceptualized by Veksler [28] and McMillan [29] and it forms the basis of all modern accelerators. This principle is very important. It ensures that a package of molecules is kept together in the forward direction throughout the decelerator.

The kinetic energy $\Delta K(\phi_s)$ that the synchronous molecule loses per stage is given by $W(\phi_s) - W(\phi_s + \pi)$, the difference in Stark energy before and after switching the electric fields. When ϕ_s is chosen such that the synchronous molecule is decelerated in each stage, the switching time intervals have to be gradually increased in order to match the time it takes for the synchronous molecule to fly over a distance L with its instantaneous velocity v_s. The principle of phase stability still holds during deceleration and nonsynchronous molecules oscillate around the synchronous molecule in phase-space; the molecules are trapped in a potential well that travels with the velocity of the synchronous molecule [76].

In order to quantify the longitudinal motion of the molecules in the travelling potential well, it is useful to express the potential energy $W(\phi)$ as a Fourier series,

$$W(\phi) = \sum_{n=0}^{\infty} a_n \sin(n\phi) + b_n \cos(n\phi). \qquad (2.29)$$

From the definition of the phase angle all the even terms cancel in the expression for $\Delta K(\phi_s)$, yielding

$$\Delta K(\phi_s) = 2a_1 \sin(\phi_s) + 2a_3 \sin(\phi_s) + \dots . \qquad (2.30)$$

Here, a_i are the Fourier coefficients that have the dimension of energy. In our experiment, where the adjacent electric field stages are not too far apart, $\Delta K(\phi_s)$ is pre-dominantly determined by the first term. The kinetic energy that a molecule loses per stage can be attributed to a continuously acting force. This

approximation is valid when the longitudinal velocity difference $\Delta v = v - v_s$ between a nonsynchronous and the synchronous molecule is much smaller than v_s and when the change in velocity of the synchronous molecule per stage is small compared to its absolute velocity [65].

The equation describing the longitudinal motion of the nonsynchronous molecule relative to the motion of the synchronous molecule in the potential well is given by [65]

$$\frac{mL}{\pi}\frac{d^2\Delta\phi}{dt^2} + \frac{2a_1}{L}(\sin(\phi_s + \Delta\phi) - \sin(\phi_s)) = 0, \qquad (2.31)$$

with m the mass of the molecule and $\Delta\phi = \phi - \phi_s$ the difference between the phase of the nonsynchronous molecule and the phase ϕ_s of the synchronous molecule. For $^{14}ND_3$ molecules in our particular experimental geometry $a_1 = 0.92$ cm^{-1}. When $\Delta\phi$ is small, $\sin(\phi_s + \Delta\phi) \simeq \sin\phi_s + \Delta\phi\cos\phi_s$ and the equation of motion can be approximated by

$$\frac{mL}{\pi}\frac{d^2\Delta\phi}{dt^2} + \frac{2a_1}{L}(\Delta\phi\cos\phi_s) = 0, \qquad (2.32)$$

which is just the equation of motion for an harmonic oscillator. Eq. (2.31) can be numerically integrated to find the trajectories of the molecules through the Stark decelerator as a function of time. There is one special trajectory: the one of the synchronous molecule. Calculation of this trajectory and storing the timings when the synchronous molecule reaches its ϕ_s-positions in each of the deceleration stages yields the time sequence for the deceleration. Alternatively, an analytical expression for the time sequence that fits the numerical solution well is given in [65].

Rather than showing the equation of motion in real space it is insightful to plot the motion of the molecules in phase-space, in particular to plot the motion in phase-space relative to the synchronous molecule. In Fig. 2.15 phase-space plots are shown for equilibrium phase angles of $\phi_s = 0°$ and $\phi_s = 70°$. At a phase angle $\phi_s = 0°$ a package of molecules is not decelerated but it stays together in the longitudinal direction. The buncher described in Chapter 4 is operated at this phase angle. Typically a phase angle of $\phi_s = 70°$ is used for the deceleration experiments described in this thesis. The lines show the trajectories in phase-space for molecules starting at different initial phase angles. These trajectories are curves of equal energy in the potential well experienced by the molecules. The motion is clockwise. Around ϕ_s there is a stable, bound region in which the molecules are trapped. The area within the thick curve (separatrix) is the longitudinal acceptance of the potential well. Molecules whose energy exceeds the depth of the potential well are unbound and their trajectories lie outside the separatrix. The acceptance area is periodic in $\Delta\phi$ (periodicity $2L$) creating a train of travelling potential wells throughout the decelerator. From Fig. 2.15 it is clear that the acceptance is larger for smaller equilibrium phase
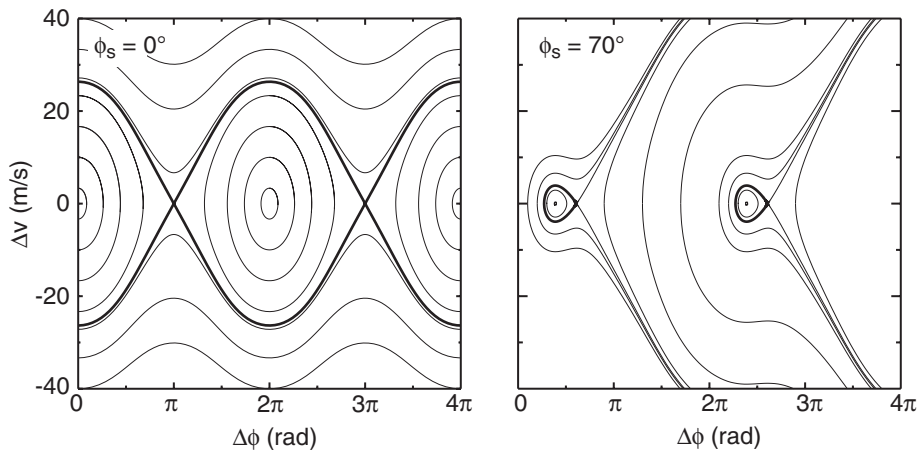
Figure 2.15: *Phase stability diagrams for $\phi_s = 0°$ and $\phi_s = 70°$, obtained via numerical integration of Eq. (2.31) with parameters as used in the experiment for $^{14}ND_3$. Thick lines indicate the longitudinal acceptance. In the experiment a difference in the phase angle of 2π corresponds to a distance of 11 mm.*

angles, i.e., in that case more molecules are transported through the decelerator. However, a lower phase angle results in a lower deceleration per stage as given by Eq. (2.30). Since both a large acceptance and efficient deceleration are desirable, there is a trade-off between the two.

The effective potential well is nearly harmonic around the equilibrium phase angle. The inner curves are nearly elliptical, easily noticeable for $\phi_s = 0$, corresponding to a nearly linear restoring force on the molecules, as can be seen from Eq. (2.32). For $^{14}ND_3$ the longitudinal oscillation frequency, given by

$$\omega_z/2\pi = \sqrt{\frac{a_1 \cos \phi_s}{2m\pi L^2}}, \tag{2.33}$$

is approximately 1.7 kHz for $\phi_s = 0°$ and 1 kHz for $\phi_s = 70°$. Further outward, the restoring force becomes more nonlinear and the oscillation frequency is lowered, approaching zero on the separatrix. The nonlinearity leads to the aforementioned filamentation of the phase-space distribution.

The longitudinal emittance of the beam at the entrance of the Stark decelerator is typically $[\Delta z \times \Delta v_z] = [30 \text{ mm} \times 40 \text{ m/s}]$ where the widths are at full width half maximum of the respective distributions. The upper graphs of Fig. 2.16 show how the longitudinal emittance of the molecular beam overlaps with the longitudinal acceptance of the Stark decelerator for a phase angle $\phi_s = 0°$ and for a phase angle $\phi_s = 70°$. The longitudinal position and velocity distributions of the molecules in the beam are in good approximation Gaussian distributions. The longitudinal emittance of the molecular beam is much larger
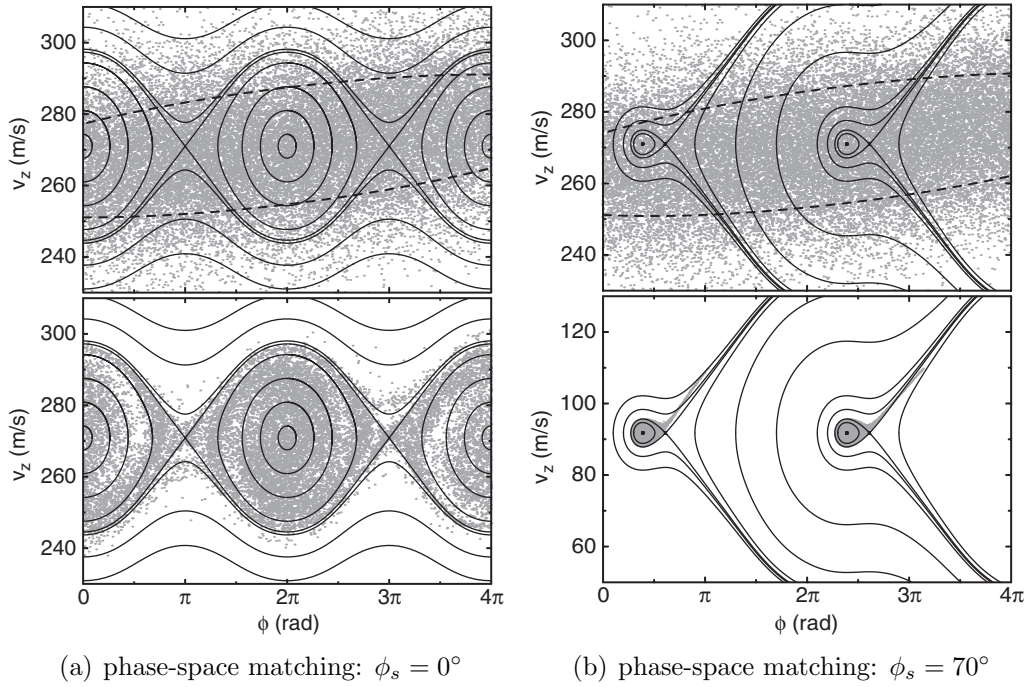
(a) phase-space matching: $\phi_s = 0°$

(b) phase-space matching: $\phi_s = 70°$

Figure 2.16: *Upper row: overlap of longitudinal emittance of the molecular beam with the longitudinal acceptance of the Stark decelerator for $\phi_s = 0°$ and $\phi_s = 70°$. The clipped ellipse (dashed lines) in the upper row indicates the full width half maximum of the density. Lower row: longitudinal phase-space distributions (emittance) at the end of the decelerator for the two phase angles.*

than the longitudinal acceptance of the Stark decelerator and the gas pulse can fill more than one bucket in the Stark decelerator. The longitudinal emittance of the Stark decelerator is shown in the lower graphs of Fig. 2.16. For a phase angle $\phi_s = 70°$ the buckets are completely filled and filamentation of the longitudinal phase-space distribution is irrelevant. For a phase angle $\phi_s = 0°$ the buckets are not completely filled and filamentation occurs, hindering phase-space matching of the Stark decelerator emittance onto the acceptance of the next beamline section. However, the Stark decelerator is normally not operated at a phase angle $\phi_s = 0°$.

Chapter 3

A prototype storage ring for neutral molecules

3.1 Introduction

In this Chapter the design and first performance testing results of a storage ring for neutral polar molecules are described. The principle of the storage ring is based on the linear, electrostatic hexapole lens that transversely confines a beam of low-field seeking molecules. By bending such a linear hexapole around into a torus, a storage ring can be created [42]. The electric field geometry of the storage ring that is actually used for the experiments, deviates from the commonly used cylindrically symmetric hexapole fields that have been discussed in Section 2.7.1. Instead, we have used a dipole configuration mainly because this simplifies the detection of the ammonia molecules. An analytical description of the potential well and the motion of the molecules is very difficult in this configuration, however, and the trajectories are calculated numerically. In the experiment, decelerated bunches of deuterated ammonia molecules are injected into the storage ring and are detected after up to six times around the ring. Each bunch contains about 10^6 molecules in a single quantum state and has a translational temperature of 10 mK.

3.2 Motion of molecules in the ring

To understand the motion of the molecules in the storage ring it is useful to look first at a ring with an electric field that has an hexapole geometry as this can be analytically described by Eq. (2.27). Later, we extend this analysis for the geometry that is actually used with numerical calculations.

This chapter is based on: F. M. H. Crompvoets, H. L. Bethlem, R. T. Jongma, and G. Meijer, Nature **411**, 174–176, 2001.
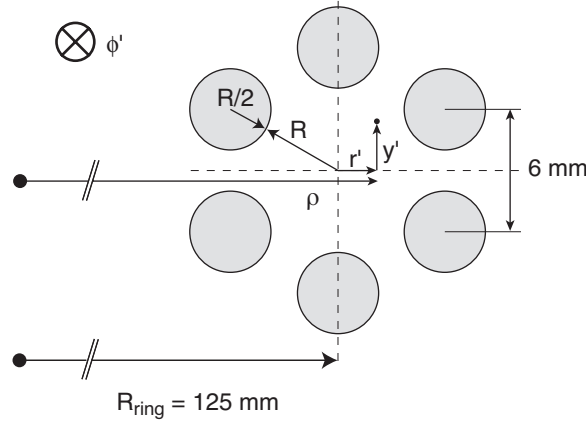
Figure 3.1: *Cross sectional view of the hexapole storage ring.*

3.2.1 Equilibrium orbit

As already mentioned, a storage ring can be created by bending an hexapole focuser around and by connecting its exit to its entrance. The electric field of the hexapole ring transversely confines low-field seeking molecules. In the forward, tangential direction they fly freely. The centripetal force required to keep the molecules in a circular orbit arises from the Stark interaction of the molecules in the inhomogeneous electric field that is created by putting high voltages on alternating rods of the hexapole. In Fig. 3.1 a cross section through the hexapole storage ring is shown. The position of a molecule with respect to the center of the hexapole geometry is given by its radial coordinate r' and its vertical coordinate y' (the z coordinate is used for the direction along the molecular beam axis throughout this thesis). The tangential coordinate ϕ' points into the plane of the paper. The position of a molecule with respect to the center of the ring is given by the radial coordinate ρ, the tangential coordinate ϕ, and the vertical coordinate y. The relation between r' and ρ is $\rho = R_{ring} + r'$, where R_{ring} is the distance from the center of the ring to the center of the hexapole. The coordinates with a prime indicate the system rotating with a angular frequency Ω at a distance R_{ring} around the origin. The coordinates without a prime indicate the inertial system fixed at the origin. It should be noted that $\rho \parallel r'$, $\phi = \phi'$, and $y = y'$.

When the hexapole inner radius, R, is small compared to the radius of the ring, R_{ring} (from the center of the ring to the center of the hexapole geometry), the electric field will only be slightly distorted. In the figure on the upper left of Fig. 3.2 the calculated electric field lines are shown for a linear hexapole. An hexapole geometry is taken with an inner radius $R = 4$ mm and with a radius of the cylindrical rods equal to $R/2$. The voltage difference between adjacent electrodes is taken to be 10 kV in these calculations. The electric field is numerically calculated using Simion [72]. When this hexapole is bent into a
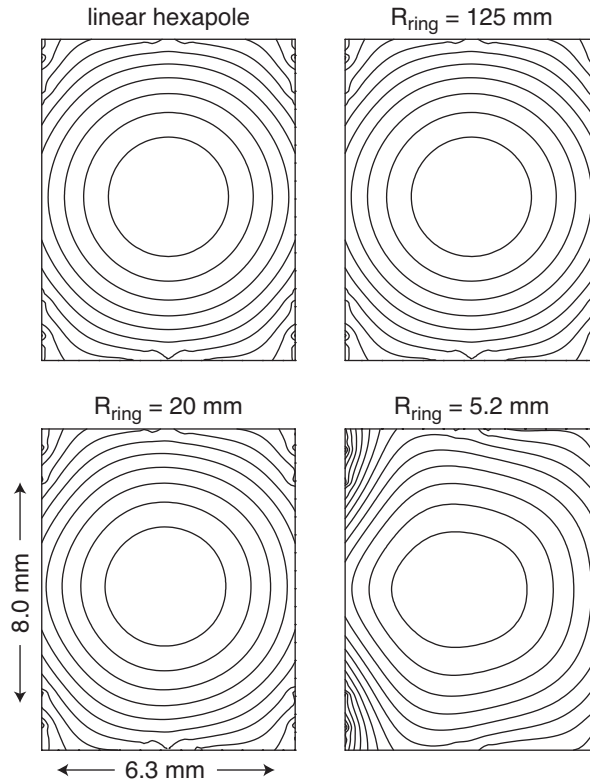
Figure 3.2: *Contour lines indicating the electric hexapole field for a linear hexapole (upper left), for a storage ring with a radius $R_{ring} = 125$ mm (upper right), with a radius $R_{ring} = 20$ mm (lower left), and with the smallest possible radius $R_{ring} = 5.2$ mm (lower right). For the latter radius, the inner ring electrodes are spheres. The inner radius $R = 4$ mm and the voltage difference between adjacent electrodes is 10 kV. The field of view that is shown has a width of 6.3 mm and a height of 8.0 mm. The center of the ring is to the left in the storage ring plots. In each graph the inner most electric field line is 5 kV/cm. Other field lines are shown at 5 kV/cm intervals.*

large torus with $R_{ring} = 125$ mm, the electric field lines are hardly distorted (upper right). By reducing the torus radius to $R_{ring} = 20$ mm (lower left) or even to the smallest radius possible $R_{ring} = 5.2$ mm (lower right), the electric field lines deviate more and more from the cylindrically symmetric electric field of the linear hexapole.

In the case of an hexapole electric field the force on the molecule is given by Eq. (2.27) and points radially inwards for a molecule in a low-field seeking state. The radial and vertical equilibrium position of the molecules can be calculated by balancing the forces in either one of these directions. In the vertical direction, the gravitational force is balanced by the vertical component of the hexapole

force

$$mg = -\frac{ky'}{\sqrt{1 + \left(\frac{W_{inv}}{kr'^2}\right)^2}} \tag{3.1}$$

where m is the mass of the molecule and g is the gravitational acceleration. In the horizontal plane, the centrifugal force is balanced by the radial component of the hexapole force

$$\frac{mv_\phi^2}{R_{ring} + r'} = \frac{kr'}{\sqrt{1 + \left(\frac{W_{inv}}{kr'^2}\right)^2}}, \tag{3.2}$$

where v_ϕ is the tangential or longitudinal velocity of the molecule in the ring. Solving Eq. (3.1) and Eq. (3.2) simultaneously for r' and y' gives the radial equilibrium position, r'_0, and the vertical equilibrium position, y'_0, respectively. In the ideal (hypothetical) case, when the inversion splitting is zero and the hexapole force is truly linear, the equilibrium radius r'_0 is found to be

$$r'_0 = \frac{R_{ring}}{2}\left[\sqrt{1 + \left(\frac{2v_\phi}{R_{ring}\omega}\right)^2} - 1\right] \approx \frac{v_\phi^2}{R_{ring}\omega^2}, \tag{3.3}$$

where $\omega = \sqrt{k/m}$ and k is given by Eq. 2.28. For a $^{14}ND_3$ molecule in the low-field seeking $|J, K\rangle = |1, 1\rangle$ state with a tangential velocity $v_\phi = 91.8$ m/s one finds in this ideal case an equilibrium radius $r'_0 = 1.90$ mm (or $\rho_0 = 126.90$ mm) and a vertical equilibrium position $y'_0 = -0.28$ μm. When the nonzero inversion splitting of deuterated ammonia is accounted for, the equilibrium radius and the vertical equilibrium position are numerically calculated to be $r'_0 = 1.95$ mm and $y'_0 = -0.29$ μm, respectively. So, the linear approximation is good enough to determine these equilibrium orbits. The effect of gravity on the motion of the molecules in the storage ring is seen to be small and will be neglected from now on. It is clear that for a given maximum attainable electric field strength, the radius of the storage ring, R_{ring}, is proportional to the square of the velocity v_ϕ. Or in other words: the maximum attainable electric field strength and the size of the ring set an upper limit on the tangential velocity of molecules that will be accepted. The availability of beams of slow neutral molecules, with a tunable absolute velocity [5, 77], is therefore an important asset in the performance testing of a storage ring for molecules.

An important consequence of the circular motion in the storage ring is that molecules with different longitudinal velocities v_ϕ have closed orbits at different equilibrium radii. If a molecule with velocity $(v_\phi)_0$ orbits at its equilibrium radius ρ_0 then a molecule with velocity $v_\phi = (v_\phi)_0 + \Delta v_\phi$ orbits at radius $\rho = \rho_0 + \Delta\rho$. Consequently, faster molecules orbiting the ring have a longer flight path while slower molecules have a shorter flight path. This difference in flight paths between faster and slower molecules counteracts the longitudinal spreading out of the molecular package, and one could wonder whether this effect

could be used to completely cancel this longitudinal spreading out. For this, the difference in round trip time ΔT between the fastest and slowest molecule has to be zero. The ring is then said to be isochronous and all molecules will arrive at the same time at the detection position. The round trip time of a molecule is given by $T = 2\pi\rho/v_\phi$. The relative change in round trip time is then given by

$$
\begin{aligned}
\frac{\Delta T}{T_0} &= \frac{\Delta\rho}{\rho_0} - \frac{\Delta v_\phi}{(v_\phi)_0} \\
&= \left[\frac{1}{\rho_0}\left(\frac{\partial\rho}{\partial v_\phi}\right) - \frac{1}{(v_\phi)_0} \right]\Delta v_\phi,
\end{aligned}
\tag{3.4}
$$

where the subscript 0 represents the molecule on the equilibrium orbit. In case of isochronous operation of the ring, the term between the square brackets of Eq. (3.4) has to be zero. Realizing that $(\partial\rho/\partial v_\phi) = (\partial r'/\partial v_\phi)$ and using Eq. (3.3) one finds for the linear case where inversion splitting is zero

$$
v_\phi = \frac{\omega^2\rho_0 R_{ring}}{2\sqrt{(v_\phi)_0^2 - \omega^2\rho_0^2}}.
\tag{3.5}
$$

This solution is real only when $(v_\phi)_0 > \omega\rho_0$. When we introduce the angular vector $\mathbf{\Omega} = \Omega\hat{\mathbf{y}}$ with which the molecules orbit in the ring, $(v_\phi)_0$ can be written as $\Omega\rho_0$. Eq. (3.4) therefore implies that isochronous operation of the storage ring is only possible when $\omega < \Omega$. On the other hand the required identity in Eq. (3.2) can be rewritten in the linear case (where inversion splitting is zero) as $\Omega^2(R_{ring} + r') = \omega^2 r'$ which is only possible when $\omega \geq \Omega$. It can thus be concluded that isochronous operation of an hexapole torus storage ring is not possible (unless $R_{ring} = 0$!). Isochronous operation of a storage ring is therefore only possible when the longitudinal momentum distribution in the ring is actively manipulated.

3.2.2 Betatron oscillations

When the molecules are stored inside the storage ring, they will oscillate around the equilibrium orbit. These oscillations are called betatron oscillations named after the oscillatory motion of charged particles first studied in betatron storage rings. In the harmonic potential well, the oscillations in the vertical and radial (horizontal) direction are not coupled, but, due to conservation of angular momentum $\mathbf{L}$, the radial motion of the molecules is coupled to the forward, tangential motion.

For the motion in a rotating system the rate of change of the position vector $\mathbf{r}$ in the inertial system is given by [78]

$$
\left(\frac{d\mathbf{r}}{dt}\right)_{inert} = \left(\frac{d\mathbf{r}}{dt}\right)_{rot} + \mathbf{\Omega}\times\mathbf{r},
\tag{3.6}
$$

where the subscripts *inert* and *rot* indicate the inertial and rotating system, respectively. For a particle rotating at a distance ρ from the center of the ring at an angular frequency $\boldsymbol{\Omega} = \Omega\hat{\mathbf{y}}$, the position vector in the rotating system (r', ϕ', y') is given by $\mathbf{r'} = (r', 0, y')$ as the particle only moves in the (r', y')-plane in the rotating system. The acceleration $\ddot{\mathbf{r}}$ of the particle in the inertial system is found by applying Eq. (3.6) twice:

$$\ddot{\mathbf{r}} = \left(\ddot{r'} - (R_{ring} + r')\Omega^2, (R_{ring} + r')\dot{\Omega} + 2\Omega\dot{r'}, \ddot{y'}\right). \qquad (3.7)$$

The angular frequency Ω is identified as the rate of change in ϕ, i.e., $\Omega = \dot{\phi}$. The equations of motion in the inertial system are then given by

$$\begin{aligned} F_\rho &= m\ddot{\rho} - m\rho\dot{\phi}^2, & (3.8) \\ F_\phi &= 0 \rightarrow \rho\ddot{\phi} + 2\dot{\phi}\dot{\rho} = 0, & (3.9) \\ F_y &= m\ddot{y}, & (3.10) \end{aligned}$$

where ρ is substituted for $(R_{ring} + r')$, $\dot{\rho}$ for $\dot{r'}$, and $\ddot{\rho}$ for $\ddot{r'}$. Multiplying Eq. (3.9) on both sides with $m\rho$ and integrating with respect to time yields

$$m\rho^2\dot{\phi} = \text{constant.} \qquad (3.11)$$

The left part of this expression is the angular momentum of a molecule orbiting the ring: $|\mathbf{L}| = m\rho v_\phi$ with $v_\phi = \rho\dot{\phi}$. It is immediately clear that a change in ρ leads to a change in v_ϕ in such a way as to keep $|\mathbf{L}|$ constant. Therefore a molecule with a radial betatron oscillation will also oscillate in the tangential direction. It is readily shown that the amplitude of the oscillation in the tangential velocity, Δv_ϕ, is proportional to the amplitude of the velocity in the radial direction with a proportionality constant of Ω/ω.

In the vertical and radial direction the forces F_y and F_ρ are given by the right hand sides of Eq. (3.1) and Eq. (3.2), respectively. These are restoring forces for low-field seeking molecules and the molecules will perform betatron oscillations around their equilibrium orbits.

The acceptance of the potential well of the hexapole ring depends on the tangential velocity of the molecules. In the vertical direction the potential well is given by

$$W(y') = \frac{1}{2}\frac{ky'^2}{\sqrt{1 + \left(\frac{W_{inv}}{kr^2}\right)^2}}. \qquad (3.12)$$

In the horizontal direction the potential well is the sum of the Stark energy in the electric field of the hexapole and a pseudo-potential energy W_{centri} associated with the centrifugal force:

$$W_{centri} = -\int \frac{mv_\phi^2}{R + r'}dr'. \qquad (3.13)$$

The constant of integration is set by our definition that $W_{centri} = 0$ for $r' = 0$. Then the potential energy is

$$W_{centri} = -mv_\phi^2 \ln|1 + \frac{r'}{R}|. \tag{3.14}$$

The potential well in the radial direction is then given by

$$W(r') = \frac{1}{2} \frac{kr'^2}{\sqrt{1 + \left(\frac{W_{inv}}{kr'^2}\right)^2}} - mv_\phi^2 \ln|1 + \frac{r'}{R}|. \tag{3.15}$$

When the tangential velocity increases, the radial equilibrium orbit moves outwards and for a fixed electric field strength the potential well depth decreases. This is shown in Fig. 3.3. Here, the dashed line is the centrifugal potential energy which is zero at $r' = 0$. The solid line is a plot of the radial potential well at $y = 0$, as given by Eq. (3.15). The plots are shown for increasing tangential velocities. At $v_\phi = 0$ m/s the radial potential well is deepest while for velocities larger than approximately 135 m/s the potential well is nonexistent as the equilibrium orbit lies beyond the radius of the hexapole ($r_0 > 4$ mm). Of course, as the tangential velocity increases and the radial potential well becomes less deep, the vertical potential well also becomes less deep. In principle, the acceptance runs up to a radius of 5.2 mm, right in between the ring electrodes where the electric field is maximum. The electrodes act like a mask, however, and cut away a part of the phase-space distribution. To put, nevertheless, a number to the acceptance, we will only take into account a radius of 4 mm, which is the radius of the circle enclosed by the ring electrodes. The rationale for this is that nonlinearities in the potential can lead to a coupling between the radial and vertical motion and a molecule originally accepted by the ring at a radius larger than 4 mm (in between the electrodes) will crash onto one of the electrodes and can be assumed lost. So, the acceptance is limited by the positions of the ring electrodes.

The longitudinal acceptance is limited by the curvature of the ring and the radial position at which the molecules are coupled into the storage ring. For instance, molecules entering the storage ring with a tangential velocity of about 90 m/s at their radial equilibrium position of $r' = 1.9$ mm are accepted only over a length of 36 mm. The accepted velocity range runs from 0 m/s to about 135 m/s, at which the molecules are no longer able to follow the curvature of the ring. The transverse acceptance depends on the tangential velocity as for higher tangential velocities the transverse potential well decreases. For a tangential velocity of 90 m/s, the radial acceptance is calculated to be $[\Delta r \times \Delta v_r] = [4.2$ mm $\times$ 12.9 m/s$]$ and the vertical acceptance is calculated to be $[\Delta y \times \Delta v_y] = [7.0$ mm $\times$ 20.8 m/s$]$.
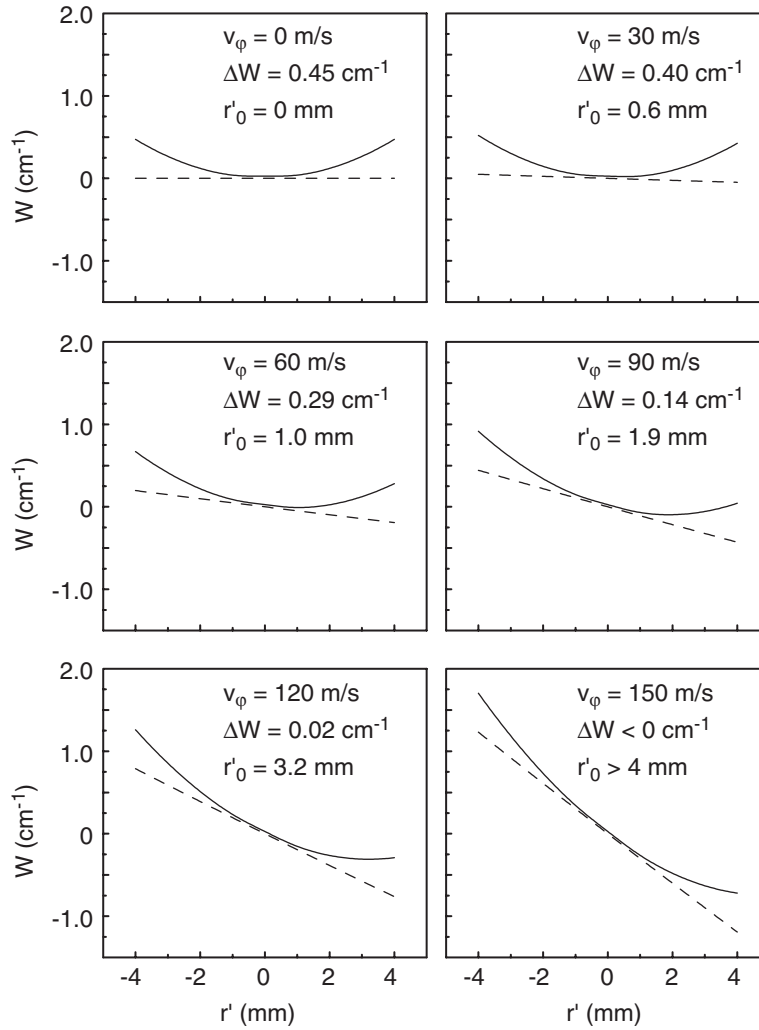
Figure 3.3: *Radial potential energy well (solid lines) for $^{14}\text{ND}_3$ for different tangential velocities. The potential well is taken at $y = 0$. The centrifugal potential energy is indicated with dashed lines.*

3.3 Dipole ring

The actual electric field geometry in our hexapole torus storage ring deviates from the cylindrically symmetric hexapole fields. The reason for this is that apart from trapping the molecules inside the storage ring, we also need to be able to detect them. As the detection of ammonia is performed via a resonance enhanced ionization scheme we need to be able to extract the laser-produced ions from the ring, which will be discussed in Section 3.4. A concomitant advantage of the electric field geometry used, is that transitions from trapped to untrapped states which can occur at zero electric field, so-called Majorana
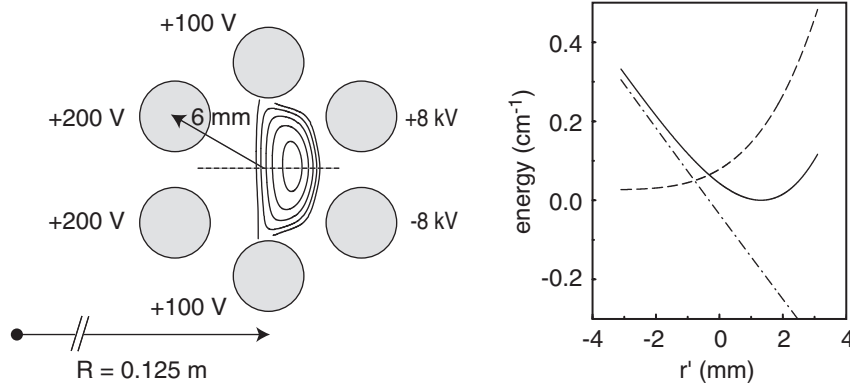
Figure 3.4: *Left: Cross section of the hexapole storage ring in the dipole configuration. Contour lines of equal potential energy for $^{14}ND_3$ molecules in the $|J,K\rangle = |1,1\rangle$ state with positive Stark-shift and with a tangential velocity of 89 m/s are shown at 0.02 cm^{-1} intervals. Right: The dashed curve shows the Stark energy as a function of the displacement from the center of the hexapole (r') in the plane of the hexapole ring (along the dashed axis as shown in the left part of the figure). The solid curve is obtained by adding the potential energy as a result of the centrifugal force for an ammonia molecule with a tangential velocity of 89 m/s (dot-dashed line) to the Stark energy (dashed line). The minimum of the resulting potential well is located 1.3 mm offset from the geometrical center of the hexapole.*

transitions, are avoided. Fig. 3.4 illustrates the voltages applied to the different rods of the ring and the equipotential lines in the shallow well experienced by deuterated ammonia molecules in the low-field seeking $|1,1\rangle$ state travelling with a tangential velocity of 89 m/s. The potential well is calculated in a similar fashion, as outlined above, for an ideal hexapole field. It is the sum of the Stark energy and the potential energy due to the centrifugal force. In this case an analytical expression for the electric field is not available and the electric field has been numerically calculated using Simion [72]. Although the shape of the potential well differs from the hexapole case, the motion of the molecules in this "dipole" ring is in principle the same as for the hexapole ring: angular momentum is a conserved quantity and the molecules perform betatron oscillations around the equilibrium orbit. The difference is the introduction of additional nonlinearity in the equations of motion as well as an asymmetry in the shape of the potential well. The trajectories of the molecules in the ring are numerically calculated by correctly incorporating the Stark energy in the equations of motion. From Fig. 3.4 it is clear that the potential well is anharmonic (equipotential lines are not ellipses) and asymmetric. Therefore the betatron oscillations of the molecules have different frequencies in the vertical and radial direction. The frequencies also depend on the position of the molecules in the
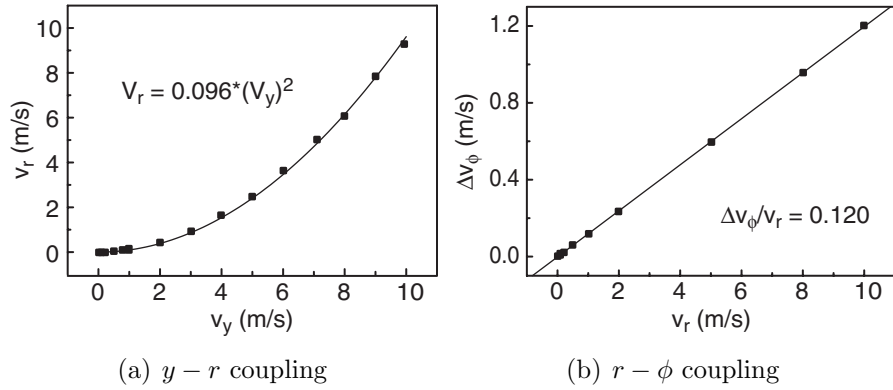
(a) $y - r$ coupling

(b) $r - \phi$ coupling

Figure 3.5: *(a) Coupling in the dipole ring between v_y and v_r. The plot shows the velocity amplitude in the radial direction as a function of the (initial) velocity amplitude in the vertical direction. (b) Coupling in the dipole ring between v_r and Δv_ϕ. The plot shows the velocity amplitude in the tangential direction as a function of the (initial) velocity amplitude in the radial direction.*

potential well. At the equilibrium orbit the oscillation frequencies in the vertical and horizontal (radial) direction for the potential well shown in Fig. 3.4 are 390 Hz and 970 Hz, respectively. This corresponds to 3.4 oscillations per round trip in the vertical direction and to 8.4 oscillations per round trip in the radial (and therefore also in the tangential) direction. These oscillation frequencies are found by numerical integration of the path that a molecule traverses through the ring. To stay in the harmonic region, the amplitude of the oscillations is chosen to be small in this simulation. Larger amplitudes lead to strong coupling between the radial and vertical motion. Fig. 3.5(a) shows the result of a numerical calculation of the coupling between v_y and v_r for different initial values of v_y. It appears that this coupling is quadratic in the dipole ring. The coupling between the radial and tangential motion is shown in Fig. 3.5(b). The coupling constant, i.e., the slope of the graph, is numerically found to be 0.120 in good agreement with the expected value of $\Omega/\omega = 0.118$.

As for the hexapole storage ring the potential well of the dipole storage ring depends on the tangential velocity. Fig. 3.6 shows the radial potential well as a function of the tangential velocity v_ϕ. In contrast to the potential well of the hexapole ring, the potential well of the dipole ring vanishes both for high and low tangential velocities. At high velocities the molecules cannot make the turn; the centrifugal force is larger than the force exerted by the electric field. At low velocities the potential well opens up at the inside of the storage ring because the Stark energy is a monotonically rising function of r'. The well is deepest around a tangential velocity of approximately 90 m/s. In contrast to the hexapole storage ring, the longitudinal velocity acceptance of the dipole ring has a lower
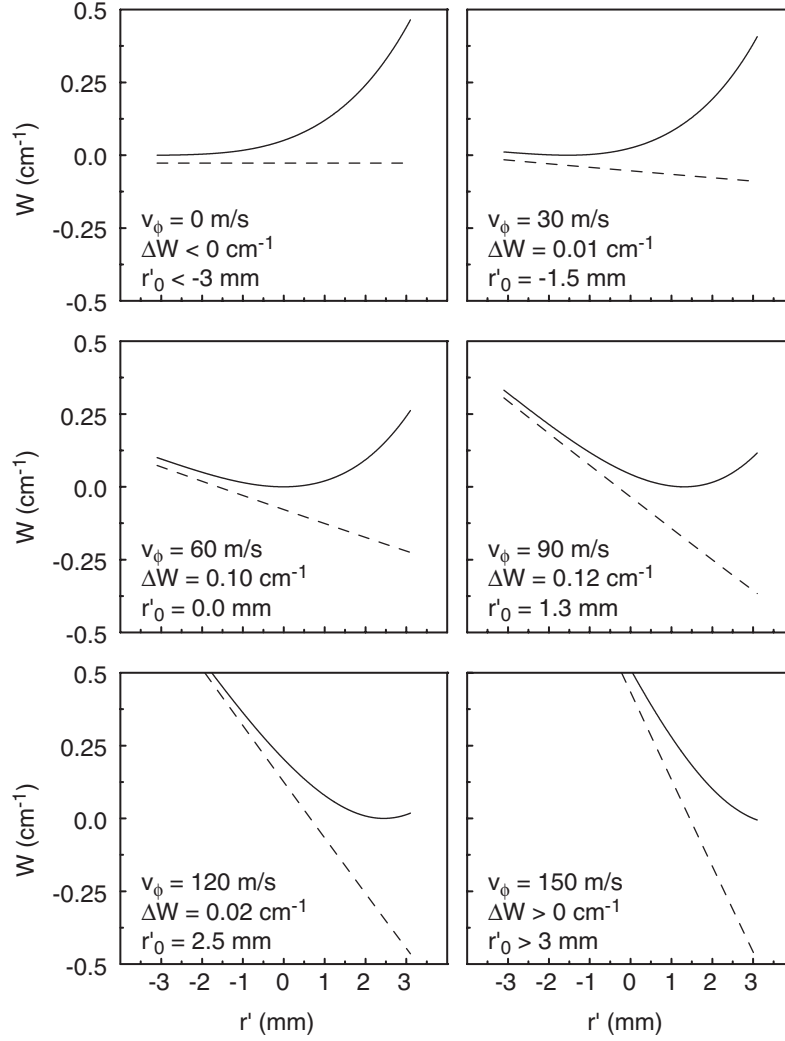
Figure 3.6: *Radial potential well ($y' = 0$) of the dipole storage ring as a function of the tangential velocity. The solid lines are the sum of the Stark energy and the potential energy due to the centrifugal energy (dashed lines).*

bound of approximately 20 m/s; the upper bound is approximately 130 m/s. The longitudinal position acceptance is 44 mm. The transverse acceptance in the radial direction for an equilibrium radius of 1.3 mm (90 m/s) is found from numerical calculation to be $[\Delta r \times \Delta v_r] = [6.2$ mm $\times 19.1$ m/s$]$. If the cutoff due the rods of the hexapole is taken into account, the effective position acceptance in the radial direction is limited to $\Delta r = 5.4$ mm. The acceptance in the vertical direction is found to be $[\Delta y \times \Delta v_y] = [7.5$ mm $\times 11.5$ m/s$]$.
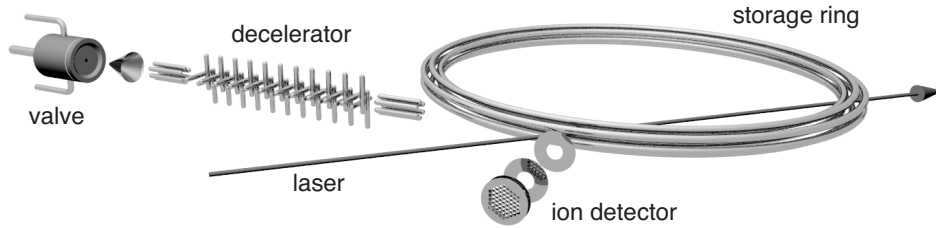
Figure 3.7: *From left to right: a gas pulse of less than 1% $^{14}ND_3$ in Xe exits a cooled (T = 200 K) pulsed valve with a mean velocity of 275 m/s. After passage through the skimmer the beam is collimated with a pulsed hexapole and sub-sets of these molecules are slowed down to velocities in the 76 m/s to 110 m/s range upon passage through the Stark decelerator. The bunches of slow molecules are tangentially injected into the electrostatic storage ring (12.5 cm radius; 4 mm diameter rods). Molecules in the detection region of the storage ring are ionized using a pulsed laser, after which they are extracted, and detected with an ion detector. The flight path of the molecules from the pulsed valve to the detection region in the storage ring is about 65 cm.*

3.4   Experimental set-up

The experimental set-up shown schematically in Fig. 3.7 consists of a compact molecular beam machine that tangentially injects molecules into an hexapole torus storage ring which has a diameter of 25 cm. A pulsed beam of deuterated ammonia is produced by expanding a $^{14}ND_3$/Xe mixture through a modified solenoid valve into vacuum. Seeding $^{14}ND_3$ in the heaviest rare gas and cooling of the pulsed valve results in a mean beam velocity of around 285 m/s (E_{kin} = 64 cm^{-1}). About 20% of the $^{14}ND_3$ molecules reside in the low-field-seeking $|J, K\rangle = |1, 1\rangle$ upper inversion level of the vibrational ground state. With the hexapoles and the decelerator only molecules are selected that are in this quantum state, i.e., molecules that gain Stark energy with increasing electric field and that are repelled from high-electric-field regions.

The $^{14}ND_3$ molecules pass through a 1.0-mm-diameter skimmer into a second, differentially pumped vacuum chamber and then fly into a short hexapole with radius $R = 3$ mm that is pulsed to 10 kV and that acts as a positive lens for the selected $^{14}ND_3$ molecules. Alternatively, one could leave the hexapole on for a much longer period, or even leave it on constantly at a lower voltage. Pulsing the hexapole at high voltage ensures that the force acting on the molecules is more linear because they are in the linear regime of the Stark shift and that all molecules are equally strongly focused. Another advantage is that it is possible to vary both the position and the strength of the hexapole lens by adjusting the timings when the hexapole is switched on and off. In addition, this approach
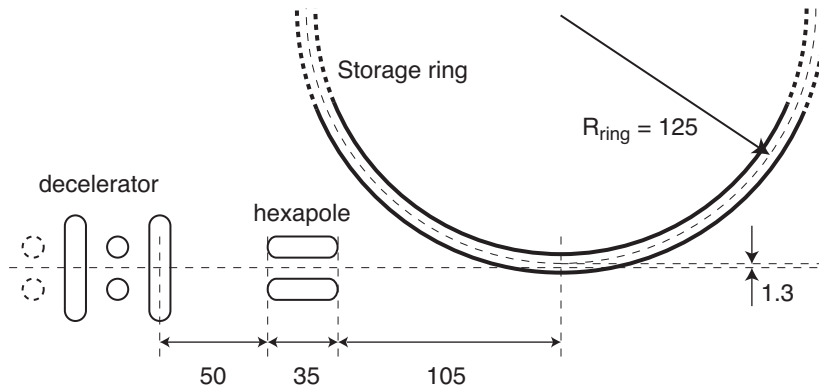
Figure 3.8: *Distances (in mm) between the Stark decelerator, the hexapole and the ring are shown schematically.*

bypasses the need for separate power supplies for each hexapole. After exiting the hexapole, the molecules enter a 35-cm-long Stark decelerator containing an array of 64 equidistant electric-field stages operated at +10/-10 kV, creating electric fields of typically up to 100 kV/cm; this decelerates the molecules while maintaining their initial phase-space density as described in Chapter 2.

A second pulsed hexapole, connected to a separate power supply, with a length of 35 mm and radius $R = 3$ mm is positioned approximately 50 mm downstream from the exit of the decelerator as shown schematically in Fig. 3.8. This hexapole focuses the decelerated molecules into the storage ring, which is placed as close as possible to the hexapole in order to minimize losses in free flight. The hexapole is switched on and off such that the signal of the molecules in the ring is maximized. The total distance from the exit of the decelerator to the ring is approximately 190 mm. The ammonia molecules enter the ring tangentially, passing through the 2-mm-wide 'slit' between two hexapole rods. Hence, only part of the transverse phase-space distribution will be coupled into the ring when the beam is too wide. The injection of the molecular beam into the ring is optimized by aligning the ring vertically and horizontally by means of mechanical actuators. As shown in Fig. 3.8 the ring is given an horizontal offset such that the molecular beam axis coincides with the radial equilibrium position of $r'_0 = 1.3$ mm for a tangential velocity of 89 m/s, which is actually used in the experiments.

The density of $^{14}ND_3$ molecules inside the storage ring is probed using the focused radiation of a pulsed laser at 317 nm, which ionizes in a 2+1 resonance enhanced multi-photon process (single color) the $^{14}ND_3$ molecules that are in the selected quantum state [65,79]. Just before firing the laser, the high voltages on the outer two ring electrodes are switched off. Then the residual electric field created by the low voltages (100 V and 200 V) on the other electrodes accelerates the ions radially outwards as shown in Fig. 3.9. The storage ring itself serves
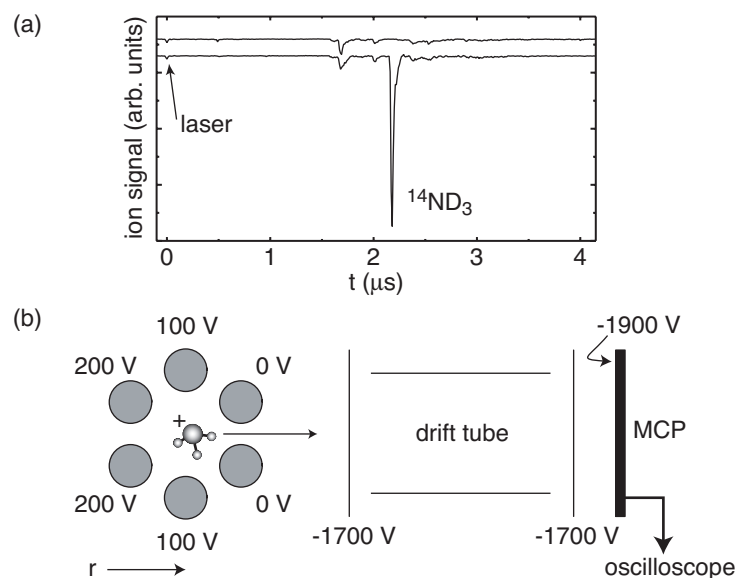
Figure 3.9: *(a) Typical time-of-flight mass spectrum as obtained with the storage ring as extraction region. Mass spectra are shown when the ammonia beam is switched off (upper trace) and when the ammonia beam is switched on (lower trace). (b) Time-of-flight mass spectrometer. The electric field created by the low voltages on the ring electrodes accelerates the positive $^{14}ND_3$-ions out of the ring. The ions are further accelerated towards a drift tube which is at -1700 V. The ions are detected with a multi-channel plate detector, which is typically at -1900 V. The ion signal is recorded on an oscilloscope.*

then as the extraction region of a linear time-of-flight mass spectrometer. The $^{14}ND_3$-ions are detected with a multi-channel plate detector which is at -1900 V and the ion signal is used as a measure for the amount of neutral ammonia molecules originally present inside the ring.

3.5   Results

Fig. 3.10 illustrates the relative density of neutral ammonia molecules in the detection region of the storage ring, as a function of the time after the molecules left the pulsed valve. Without any voltage applied to the Stark decelerator (that is, without deceleration), the ammonia density in the storage ring peaks around 2.4 ms after the molecules left the valve. This is the time it takes molecules travelling with an average velocity of around 275 m/s to cover the approximately 65-cm distance between the pulsed valve and the storage ring. The velocity spread is approximately 20% (full width at half-maximum, FWHM), implying a translational temperature of around 1.5 K in the moving frame. With the Stark
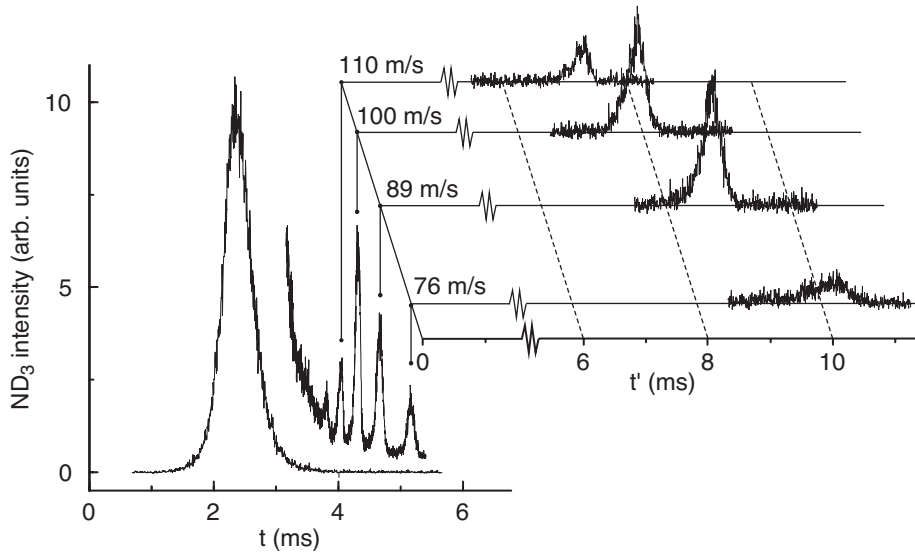
Figure 3.10: *Time-of-flight profiles. Density of ammonia molecules inside the storage ring as a function of time after opening of the pulsed valve (t), without (single large peak around 2.4 ms) and with the Stark-decelerator on (series of peaks at later arrival times). Note that the intensity of the decelerated bunches is on the same absolute scale as the original beam; the focusing effects in the decelerator typically enhance the signal on the beam axis by a factor of 5 compared to the situation that the decelerator is not switched on at all. The inset shows the density of ammonia molecules inside the storage ring measured as a function of the time after switching on the storage ring (t'). Bunches of decelerated molecules with four different center velocities are injected in the ring, with settings as shown in Fig. 3.4, and their time-of-flight distributions after the first round trip are recorded.*

decelerator switched on and configured to decelerate molecules from 275 m/s to a final velocity of 100 m/s, a series of peaks occur at later times. These different bunches, whose velocity is indicated in Fig. 3.10, originate from the spatially extended molecular gas pulse at the entrance of the decelerator. The molecules that exit the decelerator with a velocity of 110 m/s were already in the second electric-field section of the decelerator when the decelerator was switched on, and so missed one deceleration cycle. The molecules that exit the decelerator with velocities of 89 m/s and 76 m/s are molecules that entered the decelerator later, with an initial velocity that was lower than the average beam velocity. The individual bunches are still clearly separated in the probe region, which is located 19 cm away from the exit of the decelerator. The velocity spread in the decelerated bunches of molecules is only 4-5 m/s (FWHM), corresponding to a translational (longitudinal) temperature of around 10 mK. The signal we obtain corresponds to about a hundred $^{14}ND_3$-ions being generated per laser
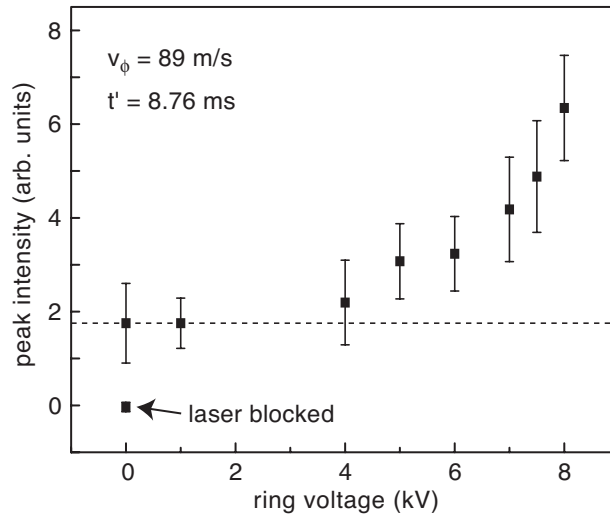
Figure 3.11: *Peak signal of the first round trip in the ring as a function of the applied voltages (+/-) to the outer ring electrodes.*

pulse. As ionization of the $^{14}ND_3$ molecules takes place only in the focus of the laser beam, the actual detection volume in our system is about 10^{-4} cm^3. Each bunch contains a minimum of about 10^6 state-selected $^{14}ND_3$ molecules. When a selected bunch of decelerated ammonia molecules has entered the storage ring, high voltages are abruptly applied to the outer two hexapole rods as indicated in Fig. 3.4. The separation between the different bunches at the entrance region of the storage ring is sufficiently large that only one selected bunch of decelerated molecules is captured. The molecules are detected after they have been stored in the ring for a certain time.

The inset to Fig. 3.10 shows the density of neutral ammonia in the detection region of the storage ring as a function of time after switching on the ring. After separately injecting each of the four selected bunches of molecules, the corresponding time-of-flight distributions after one round trip are measured. The measurements show that ammonia molecules in the velocity interval from 76 m/s to 110 m/s are captured in the ring with the settings as applied. Molecules that move significantly faster do not experience a force large enough to keep them in a circular orbit, whereas molecules that move significantly slower will be deflected too much by the repulsive outer wall of the ring, and either hit the inner hexapole rods or escape from the storage ring on the inside otherwise. With the settings that have been used, the injection efficiency is optimum for velocities around 89 m/s, where the potential well in the radial direction is deepest and hence more molecules can be captured. Fig. 3.11 shows the peak intensity of the ion signal for the first round trip ($t' = 8.76$ ms) as a function of the positive and negative high voltages on the outer ring electrodes. The dashed line indicates
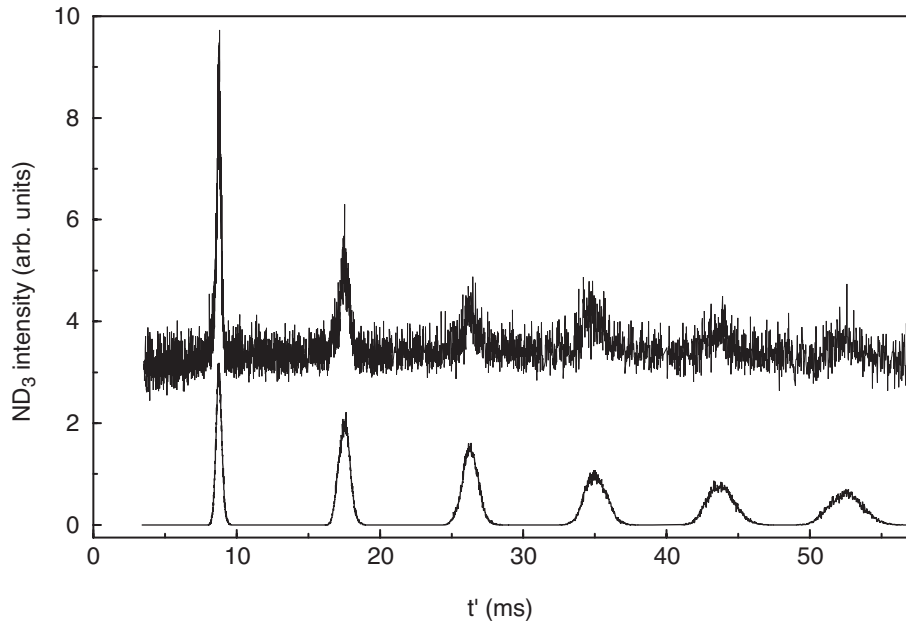
Figure 3.12: *Multiple round trips. The measurements shown in the upper trace show that bunches containing approximately a million ammonia molecules make up to six round trips in the storage ring. The package of stored molecules is seen to gradually broaden and to decrease in peak intensity, mainly due to the tangential velocity spread (dispersion). In the lower trace the results of Monte Carlo simulations, calculating trajectories of molecules through the whole experimental set-up, are shown. From the simulations a translational temperature of 10 mK is deduced for the stored bunch of molecules.*

the background level, which corresponds to the signal intensity at 0 kV. The point in the graph on the left is taken when the laser was blocked. The signal drops rapidly when the voltages decrease from +/- 8 kV to +/- 6 kV. Lowering the trapping voltages results in an increase of the equilibrium radius and in a shallower potential well, in which the molecules are less tightly confined. As a consequence, the density of molecules is lower and due to the reduced acceptance of the ring also less molecules are captured.

Upon making successive round trips the bunch of molecules spreads out gradually in the tangential direction as a result of the residual velocity spread. The experimental data in the upper trace of Fig. 3.12 demonstrate that a bunch of ammonia molecules with a velocity of 89 m/s can still be identified after it has made six round trips in the storage ring. The observed gradual broadening and decrease in peak intensity after each additional round trip is largely explained by the above-mentioned spreading out of the package along the ring, as substantiated by the results from trajectory simulations, shown in the lower

trace of Fig. 3.12. Loss of molecules from the storage ring by collisions with background gas could explain the observed faster decay of signal at early times after the gas pulse, when the background pressure is still rather high.

3.6 Conclusions

The storage ring experimentally demonstrated here can generally be used to confine polar neutral molecules. It has been shown that the motion of the molecules in the tangential direction and in the radial direction are coupled due to conservation of angular momentum. It is fundamentally impossible to operate the storage ring in isochronous mode without actively manipulating the tangential motion. Bunches of molecules can be stored in the ring over a wide range of tangential velocities and are detected for up to six round trips in the ring. This number is limited due to the residual spreading out of the package of molecules along the tangential direction. Reduction of the tangential velocity spread by means of a so-called buncher would enable the observation of more round trips.

Chapter 4

Longitudinal focusing and cooling of a molecular beam

4.1 Introduction

As discussed in the previous Chapters, a Stark decelerator can be used to decelerate pulsed beams of polar molecules to arbitrarily low velocities. Such molecular beams with a tunable absolute velocity, i.e., with a tunable de Broglie wavelength, offer fascinating perspectives for molecule optics [80, 81] as well as for collision studies [43]. The longitudinal velocity spread of these decelerated beams corresponds to a longitudinal temperature of several milliKelvin, only slightly higher than the lowest temperature He beam that has been reported [82]. Bunches of these slow and cold molecules can be stored in an electrostatic storage ring [36] or decelerated to a near standstill and trapped in an electrostatic quadrupole trap [21, 65].

In the molecular beam experiments, transverse collimation and focusing can be achieved by using electrostatic lenses, e.g., hexapole lenses and alternate gradient lenses for polar molecules in low-field seeking states and in high-field seeking states, respectively. To further increase the number density at a given point along the molecular beam axis, the molecular beam needs to be focused in the forward direction as well. Such 'spatial bunching' of the molecular beam is obviously advantageous for collision studies and can, for instance, be used to optimize the number of molecules loaded from the decelerated beam into an electrostatic trap. Spatial bunching is also highly desirable inside an electrostatic storage ring [36], as it will keep the package of molecules together in the forward direction. This will allow for instance observation of more round trips. To further reduce the longitudinal temperature of the beam, the forward velocity distribution needs to be 'focused'. Such a 'velocity bunching' keeps a package of decelerated molecules together for a longer period of time. This is highly

desirable in molecular beam diffraction studies, for instance, as it increases the phase contrast. The buncher provides us with a tool to manipulate the forward phase-space distribution of molecules. Together with hexapole lenses, that are used to manipulate the transverse phase-space distribution, the six-dimensional phase-space distribution can be manipulated.

In this Chapter we experimentally demonstrate the operation principle of a buncher for neutral polar molecules. In the buncher, a beam of polar molecules is exposed to an harmonic potential in the forward direction, i.e., along the molecular beam axis. This results in a uniform rotation of the longitudinal phase-space distribution of the ensemble of molecules. By switching the buncher on and off at the appropriate times, it can be used either to produce a narrow spatial distribution at a certain position downstream from the buncher or to produce a narrow velocity distribution. A reduction in the width of the spatial distribution is accompanied by an increase in the width of the velocity distribution, and vice versa, as the phase-space density remains constant in this process [55]. In the field of charged particle beams, where bunching-elements are routinely used, these operations are commonly referred to as re-bunching and bunch-rotation, respectively [83]. Proposals have been put forward to use time-varying magnetic fields for longitudinal focusing of atoms [84,85] and neutrons [86], both in real space and in velocity space. For atoms, where bunch-rotation is often referred to as 'δ-kick cooling', these operations have recently been experimentally demonstrated [87,88].

4.2   Experimental setup

The molecular beam machine that is used for the longitudinal focusing and cooling experiments is schematically depicted in Fig. 4.1. A beam of deuterated ammonia is formed by expanding a mixture of less than 1% $^{14}ND_3$ seeded in Xenon through a pulsed valve into vacuum. The valve is operated at a temperature of 200 K, resulting in an average velocity of the molecular beam of approximately 285 m/s. The relative velocity spread in the beam is typically 20%, corresponding to a longitudinal temperature of 1.5 K. Due to adiabatic cooling in the expansion, only the lowest rotational levels in the vibrational and electronic ground state are populated in the beam. Roughly 60% of all the ND_3 molecules in the beam reside in the $|J, K\rangle = |1, 1\rangle$ level, the ground-state level for para-ammonia molecules. For the experiments reported here, only ammonia molecules in the low-field seeking levels of the upper component of this inversion doublet are used. The molecular beam passes through a skimmer and enters the Stark decelerator, mounted in a second vacuum chamber. The 35 cm long decelerator consists of an array of 64 equidistant electric field stages. When the ammonia molecules in low-field seeking levels enter a region of high electric field (up to 90 kV/cm), they will gain Stark energy. This gain in Stark energy ('potential' energy) is compensated by a loss in kinetic energy. If the electric
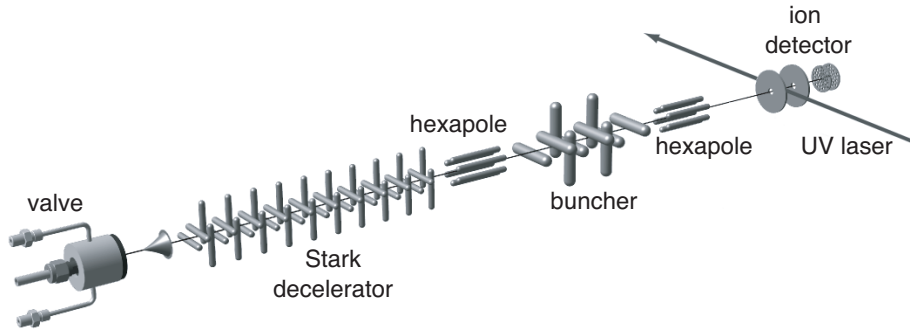
Figure 4.1: *Scheme of the experimental set-up. A pulsed beam of ammonia molecules is decelerated and passes through a buncher. The arrival time distribution of the package of molecules at the laser interaction zone is recorded using a UV-laser based ionization detection scheme.*

field is greatly reduced before the molecules have left this region, they will not regain the lost kinetic energy. This process is repeated by letting the molecules pass through the array of electric field stages, which are switched synchronously with the arrival of the package of decelerating molecules. The process in the Stark decelerator, the equivalent of a charged particle linear accelerator, can be viewed as slicing a bunch of molecules with both a narrow spatial distribution and a narrow velocity distribution (determined by the settings of the decelerator) out of the original beam, and decelerating these to arbitrarily low absolute velocities. In this process the phase-space density remains constant [76], and one can thus translate the high phase-space densities from the moving frame of the molecular beam to the laboratory frame. Detailed descriptions of the molecular beam machine and of the deceleration of ammonia using time-varying electric fields have been given in the previous Chapters.

4.3   Principle and design of the buncher

In the experiments reported here, the Stark decelerator is operated at a phase angle of 70° creating a 1 mm long bunch of ammonia molecules with an average forward velocity of 91.8 m/s and with a longitudinal velocity spread of about 6.5 m/s at the exit of the decelerator. The calculated longitudinal phase-space distribution of this initially prepared molecular beam is shown in Fig. 4.2 at $t = 0$ ms. This is the distribution relative to the position in phase-space of the synchronous molecule, at the moment that the decelerator is switched off. At this moment, the synchronous molecule is located on the molecular beam axis (z-axis) 0.6 mm upstream from the center of the last electric field stage of the decelerator, and is moving with a velocity of v_z=91.8 m/s along the z-axis. The entrance of the buncher is located some 15 cm downstream from the exit

of the decelerator. A 5 cm long hexapole is installed between the decelerator and the buncher. The hexapole is switched on for a few tens of μs once the package of ammonia molecules is completely inside it; the effective length of the hexapole is thus only a few mm. The hexapole maps the transverse phase-space distribution of the molecules in low-field seeking states from the decelerator onto the buncher. Of course, the forward phase-space distribution remains unchanged. In flying from the exit of the decelerator to the buncher the package of ammonia molecules spreads out along the molecular beam axis. This results in the elongated and tilted distribution in longitudinal phase-space as shown in Fig. 4.2 for $t = 1.743$ ms, the time that the buncher is switched on.

The buncher consists of an array of five electric field stages, with a center-to-center distance along the molecular beam axis of 11 mm. Each stage consists of two parallel cylindrical metal rods with a diameter of 6 mm, centered at a distance of 10 mm. One of the rods is connected to a positive and the other to a negative switchable high-voltage power supply. Alternating stages are connected to each other. As the electric field close to the electrodes is higher than that on the molecular beam axis, molecules in low-field seeking states will experience a force focusing them towards this axis. This focusing only occurs in the plane perpendicular to the electrodes. By alternately orienting the electric field stages horizontally and vertically, molecules are focused in either transverse direction.

When the synchronous molecule is exactly in between the first and second electric field stage of the buncher, the high voltage on the odd numbered electric field stages is switched on. The synchronous molecule is now on the downward slope of a potential well, and will be accelerated. When the synchronous molecule is 11 mm further, on the upward slope of the potential well, it is decelerated again to its original velocity. At this time the high voltage on the odd numbered stages is switched off. Molecules that are originally slightly ahead of the synchronous molecule, i.e., molecules that are originally faster, will spend more time on the upward slope than on the downward slope of the potential well, and are therefore decelerated relative to the synchronous molecule. Molecules that are originally slightly behind the synchronous molecule, i.e., molecules that are originally slower, will spend less time on the upward slope than on the downward slope of the potential well, and are therefore accelerated relative to the synchronous molecule. This process can be repeated, by switching on the high voltage on the even numbered stages when the odd numbered stages are switched off. Evidently, this can be done for a maximum of three times in our present buncher. The electric fields in the buncher are designed such, that the (series of) potential well(s) experienced by the ammonia molecules along the molecular beam axis is harmonic over an interval of approximately 1 cm around the minimum of the well. It is noted that the operation principle of the buncher is equivalent to that of the Stark decelerator at a phase angle of 0° [76]. The electrode geometry is in fact the same as the one of the decelerator except that it is scaled up by a factor two. This scaling-up increases the acceptance
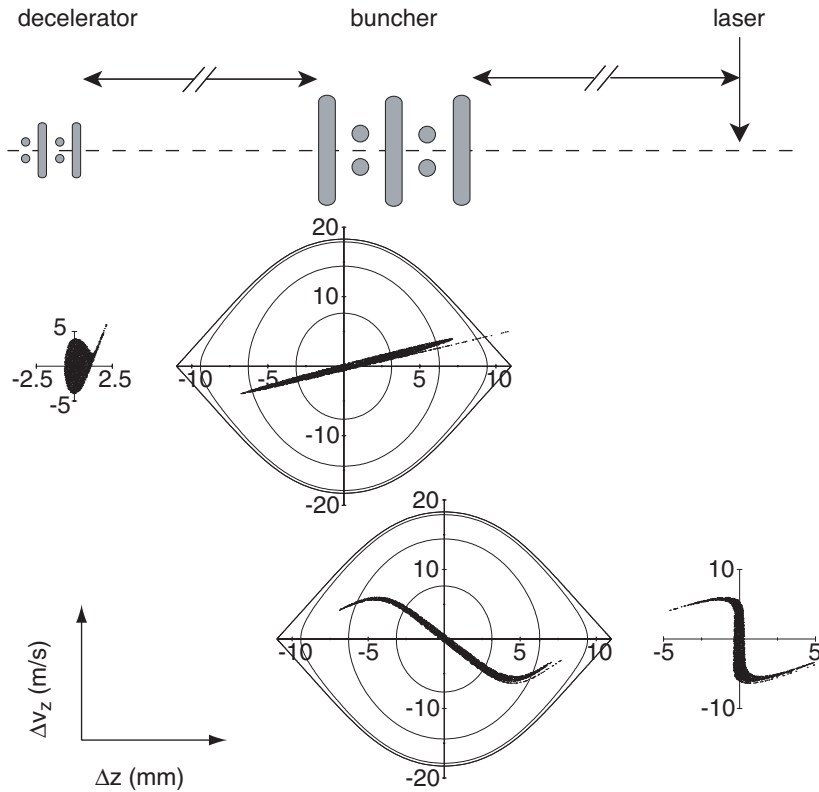
Figure 4.2: *Expanded view of the end of the decelerator, the buncher and the detection region. The calculated longitudinal phase-space distribution of the ammonia molecules is given at the exit of the Stark decelerator ($t = 0$ ms), at the entrance ($t = 1.743$ ms) and exit ($t = 2.100$ ms) of the buncher and in the laser detection region ($t = 2.652$ ms), relative to the position in phase-space of the synchronous molecule. Hexapoles are not shown in the figure.*

in position space by a factor of two but in momentum space the acceptance is reduced by a factor of two for the same voltages on the electrodes. The rotation frequency of the distribution in phase-space, given by Eq. (2.33), consequently changes as well. The a_1 coefficient is now 0.45 cm^{-1} and $L = 0.011$ m. At a phase angle of 0°, the rotation frequency is now 600 Hz.

4.4 Longitudinal focusing of a molecular beam

During the time that the buncher is on, the longitudinal phase-space distribution is rotated in the (z, v_z)-plane. The calculated distribution at $t = 2.100$ ms, i.e., at the time that the buncher is switched off, is shown in Fig. 4.2 for the case that a series of three potential wells is used in the buncher with voltages of +9.5 kV and -9.5 kV applied to the electrodes. In this figure, the contours of

equal energy for the ammonia molecules in the potential well are shown, relative to the position in phase-space of the synchronous molecule. It is seen that the rotation in phase-space is uniform, i.e., that the potential is harmonic, near the center and that the rotation is slower further outward, reaching zero at the separatrix. For optimum performance, the experiment has to be designed such that mainly the harmonic part of the acceptance diagram of the buncher is used. At the time that the buncher is switched off, slow molecules are ahead while fast molecules are lagging behind, leading to a longitudinal spatial focus further downstream. In the particular situation depicted in Fig. 4.2, the ammonia beam has a longitudinal focus with a width of about 0.5 mm, some 4.5 cm after the end of the buncher.

In the experiments the ammonia beam is probed either at a distance of 4.5 cm or at a distance of 33 cm downstream from the buncher. In the latter case, a second pulsed hexapole is used to transversely focus the ammonia beam exiting the buncher into the laser detection region. Using a (2+1)-resonance enhanced multi photon ionization scheme with a pulsed laser around 317 nm, $^{14}ND_3$ molecules in the upper component of the $|J, K\rangle = |1, 1\rangle$ inversion doublet are selectively ionized. Mass-selective detection of the parent ions is performed in a short linear time-of-flight set-up. The ion signal is proportional to the density of neutral ammonia molecules in the laser interaction region.

In Fig. 4.3 the measured time-of-flight (TOF) distributions for ammonia molecules over the 52.8 cm distance from the exit of the decelerator to the laser detection region (33 cm behind the buncher) are shown for various voltages on the buncher. The vertical scale is the same for all measurements, and the measurements are given an offset for clarity. With the buncher switched on for 239 μs, i.e., when two bunching stages are used, a longitudinal spatial focus is obtained with a voltage of +5.75 kV and -5.75 kV on the buncher. From the observed width of the TOF distribution a longitudinal spatial focus of about 2.0 mm is deduced; the magnification of the package exiting the decelerator is about a factor 2, which is what is expected with the thin-lens approximation for this geometry. With higher voltages, the beam is over-focused, resulting in a broader TOF distribution. Approximately 30 % of the molecules are within the full width half maximum of the TOF distribution when the buncher is operated at 5.75 kV. This is clear from the time-integrated signal of the bunched (5.75 kV) signal as shown in the upper graph of Fig. 4.3. In the inset, the measured TOF distributions recorded 4.5 cm behind the buncher (24.3 cm from the exit of the decelerator) and using three bunching stages are shown. A considerably tighter longitudinal spatial focus is now obtained with voltages of +9.5 kV and -9.5 kV on the buncher. The observed 6.0 μs width of the TOF distribution corresponds to a longitudinal spatial focus of approximately 0.5 mm; the calculated phase-space distributions for this particular situation are those shown already in Fig. 4.2. The observed TOF distributions are quantitatively reproduced in trajectory calculations, shown underneath the experimental data.
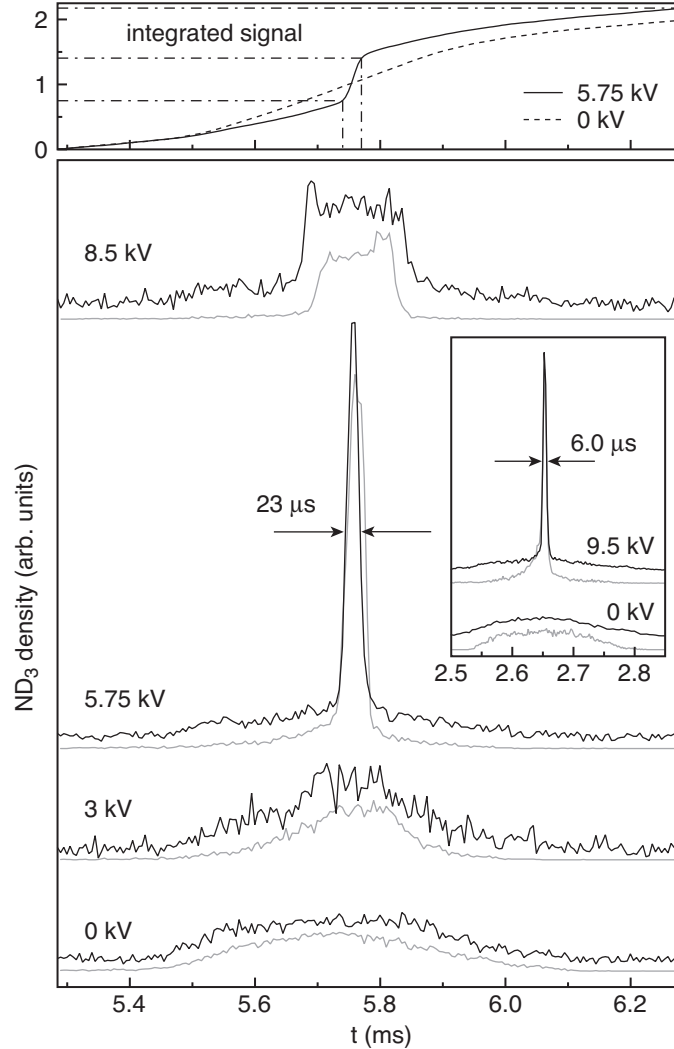
Figure 4.3: *Lower graph: density of ammonia molecules 33 cm behind the buncher as a function of time (at $t = 0$ ms the synchronous molecule is at the exit of the decelerator) for different voltages on the buncher, using two bunching stages. In the inset similar measurements recorded at a 4.5 cm distance behind the buncher, using three bunching stages, are shown. The results of trajectory calculations through the entire set-up are shown underneath the experimental data. Upper graph: integrated signals of bunched (5.75 kV) and unbunched (0 kV) molecular package.*

Figure 4.4: *Longitudinal width (FWHM) of the package of molecules as a function of the applied buncher voltage at 33 cm (circles) and 4.5 cm (triangles) behind the buncher. Arrow A indicates the voltage crossing at which the beam is in principle longitudinally collimated. Arrow B indicates the voltage crossing when there is a focus in between the two measurement positions. The situations at arrow A and arrow B are shown schematically in the lower part of the figure.*
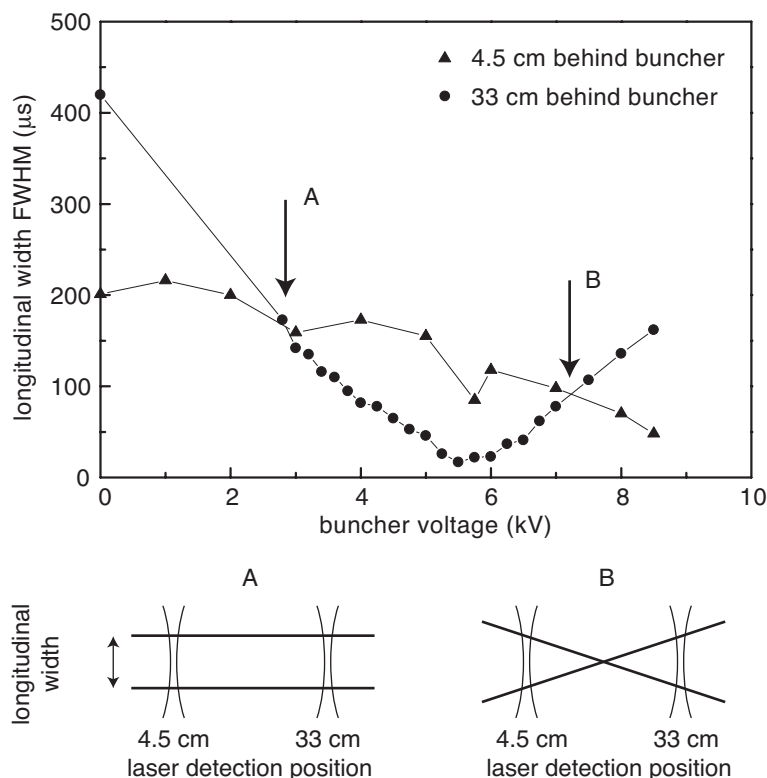
In Fig. 4.4 the widths (FWHM) of the measured TOF distributions are shown as a function of the applied buncher voltage. The data indicated with circles are measured 33 cm behind the buncher. The data indicated with triangles are measured 4.5 cm behind the buncher. The longitudinal spatial focus measured at 33 cm behind the buncher can be clearly observed in the corresponding set of measurements. The two sets of measurement points cross twice. At the voltages at which these crossings occur, the longitudinal width of the package of molecules is the same. For the higher voltage crossing, the package is spatially focused halfway between the two measurement positions at 4.5 cm and 33 cm behind the buncher. For the lower voltage crossing, the longitudinal velocity of the molecular beam is focused and the package of molecules hardly spreads out in the forward direction; the width is practically the same at both positions. The experimentally determined voltage settings where the two sets
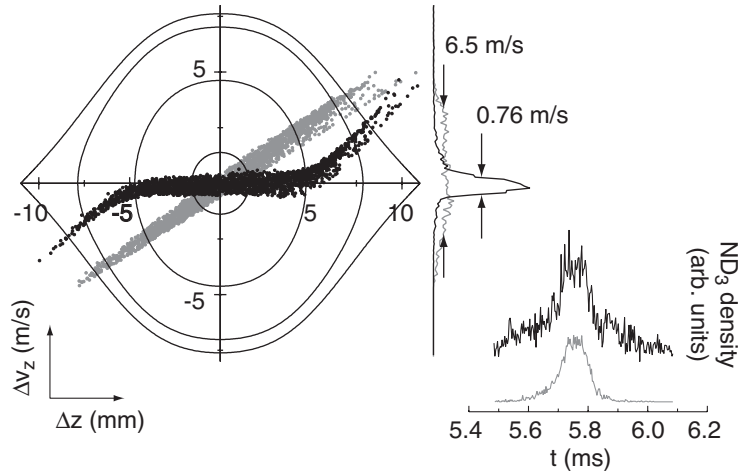
Figure 4.5: *Calculated longitudinal phase-space distribution at the moment that the buncher is switched on (t = 1.743 ms) and off (t = 1.982 ms) with voltages of +3.8 kV and -3.8 kV. The projections of the longitudinal velocity distributions on the v_z-axis are given for both cases. On the right hand side, the measured (upper trace) and calculated (lower trace) TOF distributions 33 cm behind the buncher are shown.*

of measurements cross for the first time enable thus to find the settings for the production of a package of molecules with the lowest possible longitudinal velocity spread. In turn, this corresponds to the lowest possible longitudinal temperature.

4.5   Longitudinal cooling of a molecular beam

It is evident from the description of the operation principle of the buncher that it is also possible to rotate the phase-space distribution of the bunch such that an elongated horizontal distribution is formed, i.e., that a focus is created in velocity space. The optimum settings for longitudinal cooling of the molecular beam follow directly from the experimentally determined settings for spatial focusing. In Fig. 4.5 the calculated longitudinal phase-space distribution is shown at the moment when the buncher is switched on and off. In this case two bunching stages are used, and voltages of +3.8 kV and -3.8 kV are applied.

These voltages are higher than those found from the measurements presented in Fig. 4.4. This is due to the difficulty in determining the longitudinal widths of the package of molecules close to the buncher. Near the buncher the TOF distribution is a convolution of the bunched part of the package of molecules with the unbunched part of the package. This unbunched part still has a large density directly behind the buncher and hence contributes much to the measured

longitudinal widths. This leads to an overestimate of the width of the bunched part of the package of molecules.

The projection of the phase-space distribution onto the vertical axis after bunch-rotation gives a longitudinal velocity distribution with a full width at half maximum of 0.76 m/s. This corresponds to a record-low longitudinal temperature of our molecular beam of 250 μK. The measured and calculated TOF distributions 33 cm behind the buncher are shown in the figure as well.

4.6 Conclusions

We have demonstrated a buncher for longitudinal focusing and cooling of a beam of neutral polar molecules. Tighter spatial focusing and/or further longitudinal cooling can be achieved by properly scaling and positioning the buncher. When this buncher is used in combination with electrostatic multipole lenses, full six-dimensional phase-space matching of one element onto another, for instance, of a molecular beam exiting a decelerator into a trap or storage ring, is possible.

Chapter 5

Dynamics of neutral molecules stored in a ring

5.1 Introduction

In the experiments reported in this Chapter, a package of ammonia molecules in a single ro-vibrational state and spatially oriented, is decelerated and focused and subsequently forced in circular orbits. The absolute velocity, as well as the width of the velocity distribution, of the package of molecules is under computer control, and these experiments thereby serve as a demonstration of the level of control over neutral molecules that can nowadays be achieved.

The buncher as described in the previous Chapter is used to decrease the longitudinal (tangential) velocity spread of the package of molecules prior to injecting them in the ring. The density of the package of molecules in the ring therefore drops less quickly than in the injection scheme without a buncher. Furthermore, by properly matching the transverse emittance of the Stark decelerator onto the transverse acceptance of the ring with hexapole lenses, molecules are coupled into the ring more efficiently, resulting in more observable round trips than in previous experiments as reported in Chapter 3. Together, the buncher and hexapoles enable us to control the full six-dimensional phase-space distribution of the package of molecules entering the ring: with the buncher we can control the longitudinal phase-space distribution while with the hexapole we can independently control the transverse phase-space distribution.

5.2 Experimental setup and alternative bunching scheme

The setup, consisting of the injection beamline and the storage ring, is depicted schematically in Fig. 5.1. The storage ring and the improved beamline have been described in detail in Chapters 3 and 4, respectively. Briefly, a beam of deuterated ammonia is formed by expanding a mixture of less than 1% $^{14}ND_3$ seeded in Xenon through a cooled pulsed valve (-70 °C) into vacuum. The molecular beam has a velocity of approximately 285 m/s and a longitudinal temperature of about 1.5 K. Due to the adiabatic expansion roughly 60% of all the $^{14}ND_3$ molecules in the beam reside in the $|J, K\rangle = |1, 1\rangle$ inversion doublet, the ground-state level for para-ammonia molecules.

After the beam has passed through a skimmer into a second vacuum chamber the ammonia molecules in low-field seeking states of the upper level of the inversion doublet are transversely focused with a pulsed electrostatic hexapole lens into the Stark decelerator. The package of molecules is decelerated to 91.8 m/s for the experiments described here.

At the exit of the decelerator the calculated longitudinal phase-space distribution is $[\Delta z \times \Delta v_z] = [1.1 \text{ mm} \times 5.9 \text{ m/s}]$ and the transverse phase-space distributions are $[\Delta x \times \Delta v_x] = [\Delta y \times \Delta v_y] = [1.0 \text{ mm} \times 5.0 \text{ m/s}]$, where z lies along the molecular beam axis. Here the position spread and velocity spread are the full widths at half maximum (FWHM) of a fitted Gaussian distribution. The transverse phase-space distribution is mapped onto the acceptance of the ring using a telescope of two electrostatic hexapole lenses. The acceptance of the ring is in fact set by the vertical (y) and radial (r) eigenfrequencies of the potential well which are numerically found as $f_y = 390$ Hz and $f_r = 910$ Hz near the minimum of the well for the voltage settings used. The relation between the frequency f_s, the accepted position spread Δs, and the accepted velocity spread Δv_s is given by $\Delta v_s = 2\pi f_s \Delta s$. The potential well shown in Fig. 5.1 contains both the Stark energy and the quasi-potential centrifugal energy for molecules moving in circular orbits with a tangential velocity of 91.8 m/s. It is evident from the equipotential lines in Fig. 5.1 that the potential well is asymmetric in the dipolar configuration that we have used. To load the ring the hexapoles rotate the transverse phase-space distribution of the molecules uniformly such that it matches the vertical acceptance of the ring, because in this direction the potential well is the shallowest. For this, the hexapoles are switched on for only a few tens of microseconds, corresponding to an effective length of a few millimeters for molecules moving with a velocity of 91.8 m/s. As explained in Chapter 4, the buncher creates an harmonic potential well that rotates the longitudinal phase-space distribution until the longitudinal velocity spread has been minimized. The buncher and the hexapoles are offset by a few hundred volts, creating a sufficiently large residual electric field to prevent Majorana transitions. In addition, possible transitions between low-field seeking and non-
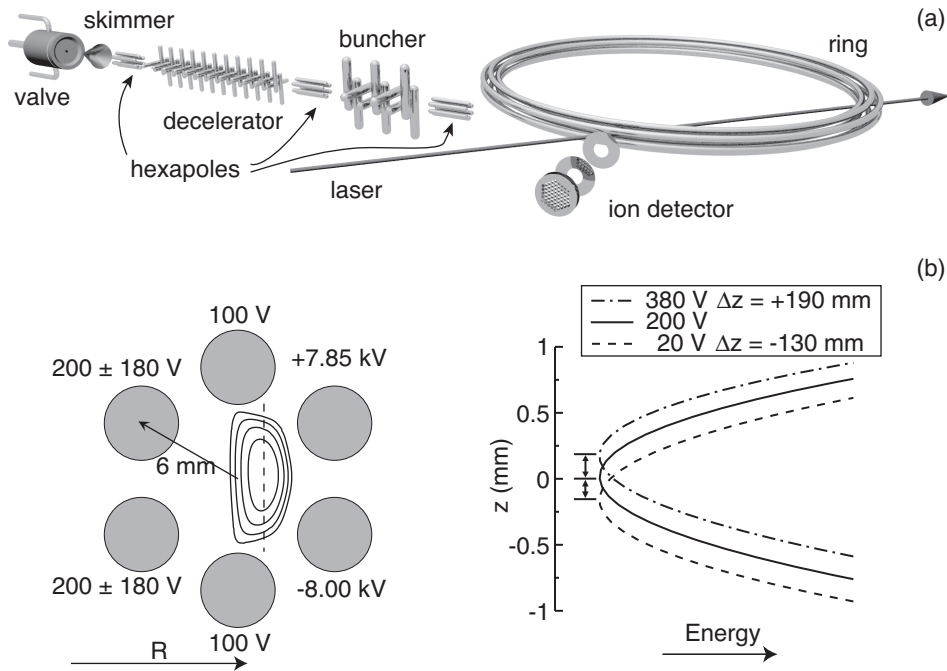
Figure 5.1: *(a) Scheme of the experimental set-up. The injection beamline consists of a pulsed valve, a Stark decelerator, hexapoles, and a buncher. (b) The molecules are trapped in a 2-dimensional potential well. The center of the ring is to the left. Equipotential lines are shown at 0.02 cm^{-1} intervals. Molecules are detected in the ring using a UV-laser based ionization detection scheme. The inset shows the vertical position of the potential well along the equilibrium radius for three values of the (AC modulation) voltage on the inner ring electrodes.*

low-field seeking hyperfine levels that can be induced by rapid switching of the high voltages, are avoided by this offset field as well.

Here, we describe and demonstrate an alternative bunching scheme. In the bunching method as detailed in the previous Chapter, the length of the longitudinal potential well was kept constant while the amount of rotation of the molecules in longitudinal phase-space was controlled by adjusting the force constant. The latter was accomplished by varying the voltages applied to the buncher electrodes. The advantage of this method is that the time intervals between switching can be kept constant; these are simply the length of the buncher stage divided by the velocity of the synchronous molecule. It is often easier to adjust a voltage than adjusting several timings.

In the experiment described here, the hexapoles before and behind the buncher and the buncher itself are electrically connected to the same positive voltage power supply. In this case only one voltage setting can be used and hence the timings for the buncher and hexapoles have to be adjusted in order to
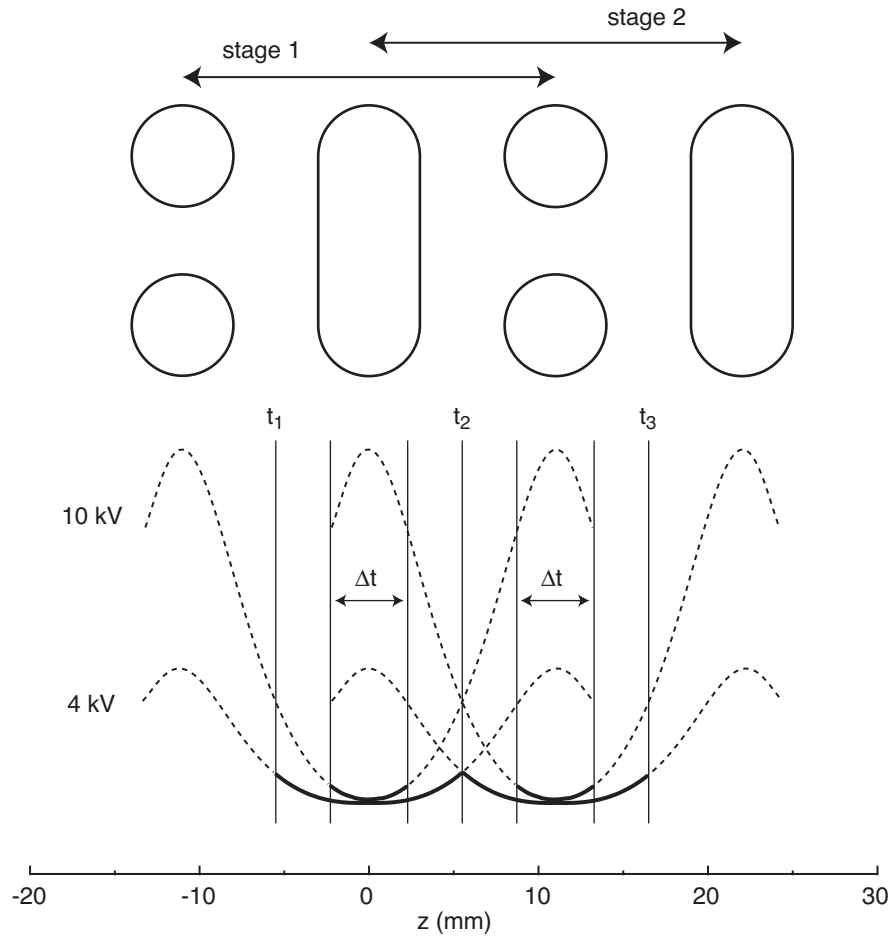
Figure 5.2: *Comparison of the longitudinal potential wells and their duration for the two bunching methods. In the figure the potential wells (thick lines) and the timings for longitudinal cooling are shown for the synchronous molecule. The position of the buncher electrodes is schematically shown above the potential wells. In the bunching method demonstrated in Chapter 4, stage 1 of the buncher is switched on at t_1. At t_2 stage 1 is switched off and stage 2 is switched on until t_3. In the alternative bunching method an extra time delay is added/substracted to the timings, shortening the length of the 10 kV potential well symmetrically around its minimum to Δt.*

obtain good longitudinal and transverse focusing, respectively. The hexapoles operate optimally at high voltages as has been discussed in Chapter 2. The voltages applied to the buncher that are necessary for longitudinal cooling, though, are only +4/-4 kV[1]. Hence, in this case the voltage difference between the rods of the hexapoles is only 4 kV and the nonlinearity in the focusing properties of the hexapoles due to the inversion splitting is more pronounced. By operating the hexapoles, and therefore also the buncher, at fixed high voltages of +10/-10 kV, the electric fields are sufficiently high such that the nonlinearity due to the inversion splitting can be neglected. This means however, that in the buncher the longitudinal phase-space distribution always rotates with a fixed angular frequency. Now, by shortening the longitudinal potential well of the buncher symmetrically around its minimum by adjusting the switching times, i.e., by adding and subtracting time-delays symmetrically around the original timings, it is possible to alter the angle over which the longitudinal phase-space distribution of the molecules rotates. The potential well is then switched on for a time duration Δt as shown in Fig. 5.2. In this way it is also possible to longitudinally cool a package of molecules. Fig. 5.3 shows the distributions of molecules in phase-space at different positions along the beamline in case of longitudinal cooling. It should be noted that by shortening the potential well in the buncher, the molecules will fly freely in between the potential wells. As free flight is a linear transformation this will not lead to an increase in effective phase-space volume.

The bunching scheme, in which the buncher is operated at constant voltage and variable duration, is compared with the bunching scheme, in which the buncher is operated at constant duration and variable voltage. We will refer to these bunching schemes from now on as f(t)-bunching and f(V)-bunching, respectively. First, we will discuss rebunching; the longitudinal spatial focusing of a molecular beam. Fig. 5.4 shows the recorded $^{14}\text{ND}_3$ parent ion signal at the detection position in the storage ring as a function of the time after the synchronous molecule has exited the decelerator. The ion signal is a measure of the ammonia density at the given time. Fig. 5.4(a) shows the time-of-flight distribution when the buncher is operated with the f(t)-bunching scheme. The voltages on the buncher electrodes are fixed to +10/-10 kV and the time, during which the buncher is on, is set to $\Delta t = 88.1$ μs. With these settings a longitudinal spatial focus is created at the detection position in the storage ring. Fig. 5.4(b) shows the time-of-flight distribution when the buncher is operated with the f(V)-bunching scheme. In this case the molecular beam is longitudinally focused at the detection position in the ring when voltages of +7.5/-7.5 kV

---

[1]It should be noted that this is 200 V more than what was stated in Chapter 4. The reason for this is that in the experiments described in Chapter 4, it was very difficult to determine the spreading out of the molecular package as in the measurements close to the buncher, the unbunched part of the package swamped the bunched part. Now, in the storage ring the spreading out of the package is easier to follow and the optimum voltage settings can be determined more accurately.
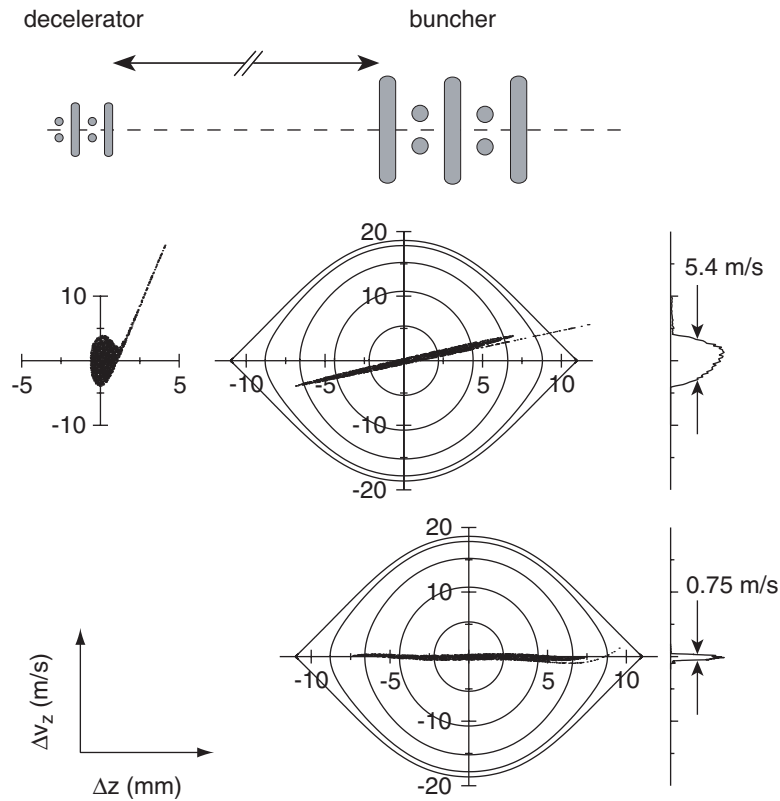
Figure 5.3: *Calculated longitudinal phase-space distributions of a package of $^{14}ND_3$ molecules are given at the exit ($t = 0$ ms) of the Stark decelerator, at the entrance ($t = 1.778$ ms), and at the exit ($t = 1.946$ ms) of the buncher, relative to the position in phase-space of the synchronous molecule. The potential well in each buncher stage is switched on for a duration $\Delta t = 49.1$ μs. Two buncher stages are used in this calculation to rotate the package of molecules in phase-space.*

are put on the buncher electrodes. It is immediately clear that there is little difference between the two bunching schemes. The longitudinal widths (FWHM) of the molecular package obtained from a Gauss fit are practically the same: $\Delta t_{f(t)} = 35.8 \pm 0.6 \mu s$ vs. $\Delta t_{f(V)} = 38.5 \pm 0.7 \mu s$, in Fig. 5.4(a) and Fig. 5.4(b), respectively. The peak position and the peak signal intensity are also practically the same for both cases. The f(t)-bunching scheme apparently works equally well as the f(V)-bunching scheme.

The main use of the buncher in between the decelerator and the storage ring is that it can be used for bunch rotation, i.e., for longitudinal cooling of the molecular beam prior to injection in the storage ring. To be able to accurately determine the width of the velocity distribution as produced by the buncher, a measurement of the time-of-flight profile needs to be done in the far
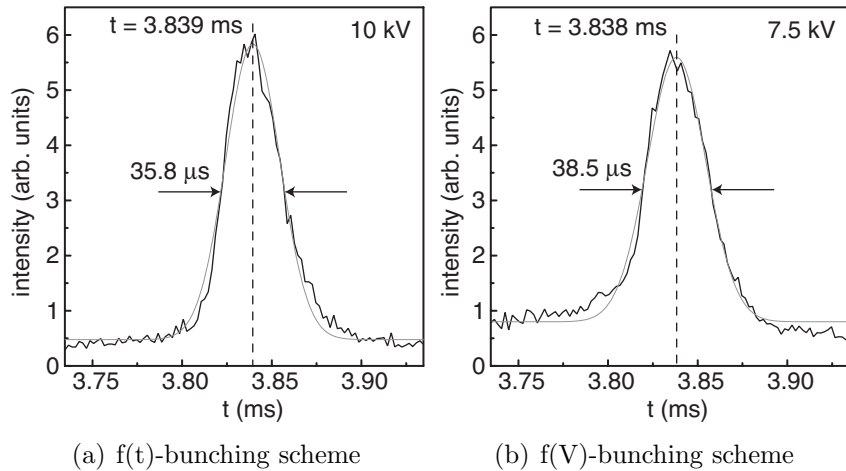
(a) f(t)-bunching scheme
(b) f(V)-bunching scheme

Figure 5.4: *Rebunching: longitudinal spatial focusing of a molecular beam. Time-of-flight distributions obtained with f(t)-bunching scheme (a) and f(V)-bunching scheme (b). The measured $^{14}ND_3$ parent ion signal is plotted as a function of time, where $t = 0$ is the moment when the synchronous molecule exits the decelerator. Peak positions as well as FWHM of the distributions are indicated.*

field, as far away from the exit of the buncher as possible. Only in that case can it be assumed that the observed width of the time-of-flight distribution is dominated by the velocity spread of the package of molecules and the initial spatial spread of the package can be neglected. Therefore, it is best to perform this measurement after many round trips in the storage ring. In the next Section such a measurement, using the f(t)-bunching scheme, is presented.

Due to the limited opening angle of the entrance slit of the ring, a part of the package of molecules is cut off by the outer pair of electrodes. The numerically calculated phase-space distribution of the package of molecules entering the ring is given by $[\Delta r \times \Delta v_r] = [2.3$ mm $\times 2.5$ m/s$]$, $[\Delta y \times \Delta v_y] = [1.4$ mm $\times 1.4$ m/s$]$, $[\Delta z \times \Delta v_z] = [9.5$ mm $\times 0.64$ m/s$]$ for the f(t)-bunching scheme.

After the molecules have entered the 25-cm diameter electrostatic storage ring, the two outer ring electrodes are rapidly (< 100 ns) switched to high voltages. This creates an electric field that delivers the centripetal force on the molecules. Just prior to detection the high voltages on these electrodes are switched off again. Then the ammonia molecules are ionized in a 2+1 resonance enhanced multi-photon ionization (REMPI) process, using 317 nm radiation. The UV-light is focused and only molecules in the approximately 3 mm long, 100 μm diameter beam waist are detected. The ions are repelled from the storage ring by the residual electric field created by the permanently present 200 V and 100 V on the inner and middle ring electrodes, respectively, and are then detected with a linear time-of-flight mass spectrometer.
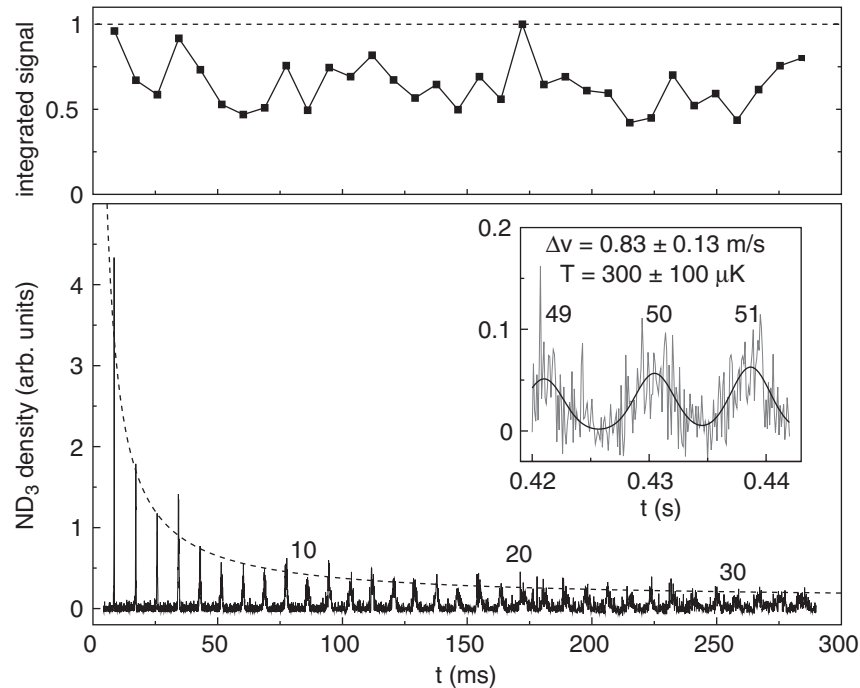
Figure 5.5: *The solid line in the lower graph shows the ammonia density at the loading position in the ring as a function of storage time. The dashed line is a 1/t plot, used to guide the eye. In the inset, a measurement of the ammonia density after 49–51 round trips is shown, together with a multi-peak Gaussian fit, from which a longitudinal temperature of $300 \pm 100 \ \mu K$ is deduced for the package of molecules in the ring. The upper graph shows the time-integrated signal after each round trip.*

5.3 Longitudinal temperature of molecules in the ring

Fig. 5.5 shows the recorded $^{14}ND_3$ parent ion signal as a function of the storage time in the ring; the origin of the time axis is at the time when the high voltages on the ring are switched on. Each data point represents the parent ion signal intensity averaged over 20 laser shots, i.e., averaged over 20 subsequent deceleration, loading and detection cycles. The experiment normally runs at a 10 Hz repetition rate. However, for the measurements that exceed 100 ms storage times in the ring the repetition rate is reduced; the laser system still runs at 10 Hz, but the effective repetition rate is reduced using a mechanical shutter. The peaks in the signal indicate the passage of a package of molecules through the laser focus. In Fig. 5.6 the center positions, determined by Gauss fits, of the first 18 peaks are plotted as a function of the round trip number. From the slope of a linear fit the round trip time can be derived, which is
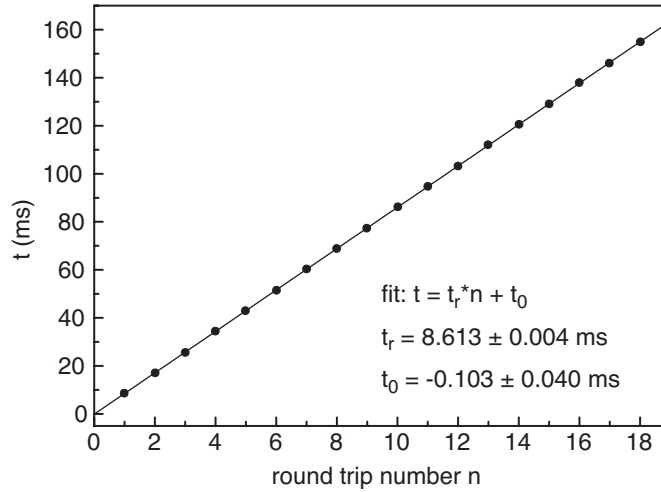
fit: $t = t_r{}^*n + t_0$

$t_r = 8.613 \pm 0.004$ ms

$t_0 = -0.103 \pm 0.040$ ms

Figure 5.6: *The center positions of the first 18 peaks are plotted as a function of the round trip number n. A linear fit (solid line) yields a value for the round trip time of $t_r = 8.613 \pm 0.004$ ms. The offset $t_0 = -0.103 \pm 0.040$ ms is caused by the delay between the arrival time of the decelerated package in the detection region of the storage ring and the moment when the ring is switched on.*

$t_r = 8.613 \pm 0.004$ ms. For a tangential velocity of 91.8 m/s and a corresponding equilibrium radius of $r'_0 = 1.3$ mm the round trip time is theoretically expected to be 8.645 ms. The discrepancy with the experimental value can be attributed to the uncertainty in the tangential velocity and in the radial position at which the package of molecules is coupled into the ring. The offset $t_0 = -0.103 \pm 0.004$ ms is caused by the fact that the ring is switched on ≈ 0.1 ms later than the arrival time of the decelerated package in the detection region of the storage ring. This delay was experimentally determined during the optimization of the round trip peak signals in the ring and probably indicates a less than perfect phase-space matching of the molecular beam emittance onto the acceptance of the ring. It is seen that the peak intensity after each round trip gradually decreases while the width of the peaks increases. This is a result of the residual tangential velocity spread of the package of molecules in the ring. Molecules with a tangential velocity of 91.8 m/s traverse the ring at the equilibrium orbit, which is a distance $r = 1.3$ mm away from the center of the hexapole geometry. Faster molecules orbit the ring at a larger radius and hence have a longer flight path; slower molecules orbit at a smaller radius and hence have a shorter flight path. This difference in flight paths between faster and slower molecules counteracts the longitudinal spreading out of the molecular package. As the relative change in orbit radius is small, however, this

effect is very limited in the present case[2]. Therefore the tangential spreading out of the package in the ring can be approximated very well by the longitudinal spreading out of a package in linear free flight. The time-spread of the signal at the n-th round trip is given by $(1/v)\sqrt{(\Delta z_0)^2 + (n\Delta v_0 t_r)^2}$, where Δz_0 is the initial longitudinal position spread, v the average velocity, and Δv_0 the longitudinal velocity spread. Without further losses from the ring, the peak density is inversely proportional to this width. When the initial position spread can be neglected, this implies an expected $1/n$ behavior for the peak intensities, as indicated with the dashed line in Fig. 5.5.

It is seen that the peak heights actually do not decrease monotonically. This is explained by the two-dimensional oscillatory motion of the package of molecules in the ring in combination with the position sensitive detection scheme. The oscillatory motion can be particularly prominent when there is a slight transverse phase-space mismatch when the molecules are injected into the ring. In the upper graph of Fig. 5.5 the time-integrated signal for each round-trip is shown. This signal clearly shows the relatively large intensity fluctuations just discussed, but it is also seen that, on average, the signal remains practically constant. Loss due to collisions with background gas can be neglected as the background pressure in the ring chamber is 10^{-9} mbar, corresponding to an anticipated 1/e decay time of several seconds. Furthermore, in the electric field geometry used in this experiment, the molecules are never in zero electric field so zero-field crossing (Majorana) transitions are avoided.

The inset of Fig. 5.5 shows the signal after 49, 50, and 51 round trips. The molecules have then been stored in the ring for about 0.43 s, corresponding to a total flight path of more than 40 m. It is seen from the data that the package of molecules has stretched out so far that it fills about half the ring, i.e., its FWHM length has become about 40 cm. A longitudinal temperature can be deduced from the relative temporal width of the signal from the 50th round trip. After such a long flight distance, the contribution of the initial position spread to the width can be neglected, and the relative temporal width is in a good approximation equal to $\Delta v/v$. From the multi-peak Gaussian fit of the data (dark solid line), in combination with the known 91.8 m/s tangential velocity of the molecules, the absolute longitudinal velocity spread is found as 0.83 ± 0.13 m/s. This corresponds to a longitudinal temperature of 300 ± 100 μK, in close agreement with the numerically calculated value at the entrance of the ring.

This value for the longitudinal velocity spread is obtained with the f(t)-bunching scheme and is almost identical to the value of 0.76 m/s found in Chapter 4 when the buncher is operated with the f(V)-bunching scheme.

---

[2]Isochronous operation of the ring, where the longitudinal spreading out is completely cancelled, is fundamentally impossible as discussed earlier (see page 41).
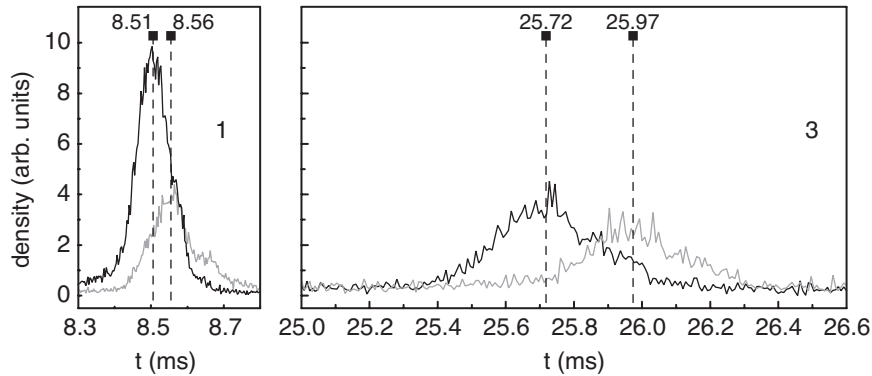
Figure 5.7: *Time-of-flight distributions of molecules in the ring for the first and the third round trip. The distributions in black are obtained with +8/-8 kV on the outer ring electrodes while the distributions in gray are obtained with +6/-6 kV on the outer ring electrodes. The vertical dashed lines indicate the centers of the peaks as obtained by fitting the peaks to Gaussian distributions. Horizontal scale and vertical scale are the same for both graphs.*

5.4 Effect of potential well strength on round trip time

As shown in Chapter 3 the equilibrium radius and hence the orbit time depends strongly on the electric field that delivers the confinement force. If the voltages on the ring electrodes are lowered then the transverse trapping potential well widens and the equilibrium radius, as well as the orbit time of the molecules, will increase given a fixed forward velocity. In Fig. 5.7 the recorded ND_3 parent ion signal is shown as a function of the storage time in the ring for the first and the third round trip. Each round trip is measured at two different voltage settings: +6/-6 kV and +8/-8 kV on the outer ring electrodes. Interestingly, while the peak density on the third round trip for the 8 kV setting is about half as large as the peak density at the first round trip, the peak density at the third round trip for the 6 kV setting is almost as large as the peak density at the first round trip. This is the result of the position sensitive detection method and a slight mismatch of the emittance of the molecular beam onto the acceptance of the storage ring, as will be discussed in Section 5.5.

It is seen from Fig. 5.7 that with the 8 kV setting the package of molecules arrives earlier than with the 6 kV setting: on average the time difference is 97 μs as deduced from fitting the peaks with Gaussians. This is a difference of about 1% in round trip time; the average round trip times are 8.61 ms and 8.71 ms for the 8 kV and 6 kV setting, respectively. As the molecules have the same tangential velocity of 91.8 m/s for both settings, it is possible to

calculate the difference in the equilibrium radii: $r'_{8kV} = 0.7$ mm and $r'_{6kV} = 2.2$ mm. This corresponds roughly to the calculated values of 1.3 mm and 1.9 mm. The discrepancy is most likely attributed to the difference between the design diameter of the ring and the actual diameter.

5.5 Observation of vertical betatron oscillations

The collective, transverse motion of the molecules in the ring can be excited by applying an AC voltage on top of the 200 V DC voltage on the inner ring electrodes. This leads to an oscillatory motion of the potential well, which, for the electric field configuration used, is almost exclusively in the vertical direction, as shown in Fig. 5.1. In the experiment, the vertical motion of the package of molecules is driven by a two-period sine-wave with an amplitude of 180 V and with a period of $t = 2.56$ ms. This modulation is started at a variable time t_{start} after the molecules have entered the ring, which is at $t = 0$. In the upper graph of Fig. 5.8 the density of ammonia molecules in the ring after ten round trips, i.e., after the molecules have been in the ring for 86 ms, is shown as a function of the time when the AC modulation starts (relative to the switching on of the ring). Each data point represents the averaged signal over 30 laser shots and is proportional to the ammonia density. The ammonia density in the laser detection area after these 10 round trips shows a strong modulation, the equivalent of a vertical betatron oscillation in charged particle storage rings. In our experimental set-up the tightly focused detection laser crosses the ring in the horizontal plane, and vertical oscillations are therefore more readily detected than radial oscillations. Although the AC modulation voltage shakes the potential well only roughly 160 μm up and down from the vertical equilibrium position, the driven vertical oscillation of the molecules is calculated to lead to an amplitude of about 1 mm. It is seen from the measurements that even when the AC modulation is induced during the first round trip, the package of molecules coherently oscillates in the vertical direction after 10 round trips. From these measurements, the eigen-frequency for the vertical oscillation in the ring can be accurately determined.

In the lower graph of Fig. 5.8 a Fourier transformation of the data is shown. The main peak in the frequency spectrum is found at 373 Hz, with a shoulder at 413 Hz, and the first overtone of this peak is visible as well. Also shown in this figure is the frequency spectrum of the two-period sine-wave (dashed), which is set to drive the fundamental vertical oscillation. The experimentally determined value of 373 Hz for this oscillation frequency is close to the calculated value of f_y=390 Hz. If detection were to be performed exactly at the center of the vertical motion, the package of molecules would pass the laser focus twice per oscillation and only the overtone would be observed. If the laser detection region would be at an extremum of the vertical motion, only the fundamental frequency would appear. The actual relative intensities of these
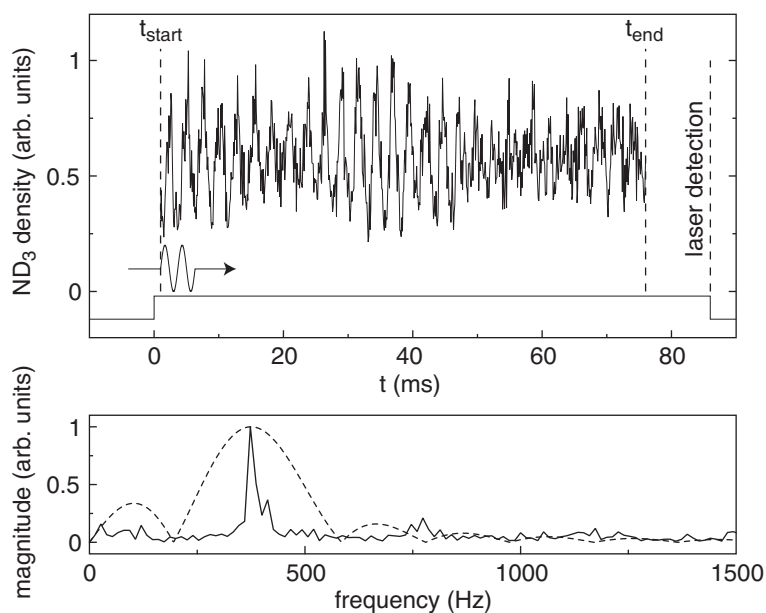
Figure 5.8: *The upper graph shows the density of ammonia molecules in the ring after 10 round trips as a function of the start time of the AC voltage modulation. The modulation signal is a two-period sine-wave with a period of $t = 2.56$ ms. The starting point of this modulation signal is scanned stepwise from t_{start} to t_{end}. The block pulse indicates the time that the molecules are confined in the ring. A Fourier transformation of the data is shown in the lower graph (solid curve) together with the frequency spectrum of the two-period sine-wave (dashed curve).*

two frequency components in the spectrum therefore depends on the details of the alignment of the laser relative to the ring as well as of the coupling of the injection beam-line to the ring. The envelope of the modulation of the ammonia density appears like a typical beating pattern, indicative of coupled motion at closely spaced oscillation frequencies. In the Fourier transformation this shows up as the 413 Hz shoulder of the main 373 Hz resonance. It turns out that, rather than being due to typical beating, the intensity of the envelope of the modulation correlates with the intensity of the corresponding time-integrated signal shown in the upper graph of Fig. 5.5; the vertical oscillation of the package of molecules shows the largest modulation depth in the detection region when this oscillation is initiated at a time when the package has the best overlap with the detection region.

Numerical calculations were performed trying to simulate the oscillatory signal of Fig. 5.8. It turned out to be practically impossible to fit the measured data. The main reason for this is that the detection of the molecules is very position sensitive. In the experiment it is practically impossible to determine

the exact detection position and hence it is difficult to find the right parameter settings for the simulations.

5.6   Effect of trapping voltage on ring dynamics

In the storage ring experiments described in the previous Section the potential well is rather nonlinear and asymmetric. Nonlinearity leads to a decrease of effective phase-space density and coupling between the radial and vertical motion of the molecules stored in the ring. Asymmetry leads to different betatron oscillation frequencies for the radial and vertical direction, which together with the nonlinear coupling leads to complex oscillatory behavior of the molecules in the ring.

The linearity and symmetry of the potential well of the storage ring can be improved by approximating the ideal hexapole electric field. An additional advantage is that the potential well does not open up at the inside of the ring, as is the case for the potential well of the dipole ring. This makes the storage ring suitable for molecules with low tangential velocities which would otherwise escape at the inside of the ring. Furthermore, an hexapole field with the same potential well strength as the field in the dipole ring can be obtained at lower voltages. A disadvantage of the hexapole field geometry is the existence of a zero electric field in the ring where the molecules can undergo Majorana transitions to untrapped states, after which they would be lost from the ring. However, as the equilibrium radius of the molecules is about 2 mm away from this zero field and as the amplitude of the betatron oscillation is not large, it is unlikely that these Majorana transitions will occur.

In this Section the effect of the trapping voltages on the dynamics of the molecules inside the hexapole ring is investigated. Altering the voltages leads to a change in betatron oscillation frequency.

The voltages on the ring electrodes for the hexapole configuration are shown in Fig. 5.9. The high voltages $HV1$ and $HV2$ are used for trapping of the molecules and are switched off for the ion extraction. The hexapole field is best approximated when $HV2 \approx HV1 + 360$ V, as is found from calculations using Simion [72].

The same injection beamline and detection scheme is used as for the dipole ring experiments. Only the timings of the hexapoles in front of and behind the buncher are adjusted to match the emittance of the molecular beam onto the slightly different acceptance of the hexapole ring. To detect the molecules, the voltages on the ring electrodes are switched to 0 V, 100 V, or 200 V as indicated in Fig 5.9. This creates an electric field that pushes the laser produced ions out of the ring towards a time-of-flight mass spectrometer. This detection scheme for deuterated ammonia molecules has been outlined in Chapter 3.

The effect of the trapping voltages on the motion of molecules in the ring is quite strong. Fig. 5.10 shows the $^{14}ND_3$ density as a function of the storage time
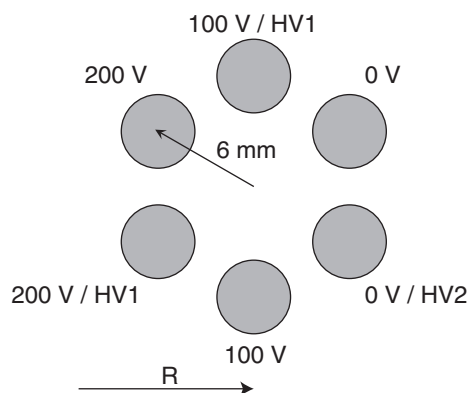
Figure 5.9: *Cross section through hexapole storage ring. Voltages on the ring electrodes are shown for the hexapole configuration. For the electrodes that are switched between two voltages both voltages are indicated.*
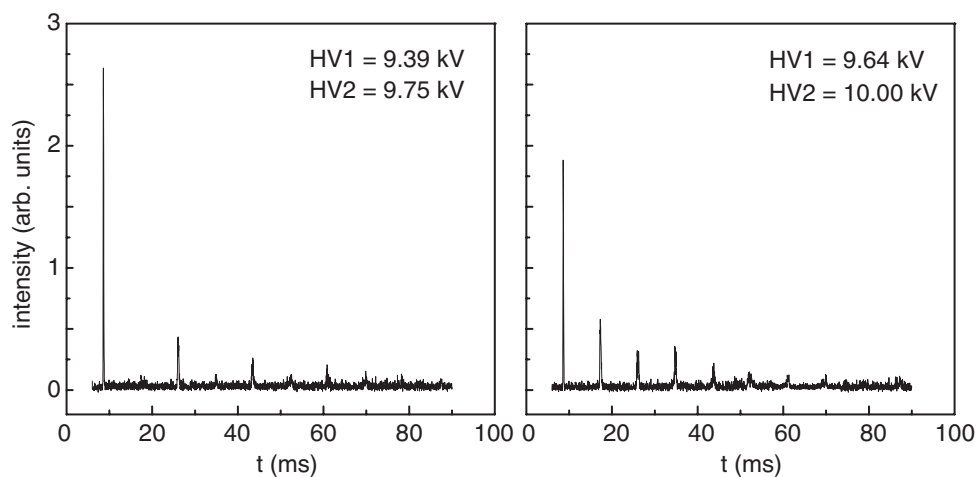
Figure 5.10: *Ammonia density in the hexapole storage ring as a function of the storage time t, shown for two different high voltage settings: left graph (HV1, HV2) = (9.39,9.75) kV and right graph (HV1, HV2) = (9.64,10.00) kV. Horizontal and vertical scales are the same for both graphs.*

in the ring for two different voltage pair settings $(HV1, HV2)$. The left graph shows the signal for $(HV1, HV2) = (9.39, 9.75)$ kV and the right graph shows the signal for $(HV1, HV2) = (9.64, 10.00)$ kV. Compared to the measurements performed with the dipole ring, the signal drops much faster over time. Now, the tenth round trip is hardly visible. As the buncher settings are the same in both cases, this is most likely explained by mismatching of the transverse emittance of the molecular beam onto the transverse acceptance of the hexapole ring. Attempts to improve the number of observable round trips by better spatial alignment of the storage ring onto the molecular beam and by optimizing hexapole and buncher timing settings proved to be unsuccessful. In particular the exact position of the ring with respect to the laser beam was difficult to control but also the combined transverse focusing effect of the hexapoles and buncher differed from the theoretically expected focusing effect. Comparing the two graphs from Fig. 5.10 it appears that the transverse motion is very sensitive to changes in the trapping voltages and hence the potential well strength. In the left graph of this figure the even round trips are missing in the time-of-flight profile whereas in the right graph all the peaks are present. Due to the improved linearity of the hexapole ring over the dipole ring the package of molecules remains more localized in phase-space (less filamentation). As the detection of the molecules is very position sensitive and the injection of the molecules into the ring might not be perfect, it is possible that for some round trips the molecules miss the laser focus and are hence not detected.

Due to this sensitive dependence on the trapping voltages on the ring electrodes, the motion of the molecules in the ring can be investigated as a function of these voltages. The wavelengths of the betatron oscillations that the molecules make in the hexapole ring are the same in the vertical and radial direction because the potential well of the hexapole ring is cylindrically symmetric. The betatron wavelength depends on the hexapole force constant k given by Eq. (2.28) in the following way:

$$\lambda = 2\pi v_\phi \sqrt{\frac{m}{k}} \propto \sqrt{\frac{1}{V}}. \qquad (5.1)$$

Here, λ is the wavelength of the betatron oscillation, v_ϕ is the tangential velocity, m is the mass of the molecule and V is the voltage difference between the adjacent electrodes of the hexapole storage ring. The inversion splitting is neglected here but near the hexapole axis, where the electric field is relatively small, the force constant k is effectively reduced and hence the wavelength is effectively increased. It is clear from this equation that it is possible to scan the wavelength of the betatron oscillations by altering the voltage on the hexapole ring .

Fig. 5.11 shows the ammonia density at the third round trip ($t = 25.93$ ms) as a function of the ring voltage $HV2$. $HV1$ is scanned together with $HV2$ such that the difference between the two remains constant. The measurement
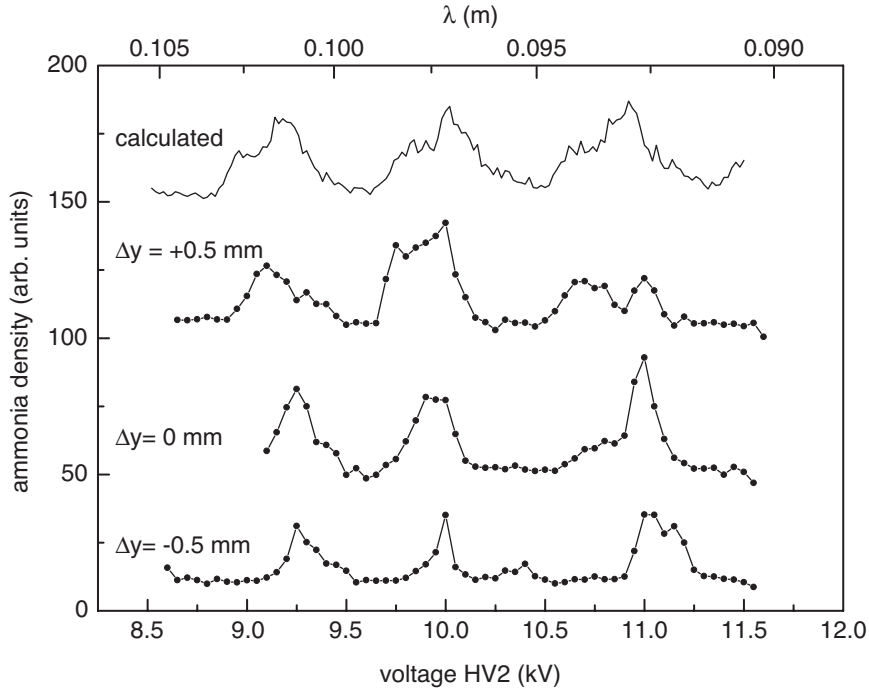
Figure 5.11: *Ammonia density at third round trip ($t = 25.93$ ms) as a function of the voltage on the ring electrodes ($HV2 = HV1 + 360$ V) for three different heights of the laser beam: $\Delta y = -0.5$ mm, $\Delta y = 0$ mm, and $\Delta y = +0.5$ mm. Upper curve is a numerical simulation of the $\Delta y = +0.5$ mm measurement. The curves are given an offset for clarity. The top axis indicates the corresponding wavelength scale.*

is performed for three different vertical laser detection positions. Instead of translating the laser focus vertically, it was experimentally easier and more accurate to translate the ring vertically. The ring is translated vertically from $\Delta y = +0.5$ mm to $\Delta y = -0.5$ mm. It is clear that the oscillations depend on the detection position as the peak positions shift and the peak shapes change. At all three detection positions the signal shows an oscillatory behavior. This can be attributed to the mismatching of the emittance of the molecular beam onto the acceptance of the ring and to the position sensitive detection scheme that is employed. For certain voltage settings the density of ammonia molecules that are detected in the laser focus has a maximum. The laser focus overlaps then optimally with the path of the package of molecules. For other voltage settings the density is almost zero. In this case the overlap of the laser focus with the path of the molecules is minimal. The top axis of Fig. 5.11 indicates the betatron wavelength, which is calculated using Eq. (5.1) assuming no inversion splitting. The wavelengths λ_{peak} corresponding to the peak positions are determined from a fit. At the third round trip the synchronous molecule has travelled a distance

	$HV2$ (kV)	λ_{peak} (m)	n
peak 1	9.14	0.102	23.3
peak 2	9.90	0.0977	24.3
peak 3	10.8	0.0934	25.5

Table 5.1: *Trapping voltages $HV2$, the corresponding wavelengths λ_{peak}, and the number of betatron oscillations n for the three peaks of the $\Delta y = +0.5$ mm signal shown in Fig. 5.11.*

of 2.38 m. Dividing this distance by the wavelengths found gives the number of betatron oscillations n that have occurred up to the third round trip for the given voltage settings. The relevant data are listed in Table 5.1. The wavelengths correspond to oscillation frequencies of about 940 Hz which agrees very well with the calculated value.

The voltage scan is numerically simulated in order to analyze the signal. The input phase-space distribution is taken from the calculated values in Section 5.2. From the calculations it is again found that the oscillating signal is rather sensitive to the vertical laser detection position and to the alignment of the ring onto the molecular beam, due to the detection method. A numerical simulation is shown in Fig. 5.11 and corresponds to a vertical shift in detection position of $\Delta y = +0.5$ mm. A qualitative fit of the experimental data is obtained when the vertical position of the ring relative to the incoming molecular beam is set to $\Delta y = -0.5$ mm. The peak positions agree rather well. The asymmetric shapes result from the asymmetry between the radial and vertical phase-space distributions. Calculations with radially and vertically symmetric phase-space distributions show that the peaks are smoother and more symmetric.

5.7 Conclusions

By optimizing the transverse phase-space matching of the injection beam-line onto the storage ring using hexapole lenses and by reducing the longitudinal temperature of the package of molecules prior to injection using a buncher, we have been able to detect ammonia molecules in a 80 cm circumference storage ring after more than 50 round trips. The ammonia molecules are actually stored in the ring considerably longer than this, but they fill up the whole ring with a nearly constant density and the fast molecules from the n-th round trip can then experimentally no longer be distinguished from the slow molecules in the $(n+1)$-th round trip. The transverse oscillations in the ring can be driven with relatively low AC voltages, and, in combination with position sensitive detection schemes, this can be used for an accurate measurement of the fundamental betatron oscillation frequencies. Alternatively, the wavelength of the betatron

oscillation can be determined by scanning the trapping voltages on the ring electrodes.

This opens the way for more detailed studies of the dynamics of polar molecules in an electrostatic storage ring. It is well-known that in ion traps, for instance, strong resonances occur when the axial and radial frequencies are in tune [89]. Similar effects will be present in the storage ring for neutral molecules as well, and at certain parameter-settings molecular trajectories might become highly unstable. Investigation and a detailed understanding of these ring dynamics is important for the design and construction of future sectional storage rings [90].

Chapter 6

Design of a sectional storage ring

6.1 Introduction

The molecular package is transversely confined in the current storage ring but it still spreads out in the tangential direction. As a consequence, the density of molecules stored in the ring decreases with $1/t$, where t is the storage time. To prevent this decrease in density it is necessary to build a buncher inside the storage ring. The purpose of the buncher is to keep the package of molecules together in the ring. To implement such a buncher, the storage ring has to be split up into sections as shown in Fig. 6.1. The sectional storage ring that is shown here schematically consists of bend sections, focusing sections, buncher sections, and free flight sections (gaps). Ideally, all these sections should do solely what they are designed for. It is inevitable, though, that some sections have a combined task. This follows from the requirement that the divergence of the electric field must be zero in absence of free charges, $\nabla \cdot \mathbf{E} = 0$. It is therefore fundamentally impossible to design an electrode geometry that only bends the molecules without focusing them.

In the current storage ring the transverse potential well is the same at every tangential position along the ring and the orbits of the molecules in the ring are stable as long as the kinetic energy of the molecules does not exceed the depth of the potential well. In a sectional storage ring, the strength of the potential well and hence the confinement force changes when the molecules move from one section to the next. If these changes occur at certain intervals it can lead to parametric amplification of the betatron motion and eventually, the molecules will be expelled from the storage ring.

The sectional storage ring presented in this Chapter incorporates all the required bending, bunching and focusing sections in a very simple and compact design. The number of sections is kept to a minimum in order to make construction and operation of the ring easier. The conditions for stable operation of this sectional storage ring are discussed.
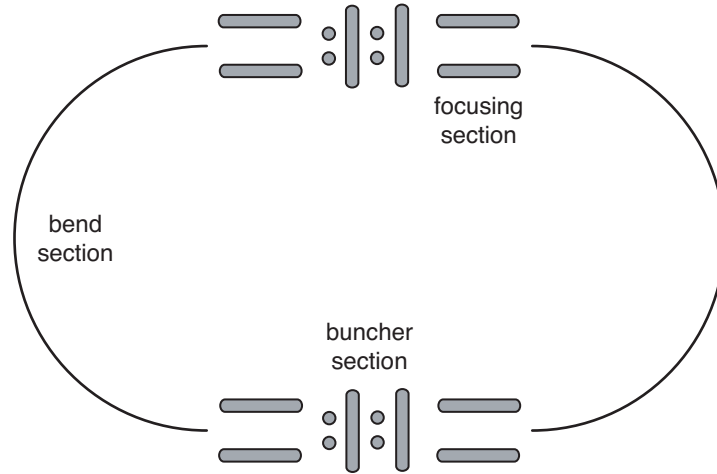
Figure 6.1: *Example of a sectional storage ring consisting of bend sections, focusing sections, and buncher sections with gaps in between them.*

6.2 Transverse stability in a sectional storage ring

In this Section the transverse stability is investigated for the simplest sectional storage ring possible: two bend sections with a small gap between them. The bend sections are 180°-bent hexapole focusers and the gaps between the bend sections are the free flight sections. The longitudinal motion of the molecules and the buncher are disregarded here. In first order approximation, when all the forces are assumed to be perfectly linear (no inversion splitting), the transverse motion of the molecules in phase-space can be conveniently described with the matrix method [48]. The matrix method is used extensively in the design of charged particle storage rings and gives a first order estimate of the stability of a storage ring. The transformation of the position and velocity coordinates of the molecules by each section of the ring is given by a single matrix. In order to calculate the transformation matrix of the entire storage ring it is useful to divide the ring in cells. Each cell is a block of one or more ring sections and it can occur many times in the ring. The simple sectional storage ring presented here consists of two cells, where each cell consists of one hexapole bend section and a free flight section.

The transformation matrix M_{ring} for one round trip through the ring is a multiplication of two cell matrices M_{cell}. The matrix M_{cell} is again a multiplication of an hexapole focusing matrix and a free flight matrix as given in Eq. (2.11) and Eq. (2.10), respectively. For stable operation of the ring it has to be shown now that the motion of the molecules in the ring remains bound after n propagations through the matrix M_{cell}. This requires that $-2 \leq \text{Tr}(M_{cell}) \leq 2$,

where $\mathrm{Tr}(M_{cell})$ is the trace of the matrix M_{cell} [30]. In this case, the stability criterium is found to be

$$-2 \leq 2\cos(\omega L_{hex}/v) - (\omega L_{gap}/v)\sin(\omega L_{hex}/v) \leq 2, \qquad (6.1)$$

where ω is the oscillation frequency of the molecules in the hexapoles, v is the velocity of the molecules, L_{hex} is the length of the hexapoles, and L_{gap} is the free flight path length.

When the inversion splitting is taken into account, the matrix formalism can no longer be used. Now, a numerical calculation has to be performed to investigate the transverse stability of a sectional storage ring. In good approximation the bend section can be taken as a straight focusing hexapole, since for large ring radii the electric field inside a bent hexapole is practically the same as for a straight hexapole (see Fig. 3.2). The trajectories of 100 $^{14}\mathrm{ND}_3$ molecules in the $|J,K\rangle = |1,1\rangle$ state are numerically calculated while flying through this ring with a tangential velocity of 91.8 m/s. The length of the hexapoles is chosen to be $L_{hex} = 39.3$ cm. The initial transverse phase-space distributions are taken to be $[\Delta r \times \Delta v_r] = [\Delta y \times \Delta v_y] = [1\,\mathrm{mm} \times 5\,\mathrm{m/s}]$, with r and y in the horizontal (radial) and vertical direction, respectively. Here, the widths are at FWHM of gaussian distributions. The number of molecules that are still in the ring after 100 round trips are counted. The ratio of this number to the number of molecules injected into the ring can be regarded as the transmission efficiency of the ring for the parameters used. Fig. 6.2(a) shows a plot of the transmission efficiency as a function of k_{hex} and L_{gap}. The horizontal axis is linear in the voltage difference between the hexapole electrodes. The maximum value of $k_{hex} = 0.06$ cm^{-1}/mm^2 corresponds to a voltage of 10.18 kV for an hexapole with an inner radius of $R = 4$ mm. The design voltage of 8 kV for the sectional storage ring corresponds to 0.047 cm^{-1}/mm^2. The dark bands in the diagram indicate the regions of stability. At larger values of k_{hex} the transmission efficiency decreases strongly when the free flight path length L_{gap} is increased. Fig. 6.2(b) shows the same calculation but now for the hypothetical case when the molecules have no inversion splitting. In this case the hexapole force is perfectly linear. Due to the improved linearity the bands are more pronounced and extend over a wider range of free flight path lengths. The thick white horizontal lines in this figure indicate the regions of stability for $L_{gap} = 3$ cm according to Eq. (6.1) obtained with the matrix method.

As observed, for some values of k_{hex} hardly any molecule remains in the ring, even when L_{gap} approaches zero. These so-called stop bands scale with the band number n, like $k_{hex} \propto n^2$, starting with $n = 1$ for the left most band. The occurrence of these stop bands is a result of so-called half-integer resonances in the ring. These can be understood by examining the phase-space diagram shown in Fig. 6.3. Assume a molecule orbiting the ring with a round trip frequency Ω_{ring} and a betatron oscillation frequency ω_{beta}. Fig. 6.3 shows the motion of such a molecule in phase-space (inner circle). The momentum
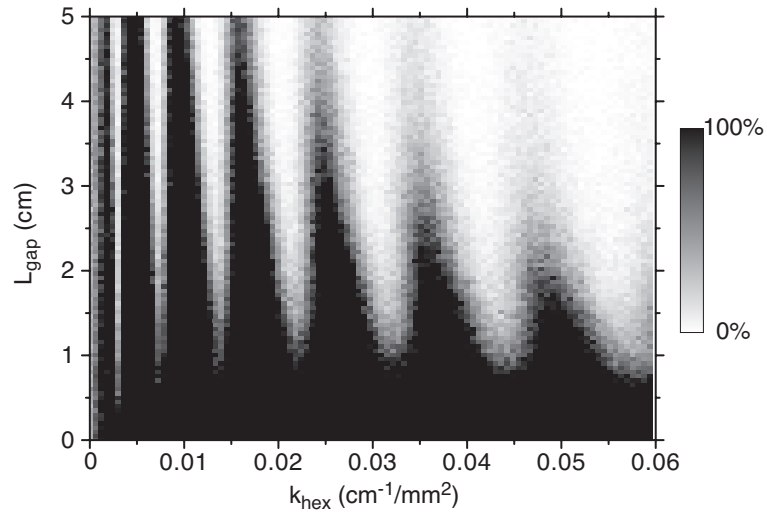
(a) With inversion splitting
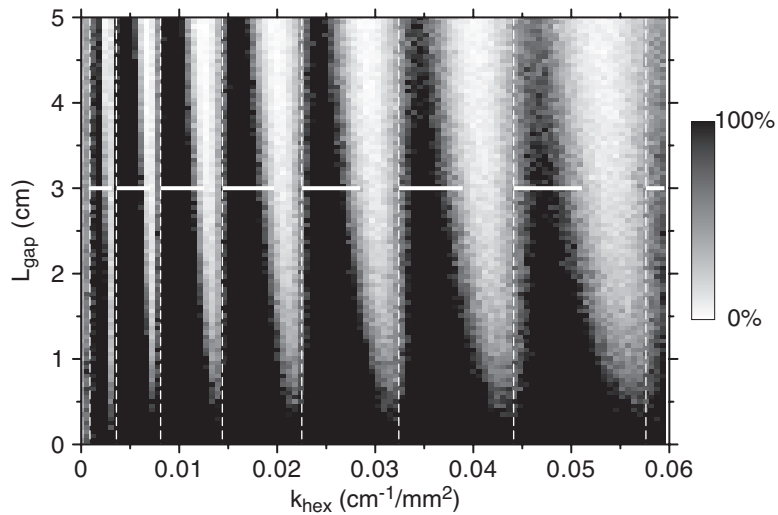
(b) Without inversion splitting

Figure 6.2: *(a) Stability diagram of the sectional storage ring consisting of two bend sections and two free flight sections. At each coordinate (k_{hex}, L_{gap}) the transmission efficiency is calculated by flying 100 ammonia molecules through the ring and determining how many molecules are still in the ring after 100 round trips. (b) Same diagram but now for the hypothetical situation when the ammonia molecules have no inversion splitting. The thick white horizontal lines indicate the regions of stability for $L_{gap} = 3$ cm according to Eq. (6.1). The vertical dashed white lines indicate the position of the stop bands according to Eq. (6.4).*
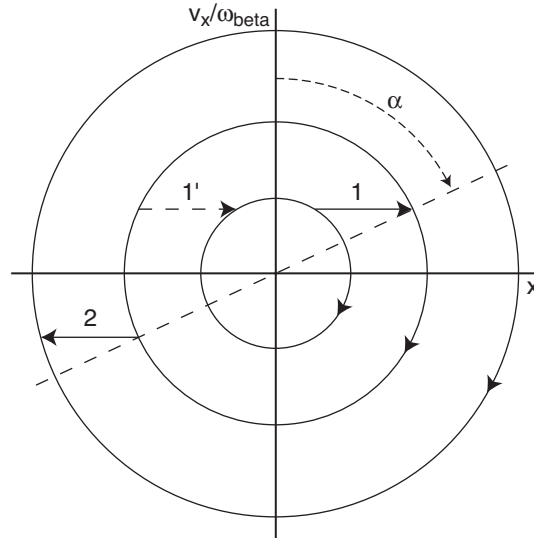
Figure 6.3: *Phase-space plot in one transverse direction showing an half-integer betatron resonance in the sectional storage ring consisting of hexapole bend sections and free flight sections. The betatron amplitude of a molecule (radius of the circles) grows without bound when the phase advance is a multiple of π. The solid arrows (1,2) indicate the free flight paths of the molecule, which occur every time the betatron phase has increased by π. The dashed arrow (1') brings the molecule back to its original phase-space trajectory.*

axis is divided by ω_{beta} to make the trajectories in phase-space perfect circles. Inversion splitting is neglected. At a certain orbital position in the ring the molecule exits an hexapole bend section and enters a free flight section. The position of the molecule in phase space shifts horizontally during free flight as indicated by arrow 1 in Fig. 6.3. Then the molecule enters the next hexapole bend section. At that moment the molecule's betatron phase is α as indicated in the figure. The trajectory of the molecule describes now a larger circle in phase-space: its betatron amplitude has grown. During its flight through the hexapole the betatron phase of the molecule increments by an amount $\Delta\alpha$. This difference, $\Delta\alpha$, between the betatron phase at the exit and the betatron phase at the entrance of an hexapole is called the phase advance of that hexapole, like in charged particle accelerators. The half-integer resonances arise when the phase advance is a multiple of π. Every time the molecule has rotated over an angle of π in phase space and it enters a free flight section, it moves to a circle with a larger radius in phase space (arrow 2 in Fig. 6.3). In this way the betatron amplitude grows quickly out of bounds and eventually the molecule escapes from the ring or crashes into the electrodes. Besides these half-integer resonances higher order resonances can also occur.

In principle, the increase in the betatron oscillation amplitude is cancelled when the molecule enters the next free flight section at the right betatron phase. Then the free flight motion brings the molecule back to its original orbit in phase-space as indicated by arrow $1'$ in Fig. 6.3. The resonances can be avoided by operating the ring such that the phase advance is not a multiple of π. In this case the betatron amplitude sometimes grows and sometimes shrinks; averaging out in the end.

The position k_{hex} of the stop bands can easily be calculated as the phase advance $\Delta\alpha$ is given by

$$\Delta\alpha = \omega_{beta}L_{hex}/v, \tag{6.2}$$

where v is the forward velocity of the molecule, ω_{beta} is the betatron angular frequency, and L_{hex} is the length of the hexapoles. As the stop bands occur when the phase advance is a multiple of π, $\Delta\alpha = n\pi$, one finds for the betatron angular frequency

$$\omega_{beta} = n\frac{\pi v}{L_{hex}}. \tag{6.3}$$

By substituting k_{hex} for ω_{beta} using the relation $\omega_{beta} = \sqrt{k_{hex}/m}$, one finds for the force constant

$$k_{hex} = n^2 \left(\frac{\pi v}{L_{hex}}\right)^2 m, \tag{6.4}$$

where m is the mass of the molecule. This explains the observed quadratic dependence of k_{hex} on n. The stability plots shown in Fig. 6.2 are calculated for $^{14}ND_3$ with $v = 91.8$ m/s and $L_{hex} = 39.3$ cm. In that case the proportionality constant between k_{hex} and n^2 is 9.0×10^{-4} cm^{-1}/mm^2. The position of stop band number 3, for instance, is then 0.0081 cm^{-1}/mm^2, which agrees well with the value found in the stability plots. The stop bands are indicated in Fig. 6.2(b) with vertical dashed white lines.

6.3 Experimental simulation of gaps in a storage ring

The voltages on the electrodes of the (current) hexapole storage ring can be switched off momentarily permitting the ammonia molecules to fly freely before they are captured again. In this way gaps in the ring can be simulated and this can be considered as a preliminary experimental test for a future sectional storage ring. The experiment is performed with the same hexapole ring setup as used for the voltage scans as discussed in Section 5.6.

First, the effect of the gap length is investigated. The molecules are injected into the hexapole storage ring and detected at a time t_{det}. The trapping voltages $HV1$ and $HV2$ are 9.64 kV and 10.00 kV, respectively. Now, the trapping voltages are switched off 5.00 ms after the molecules have entered the ring. Fig. 6.4 shows the ammonia peak density signal at the second round trip ($t_{det} =$
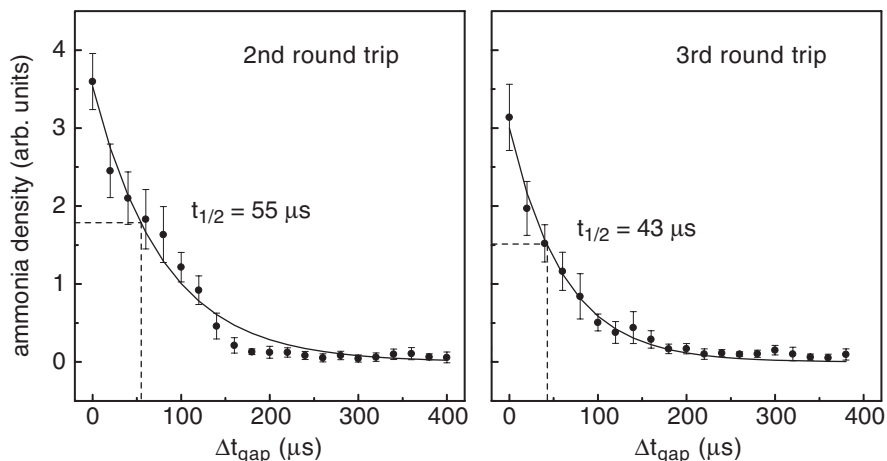
Figure 6.4: *The ammonia peak density measured at the second and third round trip in the hexapole storage ring is plotted as a function of the duration that the trapping voltages on the ring are switched off.*

17.22 ms) and third round trip ($t_{det} = 25.92$ ms) as a function of the gap length Δt_{gap}. The zero gap length corresponds to no switching off of the trapping voltages. The signal drops for increasing gap lengths but the rate at which it drops is different for the second and third round trip. The decay time at which the density has dropped to 50% is determined from an exponential decay fit and for the second round trip this decay time is 55 μs and for the third round trip it is 43 μs. Due to the gap in the ring some trajectories become unstable and molecules on those trajectories will eventually escape from the ring. The chance that this happens increases over time, explaining the more rapid decay observed at the third round trip.

In a second series of measurements, the duration of the gap is kept constant at 100 μs, which amounts to a gap length of 9.18 mm for the current tangential velocity of the synchronous molecule. Fig. 6.5 shows the ammonia peak density signal at the third round trip ($t = 25.92$ ms) as a function of the gap starting time position. The maximum measured density when a gap is present in the ring is about 40% of the "no-gap" measured density. Apparently, a number of molecules is lost from the ring anyway. Measurements where two gaps are introduced in the ring show an almost complete loss of molecules from the ring. The density oscillates with a frequency of 2 kHz as determined from fitting the data to a sine wave. This frequency corresponds to the second harmonic of the betatron oscillation frequency of the hexapole potential well. So, this is yet another method to investigate the dynamics of a package of molecules in the ring. When the molecular package oscillates around the equilibrium orbit, the phase of the betatron oscillation at the moment when the trapping voltages are switched off influences the recapture efficiency. If the phase of the betatron
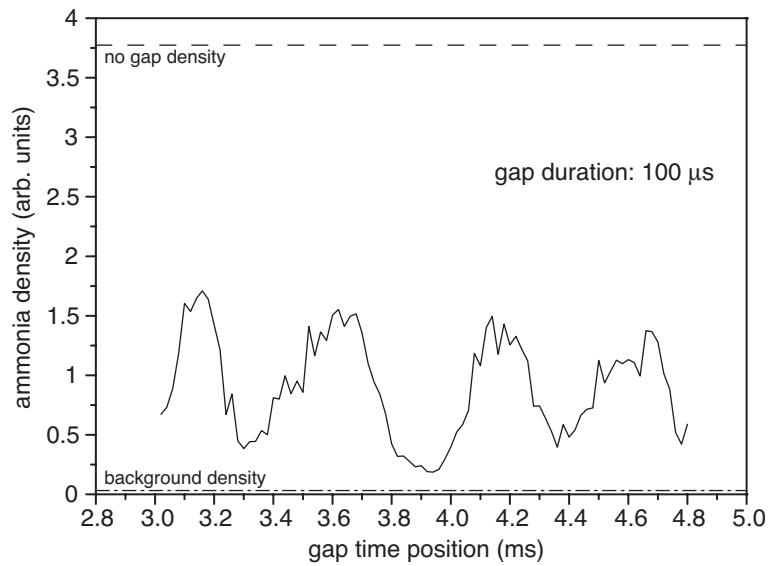
Figure 6.5: *The ammonia peak density measured at the third round trip in the hexapole storage ring is plotted as a function of the gap starting time. The gap duration is fixed at 100 μs. The dashed line (top) indicates the density when no gap is present. The dot-dashed line (bottom) indicates the background density.*

oscillation is such that the package of molecules has a velocity vector with a maximal positive or negative radial component, then the molecules are more likely to leave the storage ring. If the phase of the betatron oscillation is such that the package of molecules has a velocity vector with a minimal positive or negative radial component, then the molecules are more likely to stay in the storage ring. As these situations occur twice per oscillation period the double frequency is observed.

In conclusion, it is possible to introduce gaps in the potential well of the storage ring but there are losses. It should be noted that in the current hexapole ring the untrapped molecules will fly straight on and will not follow the curvature of the ring when the ring is switched off. If the free flight path is too long, the molecules will escape from the ring. In a sectional ring the free flight sections should ideally be made straight, facilitating an easier recapture of the molecules. An other contribution to the losses is probably imperfect phase-space matching at the entrance of the ring, which is reflected in the oscillation of the ammonia peak density shown in Fig. 6.5. Good knowledge of the transverse emittance of the molecular beam would be beneficial to improve the phase-space matching.
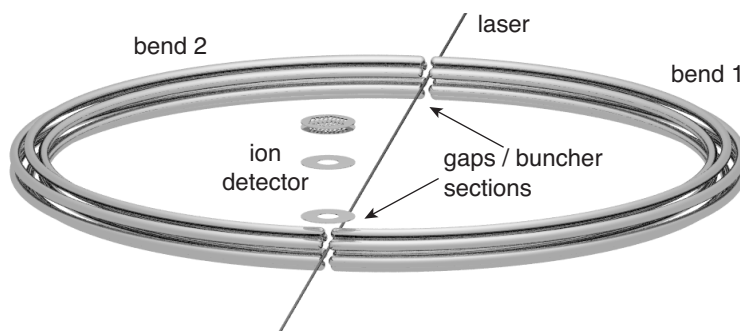
Figure 6.6: *Sectional storage ring consisting of two semi-circle hexapoles. The detection laser is shot right through the gaps, ionizing the ammonia molecules that are present in the laser focus. The parent ions are then extracted from the ring and accelerated towards an ion detector.*

6.4 A prototype sectional storage ring

The design of the sectional storage ring is kept very simple for a number of reasons. Firstly, construction and assembly have to be relatively easy. Too many sections make alignment of the individual elements more difficult. Secondly, each additional gap leads to additional beam losses as the beam is not confined. The molecules can easily make a transition from a low-field seeking, trappable state to a non-trappable state if the electric field is absent or too weak. Finally, the number of power supplies needed is limited and the timing sequence controlling the voltages on the ring is simpler. The sectional storage ring consists of two equally large 180° hexapole bend sections with a small gap in between. Fig. 6.6 shows a schematic of such a ring. In one round trip a stored molecule traverses a bend section, a straight free flight section (gap), another bend section, and another straight free flight section (other gap). Each bend section has its own high voltage power supplies and can independently be switched on and off, possibly facilitating reloading of the storage ring. Molecules are injected into the ring tangentially at the gap where they are also detected. To confine the molecules in an hexapole bend section high voltages (8 kV) are applied to the electrodes as shown in Fig. 6.7(a). The hexapole radius is taken to be $R = 4$ mm. In order to detect the molecules the voltages on the electrodes are switched to relatively low voltages as indicated in Fig. 6.7(d). Then a focused UV-laser beam is shot right through the gaps between the two sections and the laser light ionizes the molecules that are present in the gap. The parent ions are vertically accelerated out of the ring by the residual electric field and are subsequently detected with a time-of-flight mass spectrometer. The injection beamline of this sectional storage ring is similar to the one described in Chapter 5.

(a) Confinement configuration

(b) Hexapole kicker configuration

(c) Buncher configuration

(d) Detection configuration
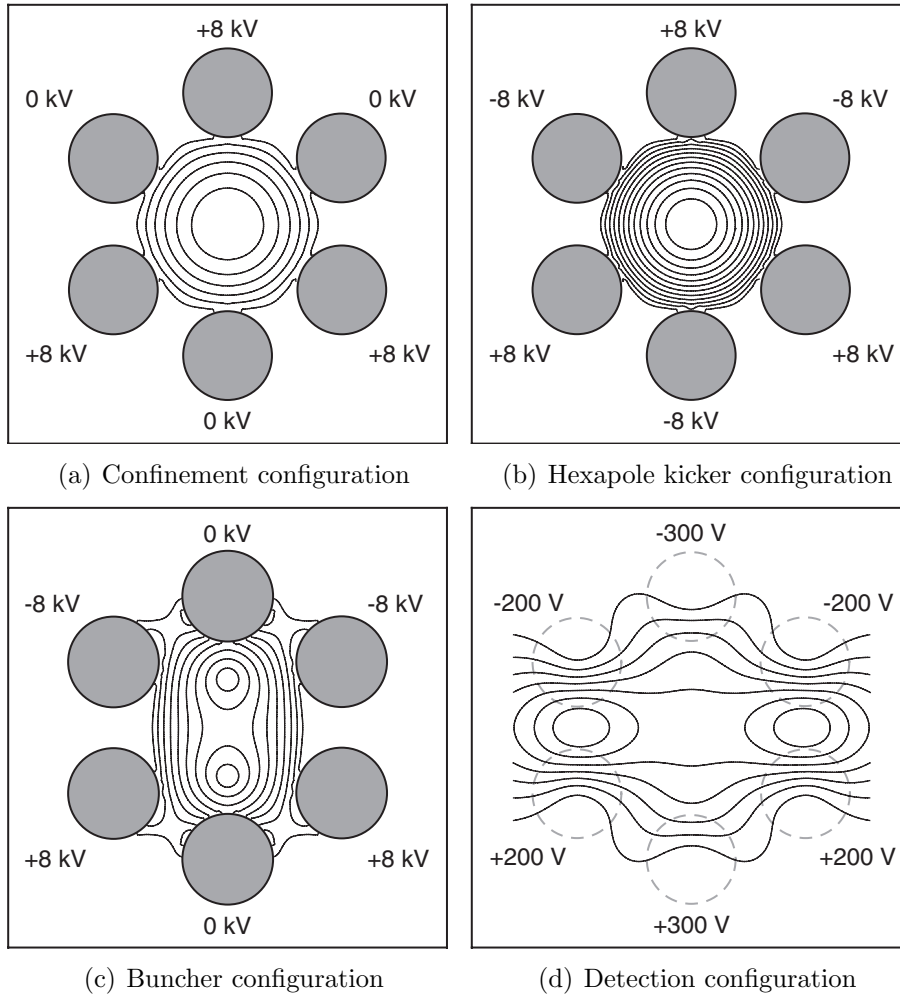
Figure 6.7: *Cross section through the hexapole bend section showing voltage settings and electric field contour lines for confinement configuration (a), hexapole kicker configuration (b), buncher configuration (c) and detection configuration (d). The latter shows the electric field in the middle of a gap. The hexapole radius is $R = 4$ mm. Contour lines are shown at 5 kV/cm intervals for (a,b,c) and 0.1 kV/cm intervals for (d). Contour lines with highest electric field value: 30 kV/cm (a), 60 kV/cm (b), 45 kV/cm (c) and 0.8 kV/cm (d).*

To achieve bunching inside the ring, molecules that are faster than the synchronous molecule have to lose kinetic energy while slower molecules have to gain kinetic energy. Bunching in the sectional storage ring is possible by making use of the gaps between the sections and by appropriately switching the high voltages on the electrodes. Firstly, a package of molecules is confined in bend section 1 with voltages applied to the electrodes as shown in Fig. 6.7(a). Just before the synchronous molecule enters one of the gaps between the two bend sections, the high voltages on the electrodes of section 1 are switched off and the molecules are not confined anymore in the transverse direction and will fly outwards. To compensate for this, it is possible to kick the molecules a little bit inwards by using the hexapole kicker configuration as shown in Fig. 6.7(b) before switching off the confinement field. The force constant of the hexapole kicker is twice as large as the force constant of the normal hexapole voltage configuration. After the hexapole kicker, the voltages on bend section 2 are switched to the bunching configuration as shown in Fig. 6.7(c). The voltages on section 1 are switched off. This creates, in the longitudinal direction, a smoothly rising potential energy curve W_1 for ammonia molecules in the low-field seeking $|J, K\rangle = |1, 1\rangle$ state as shown in Fig. 6.8. When the synchronous molecule is exactly at the center of the gap at z_0, bend section 1 is switched to the buncher configuration and bend section 2 is switched off. This creates the mirror image W_2 of the potential energy curve W_1, with respect to the center of the gap z_0. The z-direction is the longitudinal (tangential) direction. The difference between W_1 and W_2 leads to a restoring force in the longitudinal direction which is used to bunch the package of molecules inside the ring. After the synchronous molecule has entered bend section 2, a second kick is applied with the hexapole kicker configuration to get the synchronous molecule back onto the equilibrium orbit. Finally, the voltages of the bend section 2 are switched to the confinement configuration and the molecules are stored in the ring until they reach the next gap.

6.4.1 The buncher section

Now, we will look into more detail to the buncher section. When the molecules are about 4 mm in front of a gap, bend section 1 is switched off and bend section 2 is switched to the buncher configuration, as shown in Fig. 6.7(c). The potential energy for a $^{14}ND_3$ molecule in the $|J, K\rangle = |1, 1\rangle$ state is then the monotonically smooth rising potential energy function $W_1(z)$ as shown in Fig. 6.8. When the synchronous molecule is at z_0 its potential energy is given by $W_1(z_0)$. A molecule that flies at a position Δz relative to the synchronous molecule has a potential energy $W_1(z_0 + \Delta z)$. When the synchronous molecule is at z_0, the potential is changed instantaneously from $W_1(z)$ to $W_2(z)$ by swapping the voltage configurations of the bend sections. $W_2(z)$ is the mirror image of $W_1(z)$ around z_0 and is shown in Fig. 6.8 as well. The potential energy of the synchronous molecule remains unchanged in this process but the energy of the
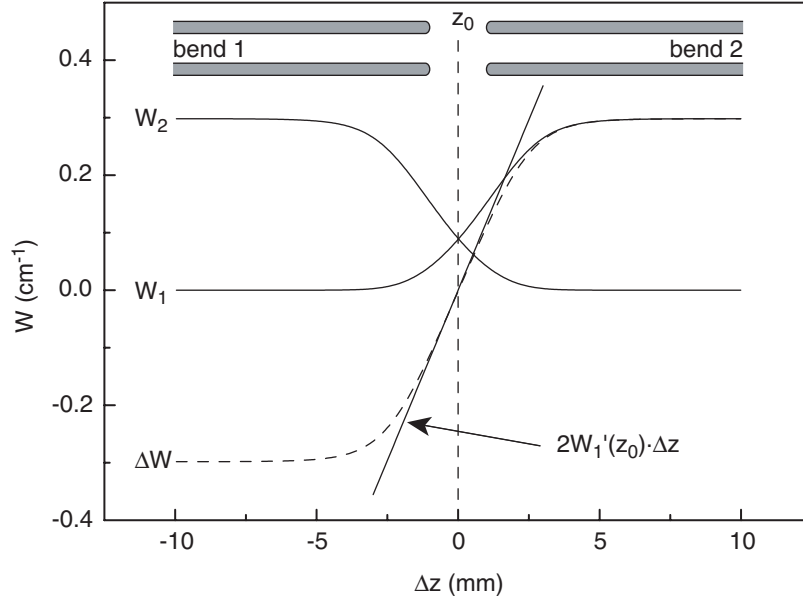
Figure 6.8: *Potential energy curves W_1 and W_2 are shown as a function of the position z of a molecule traversing the ring at r_0. The center of the gap is $z = 0$. Also shown is the potential energy difference ΔW. The slope $W_1'(z_0)$ is determined by a linear fit of ΔW.*

other molecules is changed by an amount $\Delta W(\Delta z) = W_1(z_0 + \Delta z) - W_2(z_0 + \Delta z)$, which is shown in Fig. 6.8. It is clear that a molecule that flies in front of the synchronous molecule loses kinetic energy while a molecule that lags the synchronous molecule gains kinetic energy. Because of the mirror symmetry we have $W_2(z_0 + \Delta z) = W_1(z_0 - \Delta z)$ and the potential energy difference becomes

$$\Delta W = W_1(z + \Delta z) - W_1(z - \Delta z). \tag{6.5}$$

Expanding this in a Taylor series around z_0 yields

$$\Delta W = \sum_{n=0}^{\infty} \frac{1}{n!} \left[\frac{d^n}{dz^n} W_1(z_0) \right] (\Delta z)^n - \sum_{n=0}^{\infty} \frac{1}{n!} \left[\frac{d^n}{dz^n} W_1(z_0) \right] (-\Delta z)^n. \tag{6.6}$$

Obviously, all the terms with even n cancel, while the terms with odd n add up. The change in potential energy is then given by

$$\Delta W = 2W_1'(z_0)\Delta z + \frac{1}{3} W_1'''(z_0)\Delta z^3 + \cdots, \tag{6.7}$$

where the n primes denote the n-th derivative of W_1 with respect to z. The average force $\langle F \rangle$ over one section of the ring (one gap and one bend) with length L is for small values of Δz approximately given by

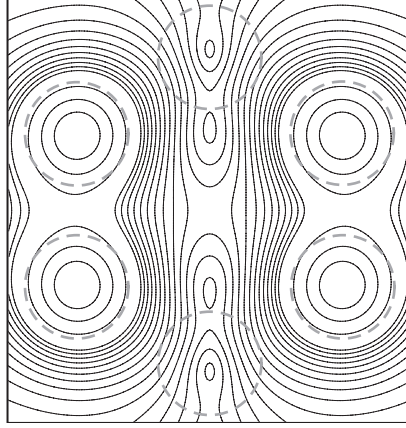$$\langle F \rangle = -\frac{2W_1'(z_0)\Delta z}{L} \tag{6.8}$$

Figure 6.9: *Contour lines showing the transverse electric field in the middle of the gap at z_0.*

This is a linear restoring force with an angular frequency given by

$$\omega_{bunch} = \sqrt{\frac{2W_1'(z_0)}{mL}}. \tag{6.9}$$

The value for $W_1'(z_0) = 0.059$ cm^{-1}/mm in case of ^{14}ND$_3$ and is found from a linear fit of ΔW through z_0. This results then in a frequency $\omega_{bunch}/2\pi = 67$ Hz for a section with length $L = 0.4$ m, amounting to one oscillation in longitudinal phase-space per 1.76 round trips. This is for one buncher in the sectional ring. With two buncher sections in the ring, the rotation is twice as fast and hence one oscillation occurs in 0.88 round trips. As the velocity spread, Δv_z, and the position spread, Δz, are related by $\Delta v_z = \omega_{bunch}\Delta z$, one finds for $\Delta z = 4$ mm, the distance over which the buncher is still linear, a velocity spread of $\Delta v_z = 1.7$ m/s. The longitudinal emittance of the decelerator is about $[\Delta z \times \Delta v_z] = [2 \text{ mm} \times 8 \text{ m/s}]$ for the currently used deceleration settings ($\phi_s = 70°$, $v_{sync} = 91.8$ m/s). To map the emittance onto the longitudinal acceptance of the ring one needs to roughly make a one to two or one to three image with the buncher in the injection beamline.

Fig. 6.9 depicts the electric field of the buncher at $z = z_0$ in the transverse direction. It is clear that the field is not homogeneous in the radial direction. Hence, the potential energy curve W_1 depends on the radial position as shown in Fig. 6.10. The effect of this radial dependency is that the molecules experience a small force towards the center of the storage ring as the electric field increases radially outwards. The radial dependency couples the longitudinal motion to the transverse motion. However, the transverse betatron oscillation frequency of about 1 kHz is much larger than the longitudinal oscillation frequency of 67 Hz and hence the coupling between the two directions is expected to be weak. Furthermore, by applying the hexapole kicker the transverse (radial) size
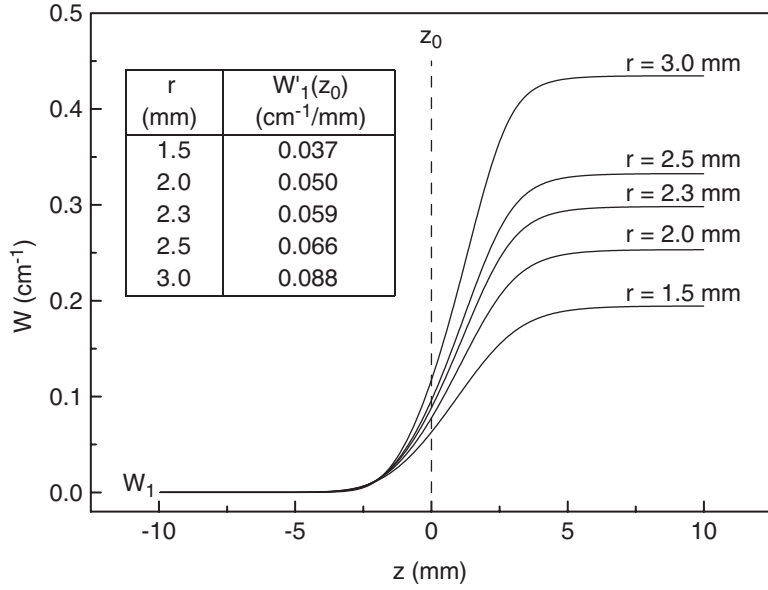
97

Figure 6.10: *Radial dependence of the buncher potential W_1. The potential energy curves are shown for $r = 1.5$, 2.0, 2.3 (equilibrium orbit), 2.5 and 3.0 mm. The inset lists $W_1'(z_0)$ for the different radii.*

of the package of molecules is reduced at the center of the gap. In this way the difference in bunching force between a molecule at the inner side of the buncher and a molecule at the outer side of the buncher is less than when the hexapole kicker is not applied.

6.4.2 Hexapole kickers

To approximate the real bend sections better, the package of molecules is injected into the ring at a horizontal (radial) offset which depends on the force constant k_{bend} and the tangential velocity of the synchronous molecules as given by Eq. (3.3). The introduction of this offset leads to a dramatic reduction of the transmission efficiency as depicted in Fig. 6.11. The diagram shows again the transmission efficiency as a function of k_{bend} and L_{gap}. For $k_{bend} < 0.03$ cm^{-1}/mm^2 no molecules are detected after 100 round trips because the force constant is too weak to keep the molecules inside the ring. Based on this diagram, only a sectional ring with small free flight path lengths seems feasible. This is unfortunate as the molecules are not well confined transversely in the buncher section over at least 10 mm.

To improve the transmission efficiency for larger gaps, the molecules can be focused more strongly using the hexapole kickers before and after the buncher section. The force constant of the hexapole kicker is twice as large as the force constant k_{bend}. The use of the hexapole kicker improves the transmission

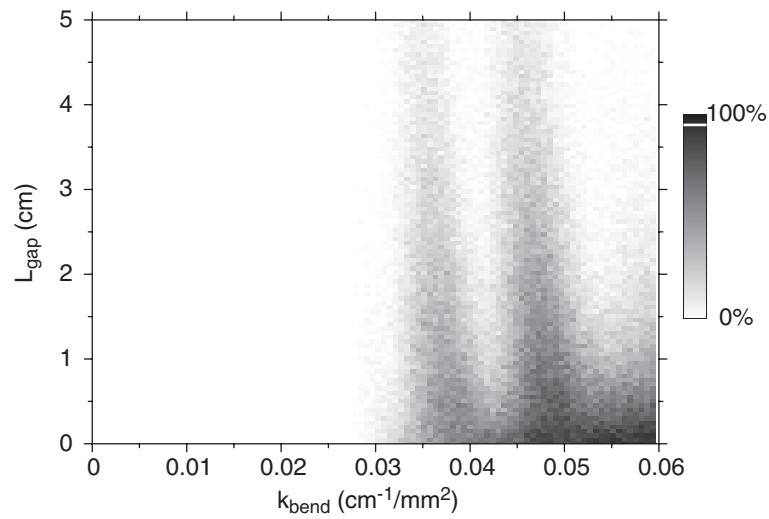**Figure 6.11:** *Stability diagram of the sectional storage ring consisting of two bend sections and two free flight sections. The package of molecules is injected into the ring at a horizontal offset which depends on the force constant k_{bend} and the tangential velocity.*
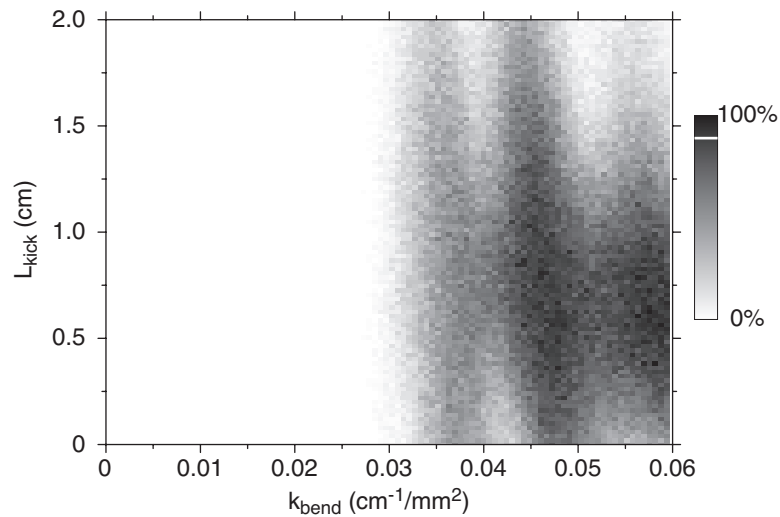
Figure 6.12: *Stability diagram of the sectional storage ring with hexapole kickers. The free flight path length is kept constant at $L_{gap} = 10$ mm.*

efficiency as shown in the diagram of Fig. 6.12. Here, the transmission efficiency is shown as a function of the force constant k_{bend} and the length L_{kick} over which the hexapole kick is applied. By using a L_{kick} of about 7 mm, the transmission efficiency for hexapole voltages of about 8 kV ($k_{bend} = 0.047$ cm^{-1}/mm^2) is much improved.

6.5 Conclusions and outlook

The numerical calculations show that for the right parameters, especially the force constant k_{bend}, free flight path length L_{gap} and hexapole kicker length L_{kick}, a sectional storage ring is feasible. Based on these calculations and the test measurements presented in this Chapter a sectional storage ring has been designed and is under construction.

Bibliography

[1] P. B. Corkum, C. Ellert, M. Mehendale, P. Dietrich, S. Hankin, S. Aseyev, D. Rayner, and D. Villeneuve, *Molecular science with strong laser fields*, Faraday Discuss. **113**, 47, 1999.

[2] H. Stapelfeldt and T. Seideman, *Colloquium: Aligning molecules with strong laser pulses*, Rev. Mod. Phys. **75**, 543, 2003.

[3] G. Scoles, editor, *Atomic and molecular beam methods*, volume 1, Oxford University Press, New York, 1988.

[4] G. Scoles, editor, *Atomic and molecular beam methods*, volume 2, Oxford University Press, New York, 1992.

[5] H. L. Bethlem, G. Berden, and G. Meijer, *Decelerating neutral dipolar molecules*, Phys. Rev. Lett. **83**, 1558, 1999.

[6] H. L. Bethlem and G. Meijer, *Production and application of translationally cold molecules*, Int. Rev. Phys. Chem. **22**, 73, 2003.

[7] E. A. Hinds, *Testing time reversal symmetry using molecules*, Phys. Scripta **T70**, 34, 1997.

[8] J. J. Hudson, B. E. Sauer, M. R. Tarbutt, and E. A. Hinds, *Measurement of the electron electric dipole moment using YbF molecules*, Phys. Rev. Lett. **89**, 023003, 2002.

[9] D. Kawall, F. Bay, S. Bickman, Y. Jiang, and D. DeMille, *Precision Zeeman-Stark spectroscopy of the metastable $a(1)[^3\Sigma^+]$ state of PbO*, Phys. Rev. Lett. **92**, 133007, 2004.

[10] M. Ziskind, C. Daussy, T. Marrel, and C. Chardonnet, *Improved sensitivity in the search for a parity-violating energy difference in the vibrational spectrum of the enantiomers of CHFClBr*, Eur. Phys. J. D **20**, 219, 2002.

[11] J.-P. Uzan, *The fundamental constants and their variation: observational and theoretical status*, Rev. Mod. Phys. **75**, 403, 2003.

[12] E. A. Cornell and C. E. Wieman, *Nobel Lecture: Bose-Einstein condensation in a dilute gas, the first 70 years and some recent experiments*, Rev. Mod. Phys. **74**, 875, 2002.

[13] W. Ketterle, *Nobel lecture: When atoms behave as waves: Bose-Einstein condensation and the atom laser*, Rev. Mod. Phys. **74**, 1131, 2002.

[14] A. G. Truscott, K. E. Strecker, W. I. McAlexander, G. B. Partridge, and R. G. Hulet, *Observation of Fermi pressure in a gas of trapped atoms*, Science **291**, 2570, 2001.

[15] U. Schramm, T. Schätz, and D. Habs, *Bunched crystalline ion beams*, Phys. Rev. Lett. **87**, 184801, 2001.

[16] L. Santos, G. V. Shlyapnikov, P. Zoller, and M. Lewenstein, *Bose-Einstein condensation in trapped dipolar gases*, Phys. Rev. Lett. **85**, 1791, 2000.

[17] M. A. Baranov, M. S. Mar'enko, V. S. Rychkov, and G. V. Shlyapnikov, *Superfluid pairing in a polarized dipolar Fermi gas*, Phys. Rev. A **66**, 013606, 2002.

[18] D. DeMille, *Quantum computation with trapped polar molecules*, Phys. Rev. Lett. **88**, 067901, 2002.

[19] H. J. Metcalf and P. van der Straten, *Laser cooling and trapping*, Springer-Verlag, New York, 1999.

[20] J. D. Weinstein, R. deCarvalho, T. Guillet, B. Friedrich, and J. M. Doyle, *Magnetic trapping of calcium monohydride molecules at millikelvin temperatures*, Nature **395**, 148, 1998.

[21] H. L. Bethlem, G. Berden, F. M. H. Crompvoets, R. T. Jongma, A. J. A. van Roij, and G. Meijer, *Electrostatic trapping of ammonia molecules*, Nature **406**, 491, 2000.

[22] T. Takekoshi, B. M. Patterson, and R. J. Knize, *Observation of optically trapped cold cesium molecules*, Phys. Rev. Lett. **81**, 5105, 1998.

[23] N. Vanhaecke, W. de Souza Melo, B. L. Tolra, D. Comparat, and P. Pillet, *Accumulation of cold cesium molecules via photoassociation in a mixed atomic and molecular trap*, Phys. Rev. Lett. **89**, 063001, 2002.

[24] S. Jochim, M. Bartenstein, A. Altmeyer, G. Hendl, S. Riedl, C. Chin, J. Hecker Denschlag, and R. Grimm, *Bose-Einstein condensation of molecules*, Science **302**, 2101, 2003.

[25] M. Greiner, C. A. Regal, and D. S. Jin, *Emergence of a molecular Bose-Einstein condensate from a Fermi gas*, Nature **426**, 537, 2003.

[26] K. Xu, T. Mukaiyama, J. R. Abo-Shaeer, J. K. Chin, D. E. Miller, and W. Ketterle, *Formation of quantum-degenerate sodium molecules*, Phys. Rev. Lett. **91**, 210402, 2003.

[27] M. W. Zwierlein, C. A. Stan, C. H. Schunck, S. M. F. Raupach, S. Gupta, Z. Hadzibabic, and W. Ketterle, *Observation of Bose-Einstein condensation of molecules*, Phys. Rev. Lett. **91**, 250401, 2003.

[28] V. I. Veksler, *A new method of acceleration of relativistic particles*, Doklady Akad. Nauk SSSR **43**, 346, 1944.

[29] E. M. McMillan, *The synchrotron – a proposed high energy particle accelerator*, Phys. Rev. **68**, 143, 1945.

[30] E. D. Courant and H. S. Snyder, *Theory of the alternating-gradient synchrotron*, Ann. Phys. **3**, 1, 1958.

[31] M. S. Livingston and J. P. Blewett, *Particle accelerators*, International series in pure and applied physics, McGraw-Hill, New York, 1962.

[32] E. J. N. Wilson, *An introduction to particle accelerators*, Oxford University Press, Oxford, 2001.

[33] J. Liouville, *Sur la théorie de la variation des constantes arbitraires*, J. Math. Pures Appl. **3**, 342, 1838.

[34] K.-J. Kügler, W. Paul, and U. Trinks, *A magnetic storage ring for neutrons*, Phys. Lett. B **72**, 422, 1978.

[35] K.-J. Kügler, K. Moritz, W. Paul, and U. Trinks, *NESTOR – a magnetic storage ring for slow neutrons*, Nucl. Instrum. Meth. A **228**, 240, 1985.

[36] F. M. H. Crompvoets, H. L. Bethlem, R. T. Jongma, and G. Meijer, *A prototype storage ring for neutral molecules*, Nature **411**, 174, 2001.

[37] J. A. Sauer, M. D. Barrett, and M. S. Chapman, *Storage ring for neutral atoms*, Phys. Rev. Lett. **87**, 270401, 2001.

[38] D. Auerbach, E. E. A. Bromberg, and L. Wharton, *Alternate-gradient focusing of molecular beams*, J. Chem. Phys. **45**, 2160, 1966.

[39] J. C. Helmer, F. B. Jacobus, and P. A. Sturrock, *Focusing molecular beams of NH_3*, J. Appl. Phys. **31**, 458, 1960.

[40] K.-R. Chien, P. B. Foreman, K. H. Castleton, and S. G. Kukolich, *Relaxation cross section measurements on NH_3 and lower state focussing in a beam maser*, Chem. Phys. **7**, 161, 1975.

[41] H. J. Loesch and B. Scheel, *Molecules on Kepler orbits: An experimental study*, Phys. Rev. Lett. **85**, 2709, 2000.

[42] D. P. Katz, *A storage ring for polar molecules*, J. Chem. Phys. **107**, 8491, 1997.

[43] K. Burnett, P. S. Julienne, P. D. Lett, E. Teisinga, and C. J. Williams, *Quantum encounters of the cold kind*, Nature **416**, 225, 2002.

[44] N. Balakrishnan and A. Dalgarno, *Chemistry at ultracold temperatures*, Chem. Phys. Lett. **341**, 652, 2001.

[45] S. van der Meer, *Stochastic damping of betatron oscillations in the ISR*, CERN internal report CERN/ISR-PO/72-31, CERN, Geneva, 1972.

[46] S. van der Meer, *Stochastic cooling and accumulation of antiprotons*, Rev. Mod. Phys. **57**, 689, 1985.

[47] V. Vuletić and S. Chu, *Laser cooling of atoms, ions, or molecules by coherent scattering*, Phys. Rev. Lett. **84**, 3787, 2000.

[48] M. Conte and W. W. MacKay, *An introduction to the physics of particle accelerators*, World Scientific Publishing Co. Pte. Ltd., Singapore, 1991.

[49] S. Chu, *The manipulation of neutral particles*, Rev. Mod. Phys. **70**, 685, 1998.

[50] C. N. Cohen-Tannoudji, *Manipulating atoms with photons*, Rev. Mod. Phys. **70**, 707, 1998.

[51] W. D. Phillips, *Laser cooling and trapping of neutral atoms*, Rev. Mod. Phys. **70**, 721, 1998.

[52] W. Ketterle and N. J. van Druten, *Evaporative cooling of trapped atoms*, Adv. Atom. Mol. Opt. Phys. **37**, 181, 1996.

[53] M. G. Raizen, J. Koga, B. Sundaram, Y. Kishimoto, H. Takuma, and T. Tajima, *Stochastic cooling of atoms using lasers*, Phys. Rev. A **58**, 4757, 1998.

[54] D. Ivanov, S. Wallentowitz, and I. A. Walmsley, *Quantum limits of stochastic cooling of a bosonic gas*, Phys. Rev. A **67**, 061401, 2003.

[55] W. Ketterle and D. E. Pritchard, *Atom cooling by time-dependent potentials*, Phys. Rev. A **46**, 4051, 1992.

[56] F. Reif, *Fundamentals of statistical and thermal physics*, McGraw-Hill, Singapore, 1985, international edition.

[57] S. Y. T. van de Meerakker, R. T. Jongma, H. L. Bethlem, and G. Meijer, *Accumulating NH radicals in a magnetic trap*, Phys. Rev. A **64**, 041401, 2001.

[58] A. J. Lichtenberg, *Phase space dynamics of particles*, Wiley series in plasma physics, John Wiley & Sons, New York, 1969.

[59] P. Debye, *Polar molecules*, Dover Publications, New York, NY, USA, 1960, reprint edition.

[60] H. J. Loesch and A. Remscheid, *Brute force in molecular reaction dynamics: A novel technique for measuring steric effects*, J. Chem. Phys. **93**, 4779, 1990.

[61] B. Friedrich and D. R. Herschbach, *On the possibility of orienting rotationally cooled polar molecules in an electric field*, Z. Phys. D **18**, 153, 1991.

[62] J. D. Jackson, *Classical electrodynamics*, John Wiley & Sons, New York, 1998, 3rd edition.

[63] J. van Veldhoven, R. T. Jongma, B. Sartakov, W. A. Bongers, and G. Meijer, *Hyperfine structure of ND_3*, Phys. Rev. A **66**, 032501, 2002.

[64] S. G. Kukolich, *Measurement of ammonia hyperfine structure with a two-cavity maser*, Phys. Rev. **156**, 83, 1967.

[65] H. L. Bethlem, F. M. H. Crompvoets, R. T. Jongma, S. Y. T. van de Meerakker, and G. Meijer, *Deceleration and trapping of ammonia using time-varying electric fields*, Phys. Rev. A **65**, 053416, 2002.

[66] R. N. Zare, *Angular momentum*, John Wiley & Sons, New York, NY, USA, 1987.

[67] R. T. Jongma, *Molecular beam experiments and scattering studies with state-selected metastable CO*, Ph.D. thesis, Katholieke Universiteit Nijmegen, 1997.

[68] S. R. Gandhi and R. B. Bernstein, *Focusing and state selection of NH_3 and OCS by the electrostatic hexapole via first- and second-order Stark effects*, J. Chem. Phys. **87**, 6457, 1987.

[69] J. P. Gordon, H. J. Zeiger, and C. H. Townes, *Molecular microwave oscillator and new hyperfine structure in the microwave spectrum of NH_3*, Phys. Rev. **95**, 282, 1954.

[70] H. G. Bennewitz, W. Paul, and C. Schlier, *Fokussierung polarer Moleküle*, Z. Phys. **141**, 6, 1955.

[71] D. Kakati and D. C. Lainé, *Alternate-gradient focusing of a molecular beam of ammonia*, Phys. Lett. A **24**, 676, 1967.

[72] D. A. Dahl, *Simion 3D Version 6.0*, Idaho National Engineering Laboratory, Idaho Falls (USA), 1995.

[73] R. T. Jongma, T. Rasing, and G. Meijer, *Two-dimensional imaging of metastable CO molecules*, J. Chem. Phys. **102**, 1925, 1995.

[74] R. W. Anderson, *Tracks of symmetric top molecules in hexapole electric fields*, J. Phys. Chem. A **101**, 7664, 1997.

[75] H. L. Bethlem, *Deceleration and trapping of polar molecules using time-varying electric fields*, Ph.D. thesis, Katholieke Universiteit Nijmegen, 2002.

[76] H. L. Bethlem, G. Berden, A. J. A. van Roij, F. M. H. Crompvoets, and G. Meijer, *Trapping neutral molecules in a traveling potential well*, Phys. Rev. Lett. **84**, 5744, 2000.

[77] M. Gupta and D. Herschbach, *A mechanical means to produce intense beams of slow molecules*, J. Phys. Chem. A **103**, 10670, 1999.

[78] H. Goldstein, C. Poole, and J. Safko, *Classical mechanics*, Addison-Wesley, San Francisco, 2002, 3rd edition.

[79] M. N. R. Ashfold, R. N. Dixon, N. Little, R. J. Stickland, and C. M. Western, *The $\widetilde{B}^1 E''$ state of ammonia: sub-Doppler spectroscopy at vacuum ultraviolet energies*, J. Chem. Phys. **89**, 1754, 1988.

[80] W. Schöllkopf and J. P. Toennies, *Nondestructive mass selection of small van der Waals clusters*, Science **266**, 1345, 1994.

[81] M. Arndt, O. Nairz, J. Vos-Andreae, C. Keller, G. van der Zouw, and A. Zeilinger, *Wave-particle duality of C_{60} molecules*, Nature **401**, 680, 1999.

[82] J. Wang, V. A. Shamamian, B. R. Thomas, J. M. Wilkinson, J. Riley, C. F. Giese, and W. R. Gentry, *Speed ratios greater than 1000 and temperatures less than 1 mK in a pulsed He beam*, Phys. Rev. Lett. **60**, 696, 1988.

[83] S. Humphries Jr., *Charged particle beams*, John Wiley & Sons, New York, 1990, digital edition.

[84] S. Chu, J. E. Bjorkholm, A. Ashkin, J. P. Gordon, and L. W. Hollberg, *Proposal for optically cooling atoms to temperatures of the order of 10^{-6} K*, Opt. Lett. **11**, 73, 1986.

[85] H. Ammann and N. Christensen, *Delta kick cooling: a new method for cooling atoms*, Phys. Rev. Lett. **78**, 2088, 1997.

[86] J. Summhammer, L. Niel, and H. Rauch, *Focusing of pulsed neutrons by traveling magnetic potentials*, Z. Phys. B **62**, 269, 1986.

[87] E. Maréchal, S. Guibal, J.-L. Bossennec, R. Barbé, J.-C. Keller, and O. Gorceix, *Longitudinal focusing of an atomic cloud using pulsed magnetic forces*, Phys. Rev. A **59**, 4636, 1999.

[88] S. H. Myrskog, J. K. Fox, H. S. Moon, J. B. Kim, and A. M. Steinberg, *Modified "δ-kick cooling" using magnetic field gradients*, Phys. Rev. A **61**, 053412, 2000.

[89] R. Alheit, T. Gudjons, S. Kleineidam, and G. Werth, *Some observations on higher-order non-linear resonances in a Paul trap*, Rapid Commun. Mass Spectrom. **10**, 583, 1996.

[90] H. Nishimura, G. Lambertson, J. G. Kalnins, and H. Gould, *Feasibility of a synchrotron storage ring for neutral polar molecules*, Rev. Sci. Instrum. **74**, 3271, 2003.

Summary

A storage ring for neutral molecules

In this thesis the experimental results of the first storage ring for neutral polar molecules are presented. Stored neutral molecules offer exciting possibilities to perform high-precision measurements and to study the interactions between molecules at very low temperatures where particles behave like waves.

A storage ring is well suited for these kind of experiments as bunches of molecules can be made to interact repeatedly, at well defined times and at distinct locations, with electromagnetic fields and/or other particles. The effect of weak interactions can be enhanced by increasing the storage time in the ring, i.e., by accumulating weak effects during many round trips.

The Stark deceleration technique is used to inject bunches of cold deuterated ammonia, $^{14}ND_3$, molecules into the storage ring. This technique uses time-varying electric fields to manipulate the forward motion of a bunch of neutral polar molecules. The bunches of molecules are created in a pulsed supersonic expansion and are subsequently decelerated using a Stark decelerator. Deuterated ammonia is chosen over normal ammonia, $^{14}NH_3$, because it has a more favorable Stark effect. Reducing the forward velocity of the molecules injected into the storage ring makes a very compact storage ring design possible.

The physics of decelerating and storing neutral particles shows great similarities with the physics of charged particle accelerators. The important difference between charged particles and neutral particles is that the force on a charged particle in an electric field is proportional to the field while the force on a neutral particle is proportional to the gradient of the electric field strength.

A central theme in particle physics is the concept of phase-space, which is the 6-dimensional position-momentum space. Liouville's theorem states that the phase-space density for a group of particles, i.e., the number of particles per unit volume position-momentum space, remains constant in the absence of dissipative forces. However, nonlinear forces acting on particles lead to a spiralization of the phase-space distribution and this reduces the effective phase-space density. This proces is irreversible and should thus be avoided.

The phase-space distribution of the molecules at the exit of the Stark decelerator, the emittance, has to be mapped onto the acceptance of the storage ring in order to store as many molecules as possible in the storage ring. This

mapping is called phase-space matching. The aforementioned spiralization of the phase-space distribution makes this matching less than perfect.

The principle of the storage ring for neutral molecules is based on the linear, electrostatic hexapole lens that transversely confines a beam of low-field seeking molecules. By bending such a linear hexapole around into a torus, a storage ring can be created. The electric field generated by appropriately chosen high voltages on the ring electrodes provides the centripetal force that keeps the molecules in orbit. Molecules that are not injected onto the equilibrium orbit start to oscillate around this orbit. These oscillations are called betatron oscillations.

The asymmetric geometry of the applied electric field deviates from the commonly used hexapole field to facilitate the laser ionization based detection of the molecules in the ring. The asymmetry leads to a coupling between the radial and vertical motion of the molecules. Furthermore, conservation of angular momentum couples the radial motion to the forward, tangential motion. It is shown theoretically that without active manipulation in the tangential direction an isochronous operation of the ring, when all molecules have the same round trip time, is impossible.

It is shown experimentally that decelerated packages of molecules in single rotational and vibrational quantum state are stored in the ring at different tangential velocities. Up to six round trips in the ring are observed at an optimum tangential velocity of 89 m/s. This number is limited due to the velocity spread in the tangential direction of the package of molecules. Based on numerical trajectory calculations a translational temperature of 10 mK can be attributed to the packages of molecules stored in the ring.

The spreading out of the package of molecules can be reduced using a buncher. The electric field in the buncher is designed such that molecules experience an harmonic force in the longitudinal (forward) direction. This force rotates the longitudinal phase-space distribution of a package of molecules at a constant angular frequency. In this way, packages of molecules have been created that have either a minimal longitudinal position spread of 0.5 mm or a minimal longitudinal velocity spread of 0.76 m/s, which corresponds to a longitudinal temperature of 250 μK.

The buncher combined with hexapoles is used to match the six-dimensional phase-space distribution of a package of molecules at the exit of the Stark decelerator onto the acceptance of the ring. The hexapoles map the transverse phase-space distribution while the buncher is used to map the longitudinal distribution, i.e., to minimize the tangential velocity spread. By doing so, a package of molecules injected into the storage ring can be observed after more than 50 round trips. This corresponds to a total flight path of 40 m and a storage time of 0.5 s.

The betatron oscillation of the molecules in the storage ring can be driven with a small AC voltage on top of the DC voltages on the ring electrodes. In combination with the position sensitive detection method this is used to

110

determine the frequency of the vertical betatron oscillations of the molecules in the ring. The experimentally obtained frequency of 373 Hz agrees well with the theoretically expected eigenfrequency of the potential well. In a similar fashion, the betatron wavelength has been determined by altering the high voltages on the ring electrodes and by hence altering the strength of the potential well.

In the current storage ring the package of molecules still spreads out in the tangential direction due to the, all be it small, velocity spread. In the end, this limits the number of observable round trips. Incorporating bunchers in the storage ring makes it possible to keep the package of molecules together inside the ring. For that, the storage ring has to be split up in separate sections. This introduces gaps in the ring leading to abrupt changes in the transverse potential well. As these changes occur periodically it is possible that the betatron motion of the molecules is parametrically amplified and eventually the molecules will be expelled from the ring. By switching the current storage ring momentarily off, allowing the molecules to fly freely before they are recaptured, it is shown experimentally that it is in principle possible to create gaps in the ring.

In the design of the sectional storage ring the number of sections is kept to a minimum in order to make construction and operation of the ring easier. The transverse stability of the trajectories is investigated numerically. It is shown that for experimentally accessible parameter settings stable operation of a sectional storage ring is possible. The sectional storage ring proposed here incorporates all the required bending, bunching and focusing sections in a very simple and compact design.

Samenvatting

Een opslagring voor neutrale moleculen

In dit proefschrift worden de experimentele resultaten gepresenteerd van de eerste opslagring voor neutrale, polaire moleculen. Opgeslagen moleculen bieden interessante mogelijkheden voor hoge-resolutie metingen en voor het bestuderen van wisselwerkingen tussen moleculen bij zeer lage temperaturen, waar deeltjes zich gedragen als golven.

Een opslagring is zeer geschikt voor dit soort experimenten omdat pakketjes moleculen herhaaldelijk op gezette tijden en op precieze plekken kunnen wisselwerken met electromagnetische velden en/of andere deeltjes. Het effect van zwakke interacties kan versterkt worden door deze te accumuleren gedurende vele rondjes in de ring.

De Stark-afremtechniek is gebruikt om pakketjes koude, gedeutereerde ammoniakmoleculen, $^{14}ND_3$, in de opslagring te injecteren. Deze techniek maakt gebruik van tijdsvariërende velden om de voorwaartse beweging van een pakketje neutrale moleculen te manipuleren. De pakketjes moleculen worden in een gepulste supersonische expansie gevormd en vervolgens afgeremd met een Starkafremmer. Gedeutereerd ammoniak is verkozen boven gewoon ammoniak, $^{14}NH_3$, omdat dat een gunstiger Stark-effect heeft. Door de voorwaartse snelheid van de moleculen te reduceren kan een zeer compacte opslagring gemaakt worden.

De fysica van het afremmen en opslaan van neutrale deeltjes vertoont veel gelijkenis met de fysica van versnellers voor geladen deeltjes. Het grote verschil tussen geladen en neutrale deeltjes is dat de kracht op een geladen deeltje in een elektrisch veld evenredig is met het elektrische veld, terwijl de kracht op een neutraal deeltje evenredig is met de gradiënt van de elektrische veldsterkte.

Een belangrijk concept in de deeltjesfysica is faseruimte: de zes-dimensionale positie-impulsruimte. Liouvilles theorema stelt dat de faseruimtedichtheid van een verzameling deeltjes, oftewel het aantal deeltjes per eenheidsvolume positie-impulsruimte, constant blijft als er geen dissipatieve krachten op de deeltjes werken. Echter, niet-lineaire krachten leiden tot een spiralisatie in de faseruimteverdeling en dit reduceert de effectieve faseruimtedichtheid. Dit proces is onomkeerbaar en moet daarom vermeden worden.

De faseruimteverdeling van de moleculen aan het einde van de Stark-afrem-

mer, de emittantie, moet afgebeeld worden op de acceptatie van de opslagring. Deze faseruimte-afbeelding moet zo goed mogelijk gebeuren teneinde zoveel mogelijk moleculen in de ring op te slaan. De reeds genoemde spiralisatie van de faseruimteverdeling leidt tot aberraties in deze afbeelding.

De werking van de opslagring voor neutrale moleculen is gebaseerd op de lineaire, electrostatische hexapoollens die een bundel laagveldzoekende moleculen zijdelings bijeenhoudt. Door zo'n hexapool in een cirkel te buigen ontstaat een opslagring. Door de juiste hoogspanningen aan te leggen op de zes ring-electrodes wordt een elektrisch veld gecreëerd, dat de centripetale kracht levert, die de moleculen in de ring houdt. De moleculen die niet op hun evenwichts-baan ingekoppeld worden in de ring maken een oscillerende beweging rond de evenwichtsbaan. Deze oscillaties worden betatronoscillaties genoemd.

Het aangelegde elektrische veld wijkt af van het gebruikelijke hexapoolveld. Dit is gedaan om de op laser-ionisatie gebaseerde detectie van de moleculen te vereenvoudigen. De asymmetrie van het aangelegde elektrische veld leidt tot een koppeling tussen de radiële en verticale beweging van de moleculen. Het hoekmoment koppelt tevens de radiële beweging aan de tangentiële, voorwaartse beweging. Verder is aangetoond dat zonder actieve manipulatie in de tangentiële richting een isochrone werking van de ring, waarbij alle moleculen dezelfde rondetijden hebben, onmogelijk is.

Experimenteel is aangetoond dat afgeremde pakketjes moleculen in een enkele rotationele en vibrationele toestand opgeslagen kunnen worden in de opslagring. Moleculen die rondvliegen met tangentiële snelheden tussen 76 m/s en 110 m/s kunnen ingevangen worden bij een vaste instelling van de hoogspanningen op de ringelectrodes. Bij een snelheid van ongeveer 89 m/s kunnen pakketjes moleculen ook nog na zes rondjes gedetecteerd worden. Dit aantal wordt gelimiteerd door het uitspreiden van het pakketje moleculen in de tangentiële richting. Op basis van numerieke baanberekeningen kan aan een opgeslagen pakketje moleculen een translationele temperatuur van 10 mK worden toegekend.

Het uitspreiden van een pakketje moleculen kan tegengegaan worden met behulp van een zogeheten 'buncher'. Het electrisch veld in de buncher is zodanig ontworpen dat een bundel polaire moleculen een harmonische kracht ondervindt in de longitudinale (voorwaartse) richting. Deze kracht laat de longitudinale fase-ruimte verdeling van een pakketje moleculen draaien met een constante hoekfrequentie. Op deze wijze zijn pakketjes moleculen verkregen die of een minimale lengte van 0.5 mm of juist een minimale snelheidsspreiding hebben 0.76 m/s, wat overeenkomt met een longitudinale temperatuur van 250 μK.

De buncher samen met hexapoollensen worden nu gebruikt om de zesdimensionale fase-ruimte verdeling van een pakketje moleculen aan het einde van de Stark-afremmer zo goed mogelijk af te beelden op de acceptatie van de ring. De hexapolen beelden de zijwaartse faseruimteverdeling af, terwijl de buncher gebruikt wordt om de longitudinale faseruimteverdeling af te beelden; in dit

geval het minimaliseren van de tangentiële snelheidsspreiding. Op deze wijze kan een pakketje moleculen nog na 50 rondjes, oftewel na een vluchtlengte van 40 m en een opslagtijd van 0.5 s, in de ring geobserveerd worden.

De zijwaartse beweging van de moleculen in de ring kan aangedreven worden door kleine wisselspanningen te superponeren op de constante spanningen op de ringelectrodes. In combinatie met de zeer plaatsgevoelige detectiemethode is dit gebruikt om de frequentie van de verticale betatronoscillaties nauwkeurig te meten. De experimenteel gevonden frequentie van 373 Hz is in overeenstemming met de theoretisch verwachte eigenfrequentie van de potentiaalput. Vergelijkbare informatie kan verkregen worden door de hoogspanningen op de ringelectrodes en daarmee de sterkte van de potentiaalput te wijzigen.

In de huidige opslagring spreidt het pakketje nog altijd uit in de tangentiële richting door de — weliswaar kleine — resterende snelheidsspreiding. Uiteindelijk beperkt dit het aantal waarneembare rondjes in de ring. Door bunchers in te bouwen ín de ring kan het uitspreiden teniet gedaan worden. Daartoe moet de huidige ring in afzonderlijke secties opgesplitst worden. Noodzakelijkerwijs ontstaan er hierdoor gaten tussen de secties, hetgeen leidt tot abrupte veranderingen in de zijwaartse potentiaalput. Omdat deze veranderingen periodiek zijn in de ring, kan de betatronoscillatie van moleculen parametrisch versterkt worden. Hierdoor ontsnappen de moleculen uiteindelijk uit de ring. Door de huidige ring tijdelijk uit te zetten, waardoor de moleculen vrijuit kunnen bewegen voordat ze weer gevangen worden in de potentiaalput, is experimenteel aangetoond dat het in principe mogelijk is om gaten te maken in de ring.

In het ontwerp van de sectionele opslagring is het aantal secties tot een minimum beperkt teneinde de constructie en het gebruik van de ring te vereenvoudigen. De zijwaartse stabiliteit van banen die de moleculen in de ring beschrijven is numeriek onderzocht. Het blijkt dat met de juiste parameterinstellingen, die experimenteel ook realiseerbaar zijn, een stabiele werking van een sectionele opslagring mogelijk is. De sectionele opslagring die in dit proefschrift gepresenteerd wordt, heeft alle vereiste bocht-, buncher- en focussecties verenigd in een zeer eenvoudig en compact ontwerp.

Curriculum vitae

Floris Maria Hermansz Crompvoets
Born on February 27th 1976 in Meijel, The Netherlands

1988 - 1994   Secondary education ('Voorbereidend Wetenschappelijk On-
derwijs' degree) at the Peelland College in Deurne.

1994 - 1999   Physics studies at the University of Nijmegen. Research for
master thesis performed in the Applied Physics group under
supervision of dr. N. J. Dam, dr. ir. N. M. Sijtsema, and Prof.
dr. J. J. ter Meulen. Subject of master thesis: 'Laser pulse
compression by stimulated Brillouin scattering'. Graduated
with distinction in Experimental Physics.

March - June   Astrophysics research project at the Isaac Newton Group of
1999   Telescopes (La Palma) under supervision of dr. S. J. Smartt
and Prof. dr. J. Kuijpers. Research subject: 'Wavelength de-
pendent pixel-to-pixel response variations of a typical EEV42-
80 CCD: the role of flat-fielding astronomical data'.

1999 - 2004   Ph.D. student employed by the 'Stichting Fundamenteel On-
derzoek der Materie' (FOM) in the group of Prof. dr. G.
J. M. Meijer at the University of Nijmegen (now Radboud
University Nijmegen). Research topic: 'a storage ring for
neutral molecules'. The results of this research are described
in this thesis. As from August 2000, the research was per-
formed at the FOM-institute for Plasma Physics 'Rijnhuizen'
in Nieuwegein.

2004 - now   Senior scientist at Philips Research in Eindhoven.

List of publications

- *Dynamics of neutral molecules stored in a ring*
  Floris M. H. Crompvoets, Hendrick L. Bethlem, Jochen Küpper, André
  J. A. van Roij, and Gerard Meijer
  Phys. Rev. A **69**, 063406 (2004).

- *Longitudinal focusing and cooling of a molecular beam*
  Floris M. H. Crompvoets, Rienk T. Jongma, Hendrick L. Bethlem, and
  Gerard Meijer
  Phys. Rev. Lett. **89**, 093004 (2002).

- *Deceleration and trapping of ammonia using time-varying electric fields*
  Hendrick L. Bethlem, Floris M. H. Crompvoets, Rienk T. Jongma, Sebastiaan Y. T. van de Meerakker, and Gerard Meijer
  Phys. Rev. A **65**, 053416 (2002).

- *Moleculen dolgedraaid*
  Floris Crompvoets, Rick Bethlem en Rienk Jongma
  Nederlands Tijdschrift voor Natuurkunde, **67**(6), 172 (2001).

- *A prototype storage ring for neutral molecules*
  Floris M. H. Crompvoets, Hendrick L. Bethlem, Rienk T. Jongma, and
  Gerard Meijer
  Nature (London) **411**, 174 (2001).

- *Electrostatic trapping of ammonia molecules*
  Hendrick L. Bethlem, Giel Berden, Floris M. H. Crompvoets, Rienk T.
  Jongma, André J.A. van Roij, and Gerard Meijer
  Nature (London) **406**, 491 (2000).

- *Trapping neutral molecules in a traveling potential well*
  Hendrick L. Bethlem, Giel Berden, André J.A. van Roij, Floris M. H.
  Crompvoets, and Gerard Meijer
  Phys. Rev. Lett. **84**, 5744 (2000).